รายงานการวิจัยฉบับสมบูรณ์

โครงการ การพัฒนาวิธีการเตรียมและวิธีการวิเคราะห์อนุภาค
ระดับนาโนเมตรและไมโครเมตรเพื่อประยุกต์ใช้เป็น
อนุภาคนำส่งสำหรับสารเสริมสุขภาพ

โดย ผศ.ดร. อทิตยา ศิริภิญญานนท์ และคณะ

มิถุนายน 2554

สัญญาเลขที่ RSA5180009

รายงานการวิจัยฉบับสมบูรณ์

การพัฒนาวิธีการเตรียมและวิธีการวิเคราะห์อนุภาคระดับนาโนเมตรและไมโครเมตรเพื่อประยุกต์ใช้เป็นอนุภาคนำส่งสำหรับสารเสริมสุขภาพ

คณะผู้วิจัย	สังกัด
1. ผศ.ดร. อทิตยา ศิริภิญญานนท์	ภาควิชาเคมี คณะวิทยาศาสตร์ มหาวิทยาลัยมหิดล
2. นางสาว วิไลวรรณ สมเชื้อ	ภาควิชาเคมี คณะวิทยาศาสตร์ มหาวิทยาลัยมหิดล
3. นางสาว อาทิตยา สามณฑา	ภาควิชาเคมี คณะวิทยาศาสตร์ มหาวิทยาลัยมหิดล
4. นางสาว กาญจนา สงศิลาวัต	ภาควิชาเคมี คณะวิทยาศาสตร์ มหาวิทยาลัยมหิดล
5. นาย วิมุฒิ เสริมศรี	ภาควิชาเคมี คณะวิทยาศาสตร์ มหาวิทยาลัยมหิดล

นักวิจัยที่ปรึกษา	สังกัด
ศ.ดร. ยุวดี เชี่ยววัฒนา	ภาควิชาเคมี คณะวิทยาศาสตร์ มหาวิทยาลัยมหิดล

สนับสนุนโดยสำนักงานกองทุนสนับสนุนการวิจัย

(ความเห็นในรายงานนี้เป็นของผู้วิจัย สกว. ไม่จำเป็นต้องเห็นด้วยเสมอไป)

สารบัญ

กิตติกรรมประกาศ

ขอขอบคุณสำนักงานกองทุนสนับสนุนการวิจัยที่ได้สนับสนุนทุนการวิจัย “ทุนพัฒนานักวิจัย” เพื่อใช้ในการดำเนินงานวิจัยในโครงการ “การพัฒนาวิธีการเตรียมและวิธีการวิเคราะห์อนุภาคระดับนาโนเมตรและไมโครเมตรเพื่อประยุกต์ใช้เป็นอนุภาคนำส่งสำหรับสารเสริมสุขภาพ” โดยมีระยะเวลาของโครงการ 3 ปี ตั้งแต่ พฤษภาคม 2551 ถึง พฤษภาคม 2554 และขอขอบคุณศูนย์ความเป็นเลิศด้านนวัตกรรมทางเคมี โครงการพัฒนาบัณฑิตศึกษาและการวิจัยทางเคมี สำหรับทุนการศึกษาของนักศึกษาวัสดุวิจัยและครุภัณฑ์บางส่วนในโครงการวิจัย และภาควิชาเคมี คณะวิทยาศาสตร์ มหาวิทยาลัยมหิดล สำหรับสถานที่ เครื่องมือและอุปกรณ์ต่างๆ

คณะผู้วิจัย

บทคัดย่อ

รหัสโครงการ: **RSA5180009**

ชื่อโครงการ: **การพัฒนาวิธีการเตรียมและวิธีการวิเคราะห์อนุภาคระดับนาโนเมตรและไมโครเมตรเพื่อประยุกต์ใช้เป็นอนุภาคนำส่งสำหรับสารเสริมสุขภาพ**

ชื่อนักวิจัย: ผศ.ดร.อทิตยา ศิริภิญญานนท์

ภาควิชาเคมี คณะวิทยาศาสตร์ มหาวิทยาลัยมหิดล

Email Address: scasp@mahidol.ac.th

ระยะเวลาโครงการ: 1 พฤษภาคม 2551 – 31 พฤษภาคม 2554

งานวิจัยนี้ได้แบ่งออกเป็นสองตอนหลักๆ ตอนที่หนึ่งเกี่ยวข้องกับการศึกษาสารอาหารไวตามินอี โดยได้ศึกษาถึงความสามารถของโปรตีนสองชนิด คือ โปรตีนแลคโทโกลบูลินและโปรตีนไข่ขาว ในการกักเก็บไวตามินอีในอนุภาคของโปรตีนหลังจากมีการเติมเกลือลงในโปรตีนซึ่งเกลือทำให้โปรตีนเกิดการจับรวมตัวกัน ได้ทำการศึกษาถึงปัจจัยต่างๆ ที่ส่งผลต่อความสามารถในการกักเก็บไวตามินอี ได้แก่ ประเภทของเกลือ ความเข้มข้นของเกลือ โปรตีน และ ไวตามินอี พบว่าความเข้มข้นของโปรตีนและไวตามินอีมีอิทธิพลต่อความสามารถในการกักเก็บไวตามินอี จากการประเมินโดยระบบหลอดแก้ว พบว่าในสภาวะจำลองการย่อยของกระเพาะอาหาร สามารถปลดปล่อยไวตามินอีได้ถึงเกือบหนึ่งร้อยเปอร์เซนต์ จึงใช้อัลจิเนทในการเคลือบอนุภาคโปรตีนเพื่อชะลอการปลดปล่อยไวตามินอีในสภาวะกระเพาะอาหารแต่ให้ปลดปล่อยในสภาวะการดูดซึมสารอาหารของลำไส้เล็ก และได้ใช้เทคนิคการแยกแบบไหลภายใต้สนามในการศึกษาผลของไวตามินอีในการขยายขนาดของอนุภาคทองระดับนาโนเมตร

งานวิจัยในตอนที่สอง เป็นการประยุกต์ใช้เทคนิคการแยกแบบไหลภายใต้สนามในการวิเคราะห์ขนาดอนุภาคของอนุภาคขนาดนาโนเมตรสองชนิด คือ อนุภาคไทเทเนียมไดออกไซด์และอนุภาคเงินขนาดนาโนเมตร ได้ศึกษาถึงขนาดและการกระจายตัวของขนาดอนุภาคของอนุภาคไทเทเนียมไดออกไซด์ในผลิตภัณฑ์ครีมกันแดดที่มีค่า SPF ต่างกัน ความเข้มข้นของไทเทเนียมมากในผลิตภัณฑ์ที่มีค่า SPF สูง และได้ศึกษาขนาดและการกระจายตัวของขนาดอนุภาคเงินขนาดนาโนเมตรที่ใช้สารเพิ่มเสถียรภาพที่แตกต่างกัน คือ ซิเทรท เพ็คทิน และ อัลจิเนท อีกทั้งได้ศึกษาถึงการเกิดการเปลี่ยนแปลงขนาดของขนาดอนุภาคเงินขนาดนาโนเมตรในตัวกลางน้ำที่แตกต่างกันหลายประเภท พร้อมทั้งผลของสารฮิวมิกต่อการเปลี่ยนแปลงขนาดของอนุภาคเงินขนาดนาโนเมตร

คำหลัก: การวิเคราะห์ขนาดอนุภาค เทคนิคการแยกแบบไหลภายใต้สนาม ไวตามินอี การกักเก็บ อนุภาคเงินขนาดนาโนเมตร อนุภาคไทเทเนียมไดออกไซด์ขนาดนาโนเมตร

ABSTRACT

Project Code: **RSA5180009**

Project Title: **Method Development for the Preparation and Characterization of Nano- and Micro-particles as Nutraceutical Delivery Vehicles**

Investigator: Atitaya Siripinyanond

Department of Chemistry, Faculty of Science, Mahidol University

Email Address: scasp@mahidol.ac.th

Project Period: May 1, 2008 – May 31, 2011

The works in this study are divided into two parts. Part one is related to the study of α-tocopherol (α-TOC) as a model nutraceutical compound. Two types of proteins, including β-lactoglobulin (BLG) and hen egg white protein (HEW), were examined for their ability to encapsulate α-TOC after salt-induced gelation of the proteins. Parameters affecting encapsulation efficiency were investigated including the type of salt, as well as concentrations of salt, protein, and α-TOC. Concentrations of protein and α-TOC revealed to have an influence on encapsulation efficiency. From the *in vitro* estimation, the release of α-TOC was nearly 100% in simulated gastric condition. Alginate was therefore used for coating of these encapsulated particles to prolong the release of α-TOC till simulated intestinal condition. Further, field-flow fractionation (FFF) was applied for size characterization of gold nanoparticles enlargement induced by α-tocopherol. The effects of α-tocopherol and incubation time on the enlargement of gold nanoparticles were examined.

Part two involves the application of FFF as a particle size characterization technique for engineered nanoparticles. Two types of nanoparticles were examined including titanium dioxide and silver nanoparticles. Particle size distribution of titanium dioxide particles in three brands of sunscreen products of various SPF values was investigated. The titanium dioxide concentrations were higher for the products of higher SPF values. Particle size characterization of Ag NPs stabilized by citrate, pectin, and alginate was also carried out using FFF. Further, FFF was employed to observe the changes in particle size of Ag NPs in environmental water in the absence and presence of humic acid.

Keywords: size characterization, field-flow fractionation, α-tocopherol, encapsulation, silver nanoparticles, titanium dioxide nanoparticles

Executive Summary

Project Title: Method Development for the Preparation and Characterization of Nano- and Micro-particles as Nutraceutical Delivery Vehicles

Investigaor: Atitaya Siripinyanond

Department of Chemistry, Faculty of Science, Mahidol University

Email Address: scasp@mahidol.ac.th

Project Period: May 1, 2008 – May 31, 2011

Encapsulation technologies have gained increased interest to the food industry as they are used to increase stability of the bioactive compounds during processing and storage and also to prevent undesirable interactions with the food matrix. Further, a real benefit of encapsulation is due to the ability to control the release of the incorporated ingredients and deliver them to a specific target at a suitable time. Protein hydrogel has been used as a carrier particle because of its high nutritional value and generally recognized as safe. This study was carried out to evaluate the ability of β-lactoglobulin (BLG) and hen egg white protein (HEW) aggregates induced by salt as protein-based particles for encapsulation of α-tocopherol (α-TOC). Parameters affecting encapsulation efficiency including concentrations of proteins, α-TOC, and salt were examined. The release of α-TOC from the encapsulated particles was investigated. The use of alginate coating for protection of α-TOC release in the gastric condition was also explored. This study shows a successful attempt to use protein-based particles in combination with alginate to allow delivery of α-TOC to intestinal for bioavailability improvement.

Considering the antioxidant activity of α-TOC, we hypothesized that α-tocopherol should exhibit catalytic activity on the growth of gold nanoparticles, and various α-tocopherol concentrations should result in different sizes of gold nanoparticles. A closer inspection on the influence of α-tocopherol on the size of gold nanoparticles was then carried out by using field-flow fractionation (FFF) as particle size characterization technique.

With the ability of FFF as a resourceful particle size characterization technique, two types of engineered nanoparticles, i.e., TiO_2 nanoparticles and silver nanoparticles (AgNPs), were examined. Titanium dioxide nanoparticles are often added in sunscreen cosmetics as a physical UV filter, reflecting and scattering UV radiation. An on-line coupling between FFF and inductively coupled plasma-mass

spectrometry (FFF-ICP-MS) was proposed to provide the quantitative information of titanium dioxide concentrations across particle size distribution profiles of the sunscreen samples. The necessity for sample preparation before FFF particle size characterization was evaluated. The ability of ICP-MS as an on-line detector for the fractionated titanium dioxide particles was examined. The developed FFF-ICP-MS method was applied to investigate size distribution of titanium dioxide particles in various sunscreen products of various SPF values.

As Ag NPs has been widely used and one of the important parameters that affect on the properties of NPs is their particle size. Field-flow fractionation with off-line electrothermal atomic absorption spectrometry (ETAAS) detection was developed and employed for particle size characterization of Ag NPs stabilized by citrate, pectin, and alginate. Citrate stabilized-Ag NPs were prepared from sodium borohydride reduction of silver nitrate. Sodium citrate was used as the capping agent to stabilize Ag NPs and prevent the aggregation process. Pectin stabilized- and alginate stabilized-Ag NPs were prepared from ascorbic acid reduction of silver nitrate. Pectin and alginate were used as the capping agent for pectin stabilized- and alginate stabilized-Ag NPs, respectively. Further as Ag NPs have been widely used in various consumer products, causing the release of these materials to the environment, it is crucial to understand the behaviors of these materials and how these materials interact with natural organic matters in the environmental water. Field-flow fractionation with ETAAS detection was employed to observe the aggregation of Ag NPs of various types in environmental water in the absence and presence of humic acid.

Four papers have been published in the international journals as follows:

1. Somchue, W., Sermsri, W., Shiowatana, J. & Siripinyanond, A. 2009, "Encapsulation of α-Tocopherol in Protein-based Delivery Particles", *Food Res. Int.,* vol. 42, pp. 909–914. (impact factor = 2.414)
2. Sermsri, W., Jarujamras, P., Shiowatana, J. & Siripinyanond, A. 2010, "Flow Field-Flow Fractionation: A Versatile Approach for Size Characterization of α-Tocopherol-Induced Enlargement of Gold Nanoparticles", *Anal. Bioanal. Chem.,* vol. 396, pp. 3079–3085. (impact factor = 3.480)
3. Samontha, A., Shiowatana, J. & Siripinyanond, A. 2011, "Particle Size Characterization of Titanium Dioxide in Sunscreen Products Using Sedimentation Field-Flow Fractionation-

Inductively Coupled Plasma Mass Spectrometry", *Anal. Bioanal. Chem.,* vol. 399, pp. 973–978. (impact factor = 3.480)

4. Songsilawat, K., Shiowatana, J. & Siripinyanond, A. 2011, "Flow Field-Flow Fractionation with Off-line Electrothermal Atomic Absorption Spectrometry for Size Characterization of Silver Nanoparticles", *J. Chromatogr. A,* vol. 1218, pp. 4213–4218. (impact factor = 4.101)

Five papers have been presented at the international conferences during the past three years as follows:

1. Atitaya Samontha, Juwadee Shiowatana and Atitaya Siripinyanond, Ti Size Characterization in Sunscreen Products Using Sedimentation Field-Flow Fractionation-Inductively Coupled Plasma-Mass Spectrometry, **Pure and Applied Chemistry International Conference (PACCON 2010)**, January 21 – 23, 2010, Ubon Ratchathani, Thailand.
2. Kanchana Songsilawat, Juwadee Shiowatana and Atitaya Siripinyanond, Field-Flow Fractionation Coupled with GFAAS for Size Characterization of Silver Nanoparticles, **Pure and Applied Chemistry International Conference (PACCON 2010)**, January 21 – 23, 2010, Ubon Ratchathani, Thailand.
3. Kanchana Songsilawat, Manita Untang, Juwadee Shiowatana and Atitaya Siripinyanond, Field-Flow Fractionation Coupled with GFAAS for Size Characterization of Silver Nanoparticles, **16th International Conference on Flow Injection Analysis (ICFIA),** April 25 – 30, 2010, Pattaya, Thailand.
4. Atitaya Samontha, Juwadee Shiowatana and Atitaya Siripinyanond, Investigation of Elemental Size Distribution of Nanoparticles in Household Products Using Sedimentation Field-Flow Fractionation-Inductively Coupled Plasma Mass Spectrometry (SdFFF-ICP-MS), **16th International Conference on Flow Injection Analysis (ICFIA),** April 25 – 30, 2010, Pattaya, Thailand.
5. Atitaya Siripinyanond, Kanchana Songsilawat, Supharart Sangsawong and Juwadee Shiowatana, Field-Flow Fractionation with Off-line Electrothermal Atomic Absorption Spectrometry for Size Characterization of Silver Nanoparticles, **15th International Symposium on Field- and Flow-Based Separations (FFF 2011)**, May 23 – 25, 2011, South San Francisco, California, U.S.A.

Chapter 1

Encapsulation of α-Tocopherol in Protein-based Delivery Particles

1.1 Introduction

1.2 Experimental

1.2.1 Chemicals

1.2.2 Preparation of protein solutions

1.2.3 Preparation of protein based-encapsulated α-TOC

1.2.4 Preparation of alginate coated-protein based-encapsulated α-TOC

1.2.5 Estimation of α-TOC loading

1.2.6 Estimation of in vitro release of alginate coated-protein based-encapsulated α-TOC and evaluation of α-TOC release kinetics

1.3 Results and discussion

1.3.1 Selection of divalent cation for the preparation of protein based-encapsulated α-TOC by cold gelation

1.3.2 Parameters affecting encapsulation efficiency of BLG-encapsulated α-TOC

1.3.3 Parameters affecting encapsulation efficiency of HEW-encapsulated α-TOC

1.3.4 Release of α-tocopherol from protein-based delivery particles: a comparison between BLG and HEW (with and without alginate coating)

1.4 Summary

1.5 References

1.1 Introduction

Vitamin E is an important antioxidant that can help reduce risk of diseases such as cardiovascular diseases (Blatt, Pryor, Mata & Proteau, 2004; Brigelius-Flohé & Traber, 1999; Mardones & Rigotti, 2004; Pryor, 2000; Tucker & Townsend, 2005). Although vitamin E deficiency is rare in humans, absorption of vitamin E is reduced in the patients with some diseases including pancreatic diseases, biliary obstruction, coeliac disease, and abetalipoproteinaemia. Therefore, supplementation of vitamin E is needed in some cases. Vitamin E exists in eight different forms including four tocopherols (α, β, γ, δ) and four tocotrienols (α, β, γ, δ), but vitamin E supplements are usually available in forms of relatively stable all-rac α-tocopherol acetate and all-rac α-tocopherol succinate. Nonetheless, α-tocopherol was believed to be most absorbable in human intestine. Although it was believed that tocopherol esters were hydrolyzed to free tocopherol on the duodenum (Borel, 2003; Borel et al., 2001; Cheeseman, Holley, Kelly, Wasil, Hughes & Burton, 1995) the need of hydrolytic enzyme to de-esterify the supplement cannot guarantee the efficient bioavailability. Consequently, it would be beneficial if vitamin E supplements can be prepared in the free phenol form of α-tocopherol (α-TOC). As it is relatively unstable and sensitive to temperature, oxygen, and light, encapsulation is needed for protection of α-tocopherol during shelf storage. Further, the release of vitamin E on the target digestive system should be controllable with the use of encapsulation technologies (Ubbink & Krüger, 2006).

Encapsulation technologies have gained increased interest to the food industry as they are used to increase stability of the bioactive compounds during processing and storage and also to prevent undesirable interactions with the food matrix. Further, a real benefit of encapsulation is due to the ability to control the release of the incorporated ingredients and deliver them to a specific target at a suitable time. Protein hydrogel has been used as a carrier particle because of its high nutritional value and generally recognized as safe. Various preparation techniques have been used to induce gelation of proteins (Totosaus, Montejano, Salazar & Guerrero, 2002). These include acid-induced gelation (Alting, Hamer, Kruif & Visschers, 2003), heat-induced gelation (Dumay, Laligant, Zasypkin & Cheftel, 1999), and ion-induced gelation processes (Bryant & McClements, 1998; Bryant & McClements, 2000; Croguennec, & Brulé, 2002; Maltais, Remondetto & Subirade, 2008; Simons, Kosters, Visschers, & Jongh, 2002). The cold-set gelation has gained wide interest as it offers an advantage to maintain heat-sensitive ingredients (Beaulieu, Savoie, Paquin & Subirade, 2002; Chen, Remondetto & Subirade, 2006). Two steps were used to form cold-set gel. Initially, heat treatment was used to cause globular proteins to unfold and expose multiple functional groups within the protein which could create the interaction between the active ingredients and polypeptide chains. After cooling, salt was added to the protein solution to cause aggregation of protein by electrostatic interaction (Chen et al., 2006). Various kinds of

globular proteins including soy and whey proteins, especially β-lactoglobulin (BLG), were examined for their gelation characteristics. Further, gelation behavior of hen egg white protein (HEW) has been described by many researchers.

Due to its amphiphilic nature, BLG was reported to bind with small lipid molecules such as cholesterol (Wang, Allen & Swaisgood, 1997), fatty acid (Wu, Pérez, Puyol & Sawyer, 1999), vitamin A (Pérez & Calvo, 1995), vitamin D (Wang et al., 1997), and vitamin E (Swaisgood & Allen, 2001; Voth & Miller, 1958). It was illustrated that the globular proteins were adsorbed to the emulsion interface and formed continuous and homogeneous membrane around the oil droplets through β-sheet interaction (Beaulieu et al., 2002; Lefévre & Subirade, 2003; Line, Remondetto & Subirade, 2005). Moreover, the hydrogel of BLG could entrap fat-soluble ingredients to keep them in the active form until the time of consumption (Chen et al., 2006).

Hen egg white protein, a low cost protein, has been widely used as ingredients in many food products as it possesses several excellent functional properties such as foaming, emulsification, heat setting and binding adhesion. Hen egg white is composed of various types of proteins, including 54.0% ovalbumin (44.5 kDa), 12.0% ovotransferrin (77.7 kDa), 11.0% ovomucoid (28.0 kDa), 3.5% ovomucin (5500-8300 kDa), 3.4% lysozyme (14.3 kDa), and a few other proteins. Hen egg white protein was demonstrated to form stable intermolecular β-sheet structures during the thermal denaturation (Mine, 1995). Heat caused the protein molecules to partially unfold to expose their hydrophobic residues to allow adsorption of fat-soluble components forming continuous and homogeneous membrane around the oil droplets through β-sheet interaction.

In order to control the release of active ingredients at the intestinal tract, alginate coating was employed to prevent hydrolysis of protein hydrogel from proteolytic enzymatic digestion in gastric condition (Chen & Subirade, 2006; Chen & Subirade, 2007; Pongsawatmanit, Harnsilawat & McClements, 2006; Sriamornsak & Kennedy, 2007). In gastric condition, protonation converted sodium alginate to insoluble alginic acid that could protect diffusion of the active ingredients from the alginate-coated protein hydrogel. In intestinal condition, the alginate matrix swelled allowing the release of the active ingredients (Chen et al., 2006).

This study was carried out to evaluate the ability of BLG and hen egg white protein (HEW) aggregates induced by salt as protein-based particles for encapsulation of α-TOC in its free phenol form. Parameters affecting encapsulation efficiency including concentrations of proteins, α-TOC, and salt were examined. The release of α-TOC from the encapsulated particles was investigated. The use of alginate coating for protection of α-TOC release in the gastric condition was also explored. This study shows a

successful attempt to use protein-based particles in combination with alginate to allow delivery of α-TOC to intestinal for bioavailability improvement.

1.2 Experimental

1.2.1 Chemicals

(±)-α-Tocopherol, sodium alginate, sodium phosphate monohydrate and sodium phosphate dibasic dodecahydrate were purchased from Fluka Chemie GmbH, Buchs, Germany. β-Lactoglobulin (from bovine milk, approx. 90 % purified using polyacrylamide gel electrophoresis and lyophilized), pepsin 1:10,000 (from porcine stomach mucosa, crystallized and lyophilized), pancreatin (from porcine pancreas), 2,2'-bipyridyl and $ZnCl_2$ were purchased from Sigma, St. Louis, MO, USA. $FeCl_3$ and $CaCl_2$ were purchased from Riedel-de Haën, Seelze, Germany. α-Tocopherol stock solutions of the appropriate concentrations were diluted in ethanol (Lab Scan Asia Co., Ltd, Bangkok, Thailand).

1.2.2 Preparation of protein solutions

β-Lactoglobulin powder was dissolved in deionized water to obtain a stock solution of 6% (w/v). To cause BLG to unfold, the 6% (w/v) BLG solution (pH 7.5) was heated at 80 °C for 30 min and cooled to room temperature (27 °C) (Saeseaw, Shiowatana & Siripinyanond, 2006). Hen egg white protein powder was prepared using the procedure described by Croguennec et al. (2002). Hen egg white protein powder was dissolved in deionized water to obtain a stock solution of 8% (w/v). To cause HEW to unfold, the 8% (w/v) HEW solution (pH 8.0) was heated at 40 °C for 30 min and cooled to room temperature (27 °C). The proteins solutions, BLG and HEW, were filtered through 0.45 μm cellulose acetate syringe filter before use.

1.2.3 Preparation of protein based-encapsulated α-TOC

Salt induced gelation technique was used for preparation of protein based-encapsulated α-TOC. To prepare BLG-encapsulated α-TOC, appropriate concentration of α-TOC was mixed with appropriate concentration of BLG solution and subsequently $CaCl_2$ was added

to induce aggregation of BLG. The molar ratio of protein and α-TOC and salts was 2:1:1. A method to prepare HEW-encapsulated α-TOC was similar to that of the BLG-encapsulated α-TOC except that $ZnCl_2$ was added instead of $CaCl_2$ to induce aggregation. Parameters affecting encapsulation efficiency of protein-encapsulated α-TOC were examined as follows: 0.5-2% (w/v) BLG; 1-6% (w/v) HEW; 10-150 mM α-TOC; and 10-100 mM salt solutions. The incubation time was 5 h for BLG-encapsulated α-TOC and 30 min for HEW-encapsulated α-TOC.

1.2.4 Preparation of alginate coated-protein based-encapsulated α-TOC

To prepare alginate coated-BLG-encapsulated α-TOC, appropriate concentration of α-TOC was mixed with appropriate concentration of BLG solution and then appropriate concentration of sodium alginate was added to the mixture with subsequent addition of appropriate concentration of $CaCl_2$ to form gel. The molar ratio of protein and α-tocopherol and alginate and salts was 2:1:2:1. A method to prepare alginate coated-HEW-encapsulated α-TOC was similar to that of alginate coated-BLG-encapsulated α-TOC except that $ZnCl_2$ was added instead of $CaCl_2$ as a gelling and hardening agent. The incubation time was 5 h for alginate coated-BLG-encapsulated α-TOC and 30 min for alginate coated-HEW-encapsulated α-tocopherol.

1.2.5 Estimation of α-TOC loading

The protein based-encapsulated α-TOC was centrifuged at 12,000 rpm for 30 min (Beckman Allegra X-22R Centrifuge, Palo Alto, USA) to separate the unencapsulated α-TOC from the mixture. The concentration of unencapsulated α-TOC was determined by colorimetric method exploiting the ability of α-TOC to reduce Fe^{3+} into Fe^{2+} which could subsequently form red-orange color with 2,2-bipyridyl. The absorbance of the resulting solution was measured at 521 nm. Subsequently, the precipitate part containing protein aggregates was dispersed in 30 ml of simulated gastric fluid (SGF) (HCl solution, pH 1.2) with 0.1% pepsin (w/v) at 37 °C under vigorous agitation for 2 h (Chen et al., 2007). The resulting mixture was extracted by hexane solution and α-TOC concentration in the extract was determined by absorbance measurement at 297 nm with a UV–visible spectrophotometer (JASCO V530 UV-Visible Spectrophotometer, JASCO, Inc., Tokyo, Japan). The amount of α-TOC encapsulated was calculated by subtraction of the

unencapsulated α-TOC from the total amount of α-TOC added. The encapsulation efficiency (EE) was calculated from the ratio of the encapsulated α-TOC and the added α-TOC. All experiments were performed at least in five replicates ($n = 5$). Estimation of α-TOC loading and calculation of encapsulation efficiency of alginate coated-protein based-encapsulated α-TOC were performed in the same way as described for the protein based-encapsulated α-TOC. All experiments were performed at least in five replicates. Graphs were plotted with error bars showing the standard deviation of the results obtained.

1.2.6 Estimation of in vitro release of alginate coated-protein based-encapsulated α-TOC and evaluation of α-TOC release kinetics

The release of α-TOC from alginate coated-protein based-encapsulated α-TOC was determined by incubating the encapsulated particles in 30 ml of simulated gastric fluid (SGF) (HCl solution, pH 1.2) with 0.1% pepsin (w/v) at 37 °C under vigorous agitation by an incubator shaker (Grant Instrument, model SS40-D2, Cambridge, England) for 2 h and then the supernatant was separated from the swollen aggregates for further determination of α-TOC concentration. The release of α-TOC in SGF condition was determined by absorbance measurement at 297 nm after extraction of the released α-TOC from the supernatant part with hexane. Subsequently, the swollen aggregate was digested by 30 ml of simulated intestinal fluid (SIF) (phosphate buffer in saline solution, pH 7.4) with 1.0% pancreatin (w/v) at 37 °C under vigorous agitation for 4 h. The release of α-TOC in SIF condition was determined by absorbance measurement at 297 nm after extraction of the released α-TOC with hexane. The percentages of released amount of α-TOC in SGF and SIF conditions are presented as $\%R_{SGF}$ and $\%R_{SIF}$, respectively. These percentages were calculated from the ratio of the released amount from each digestion condition and the encapsulated amount in the aggregates, by which the resulting numbers were multiplied by 100.

To evaluate the release kinetics of α-TOC, the encapsulated particles were incubated in simulated gastric fluid for 2 h and subsequently in simulated intestinal fluid at various incubation times of 10, 20, 30, 60, 90, 120, 180, 240, 300, 360 min. Hexane was added to allow extraction of the released α-TOC into the hexane portion followed by absorbance measurement at 297 nm.

1.3 Results and discussion

1.3.1 Selection of divalent cation for the preparation of protein based-encapsulated α-TOC by cold gelation

Cold gelation of protein can be achieved by adding salts including monovalent or divalent cations, e.g., Na^{+}; Ca^{2+}; or Zn^{2+} to the solution containing charged protein molecules (Foegeding, Kuhn & Hardin, 1992; Saeseaw et al., 2006). To perform salt induced gelation of proteins, $CaCl_2$ and $ZnCl_2$ were used as they are listed as generally recognized as safe (GRAS) by the United States of America Food and Drug Administration when used in accordance with good manufacturing practice (FDA, 2008). Our earlier investigations indicated that salt induced gelation of BLG or HEW was best achieved by $CaCl_2$ or $ZnCl_2$, respectively (Saeseaw et al., 2006; Samontha, Nipattamanon, Shiowatana & Siripinyanond, 2008). One might argue that aggregate formation could already be obtained by mixing BLG with α-TOC. Without addition of $CaCl_2$, however, the added α-TOC was mostly found in the supernatant part suggesting that they were not encapsulated in BLG aggregates. Conversely, without addition of $ZnCl_2$ to the mixture of HEW and α-TOC, the added α-TOC was found in the aggregate part suggesting that α-TOC was encapsulated in HEW particles. Nonetheless, addition of $ZnCl_2$ to the mixture was carried out as salt was used not only to induce gel formation, but the added $CaCl_2$ or $ZnCl_2$ also acted as a hardening agent for the alginate coating of the encapsulated products.

1.3.2 Parameters affecting encapsulation efficiency of BLG-encapsulated α-TOC

The concentrations of BLG and α-TOC showed combined influence on encapsulation efficiency of BLG-encapsulated α-TOC as illustrated in Figure 1.1. At fixed concentration of BLG, the encapsulation efficiency decreased with increasing concentration of α-TOC for each BLG concentration (Figure 1.1a-c). Nonetheless, the mole amount of α-TOC in the aggregate increased with increasing concentration of α-TOC added and reached a plateau at a certain concentration of α-TOC because of the limited amount of BLG. Figure 1.1d shows the relationship between the added α-TOC concentration and the mole amount of α-TOC encapsulated at various BLG concentrations. In the excess of BLG at 2% (w/v), a straight line relationship was obtained. Deviation from the straight line was observed when BLG was not adequate for encapsulation of α-TOC. At the plateau, the mole ratio of

α-TOC and BLG was calculated to be 140 and 104 for BLG of 0.5% (w/v) and 1% (w/v), respectively, suggesting that the average mole ratio of the two compounds might be at approximately 120. In general, higher protein concentrations can hold higher amount of α-TOC at the fixed concentrations of α-TOC and $CaCl_2$. This statement was confirmed by determining the encapsulation efficiency and the mole amount of α-TOC in the aggregate at various concentrations of BLG at fixed concentrations of α-TOC and $CaCl_2$. The amount of α-TOC encapsulated increased with increasing in BLG concentration (Figure 1.1d). β-Lactoglobulin was reported to form continuous and homogeneous membranes around the α-TOC oil droplets through intermolecular β-sheets interaction because of its flexibility and amphiphilic nature (Alzagtat & Alli, 2002; Lefévre et al., 2003). At fixed concentrations of BLG and α-TOC, the change in encapsulation efficiency was not so significant with the change in $CaCl_2$ concentrations (from 10 to 100 mM), as illustrated in Figure1.2. Therefore, only small amount of Ca^{2+} was needed for neutralization of the negatively charged BLG and lowering electrostatic repulsion with the subsequent aggregates formation through intermolecular bridges (Line et al., 2005; Majhi, Vanam, Ganta, Seyrek, Giger & Dubin, 2006; Simons et al., 2002). Addition of $CaCl_2$ at concentrations higher than 100 nM was not tested, as too high concentration of salt weakened electrostatic interactions, which could suppress aggregate formation because of charge screening effects (Simons et al., 2002).

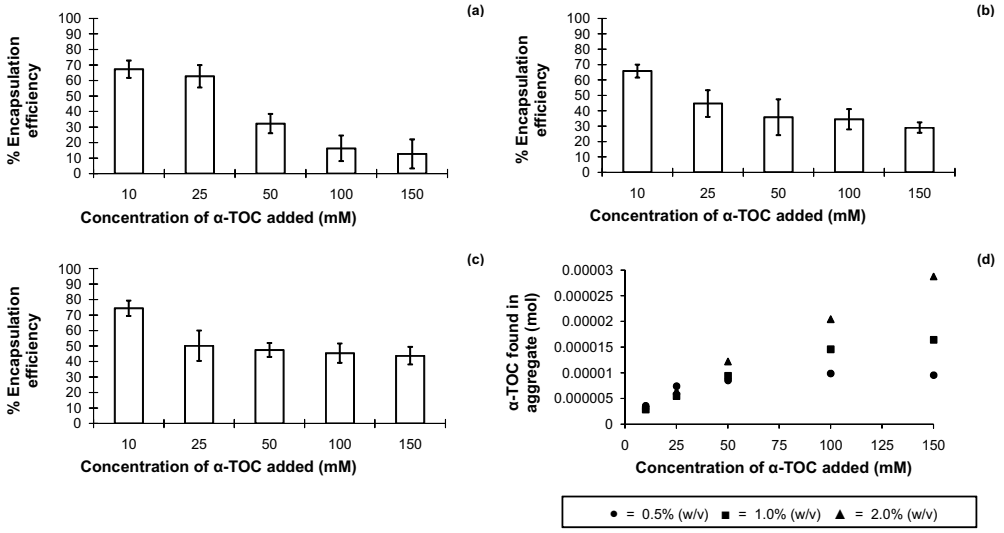

Figure 1.1 Effect of α-TOC concentration on its encapsulation efficiency in BLG particles at various concentrations of BLG; (a) 0.5% (w/v), (b) 1.0% (w/v), and (c) 2.0% (w/v), with 100 mM $CaCl_2$ as a gelling agent. (d) Relationship between concentration of α-TOC added and mole amount of α-TOC encapsulated.

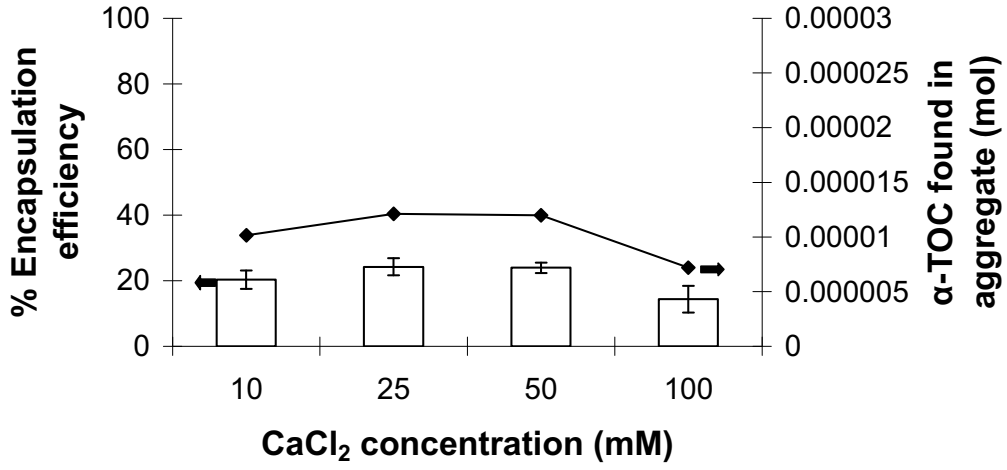

Figure 1.2 Effect of $CaCl_2$ concentration on encapsulation efficiency of α-TOC (100 mM) in 0.5% (w/v) BLG particles.

1.3.3 Parameters affecting encapsulation efficiency of HEW-encapsulated α-TOC

Similar to the case of BLG-encapsulated α-TOC, the concentrations of HEW and α-TOC showed combined influence on encapsulation efficiency of HEW-encapsulated α-TOC as illustrated in Figure 1.3. The encapsulation efficiency decreased with increasing

concentration of α-TOC for each HEW concentration (Figure 1.3a-c). At fixed concentration of HEW at 1% (w/v), the mole amount of α-TOC in the aggregate was almost constant with increasing in the concentration of α-TOC added. At higher HEW concentrations, however, mole of α-TOC in the aggregate increased with increasing concentration of α-TOC and reached a plateau at a certain concentration of α-TOC because of the limited amount of HEW. Higher protein concentrations can hold higher amount of α-TOC at the fixed concentrations of α-TOC and $ZnCl_2$. This observation was confirmed by fixing the concentrations of α-TOC and $ZnCl_2$ and determining the encapsulation efficiency and the mole amount of α-TOC in the aggregate at various concentrations of HEW (Figure 1.4). The amount of α-TOC encapsulated increased with increasing in HEW (Figure 1.4). The mole ratio of α-TOC and HEW was not calculated because the composition of HEW was rather complex consisting of various proteins. At fixed concentrations of HEW and α-TOC, the encapsulation efficiency was found to be highest at $ZnCl_2$ concentration of 25 mM (Figure 1.5). Therefore, a suitable encapsulation condition for HEW-encapsulated α-TOC was 4% (w/v) HEW with 50 mM α-TOC and 25 mM $ZnCl_2$.

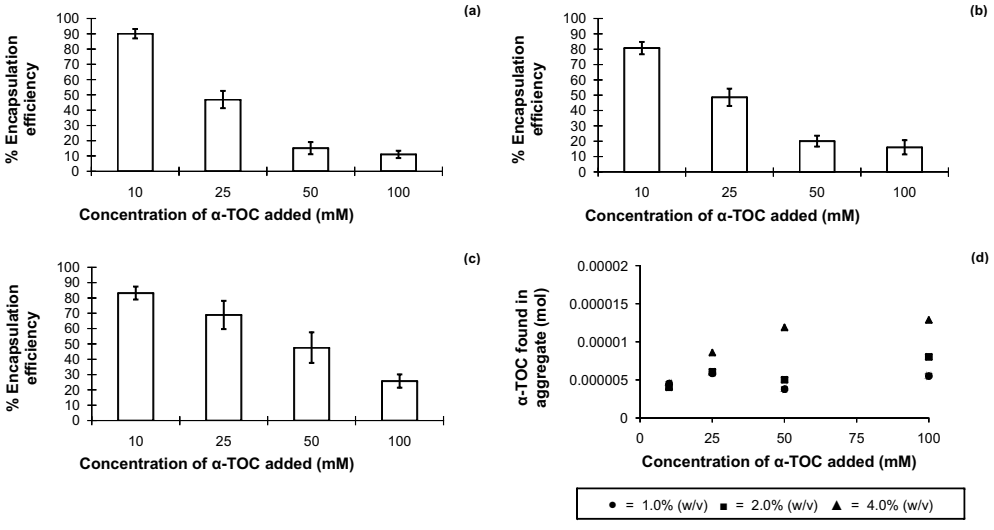

Figure 1.3 Effect of α-TOC concentration on its encapsulation efficiency in HEW particles at various concentrations of HEW; (a) 1.0% (w/v), (b) 2.0% (w/v), and (c) 4.0% (w/v), with 25 mM $ZnCl_2$ as a gelling agent. d) Relationship between concentration of α-TOC added and mole amount of α-TOC encapsulated.

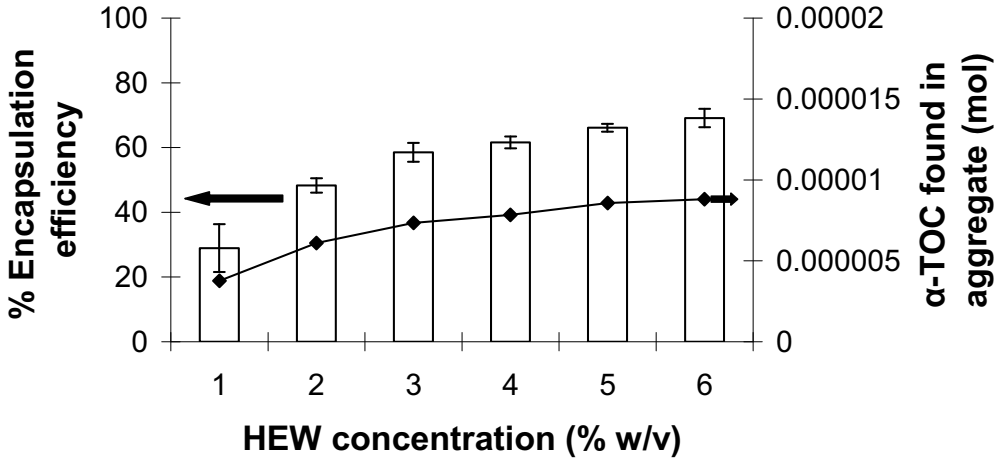

Figure 1.4 Effect of HEW concentration on encapsulation efficiency of α-TOC (50 mM) in HEW particles with 25 mM $ZnCl_2$ as a gelling agent.

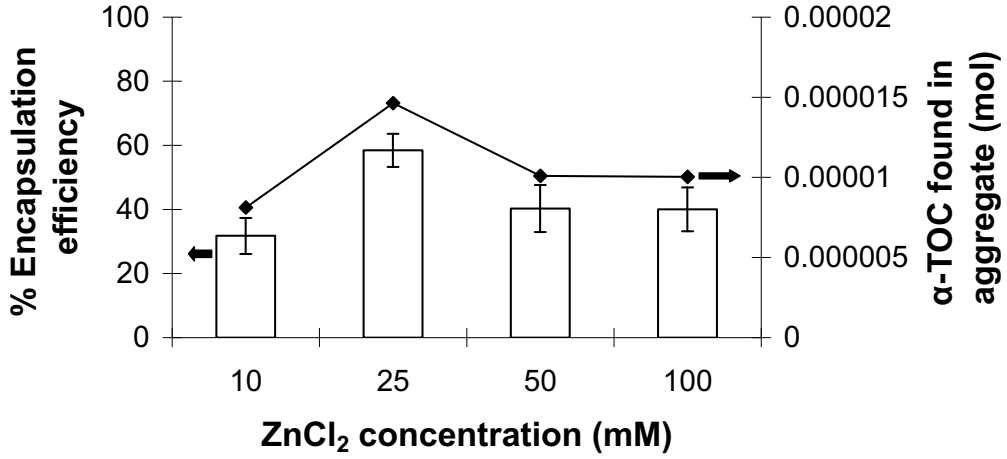

Figure 1.5 Effect of $ZnCl_2$ concentration on encapsulation efficiency of α-TOC (50 mM) in 4.0% (w/v) HEW particles.

1.3.4 Release of α-tocopherol from protein-based delivery particles: a comparison between BLG and HEW (with and without alginate coating)

To assess the suitability of BLG or HEW as a protein-based delivery particle for α-TOC, release of α-TOC from the protein particles were examined under simulated gastric and simulated intestinal digestion conditions. Table 1.1 shows that the α-TOC encapsulated was almost completely released (86.4 ± 9.9% for BLG-encapsulated α-TOC,

and 93.4 ± 10.1% for HEW-encapsulated α-TOC) in SGF condition. Considering that most nutrients and vitamins are best absorbed in intestine for further utilization in the body, α-TOC should be protected in the encapsulated particles and should not release in the SGF condition. Therefore, encapsulation of α-TOC by salt induced protein aggregates only is not adequate for such purposes. Consequently, sodium alginate was used as a coating material for these encapsulated particles as it was widely used as stabilizers, thickening or gelling agents in food products (Pongsawatmanit et al., 2006). Several reports showed that the alginate gel was very strong, rigid, and hard to swell in simulated gastric fluid (SGF) condition (Chen et al., 2006; Chen et al., 2007; Gunasekaran, Ko & Xiao, 2007). By coating with alginate, the release of α-TOC should occur in intestinal condition. Table 1.1 illustrates that the release of α-TOC in the SGF was retarded and the release was then observed in the SIF. For BLG- and HEW-encapsulated α-TOC, the released amount of α-TOC under SGF condition decreased whereas that under SIF condition increased with increasing in concentration of sodium alginate. Not only that the alginate could prolong the release of α-TOC till intestinal stage, but also it increased the encapsulation efficiency of α-TOC by BLG and HEW. The increase was prominent for HEW-encapsulated α-TOC, as the encapsulation efficiency increased from approx. 32% (without alginate coat) to approx. 85% (with alginate coat). For BLG-encapsulated α-TOC, the encapsulation efficiency was increased with the increase in concentration of alginate because the emulsion stability was improved through the formation of interfacial complex between alginate and the protein (Pongsawatmanit et al., 2006; Azzam & Omari, 2002).

Considering at the selected preparation conditions, the encapsulation efficiency obtained for HEW-encapsulated α-TOC was higher than that for BLG-encapsulated α-TOC (Table 1.1). Although encapsulation by HEW requires higher concentration than that by BLG, the cost of HEW is much less than that of BLG. With the use of alginate coating, both BLG and HEW aggregates can be employed as protein-based materials for encapsulation of α-TOC.

The release profiles of α-TOC from BLG- and HEW-encapsulated α-TOC coated with 0.25% alginate at various incubation times in simulated intestinal fluid could fit well with the diffusion-controlled release model as illustrated in Figure 1.6. This diffusion-controlled release model was considered from an empirical equation proposed by Peppas & Sahlin (1989), as described by the following equation.

$$\frac{M_t}{M_\infty} = kt^n$$

where M_t is the amount of α-TOC released up to any time t, M_∞ is the final amount of α-TOC released (the total amount of α-TOC released at 6 h in this study), k is a constant incorporating structural and geometrical characteristics, and n is a release exponent value. The α-TOC release from the two systems was therefore shown to mainly follow the diffusion-controlled model. However, other mechanisms might also involve. As the coefficients of determination (R^2) of the diffusion-controlled release profiles from the BLG- and HEW-encapsulated α-TOC coated with 0.25% alginate were 0.973 and 0.940, respectively, the release of α-TOC from BLG coated with 0.25% alginate fit with the diffusion-controlled model better than that from the HEW. Therefore, further investigation was performed for the release of α-TOC from HEW coated with 0.25% alginate. The final amount of α-TOC released from the HEW coated with 0.25% alginate was investigated at 24 h. The release profile was found to be biphasic showing a constant release with an almost instantaneous burst release. The total mole amount of α-TOC released increased from 0.000991 at 6 h to 0.005135 at 24 h. Therefore, gel erosion might also be taken place (Lin & Metters, 2006).

Table 1.1

Encapsulation efficiency and release of α-tocopherol

Samples	EE (% ± SD)	R_{SGF}*(% ± SD)	R_{SIF}**(% ± SD)
0.5% (w/v) BLG + 100 mM α-TOC + 25 mM $CaCl_2$			
Without alginate coat	18.8±6.3	86.4±9.9	
Coated with 0.125% (w/v) alginate	20.7±6.1	4.2±0.2	26.8±1.0
Coated with 0.25% (w/v) alginate	51.4±3.3	1.4±0.5	54.8±0.6
4% (w/v) HEW + 50 mM α-TOC + 25 mM $ZnCl_2$			
Without alginate coat	31.9±8.3	93.4±10.1	
Coated with 0.125% (w/v) alginate	82.1±4.3	17.5±9.5	21.8±9.9
Coated with 0.25% (w/v) alginate	85.2±2.1	7.3±2.5	38.0±3.9

* The percentages of released amount of α-TOC in simulated gastric fluid at 2 h.

** The percentages of released amount of α-TOC in simulated intestinal fluid at 4 h.

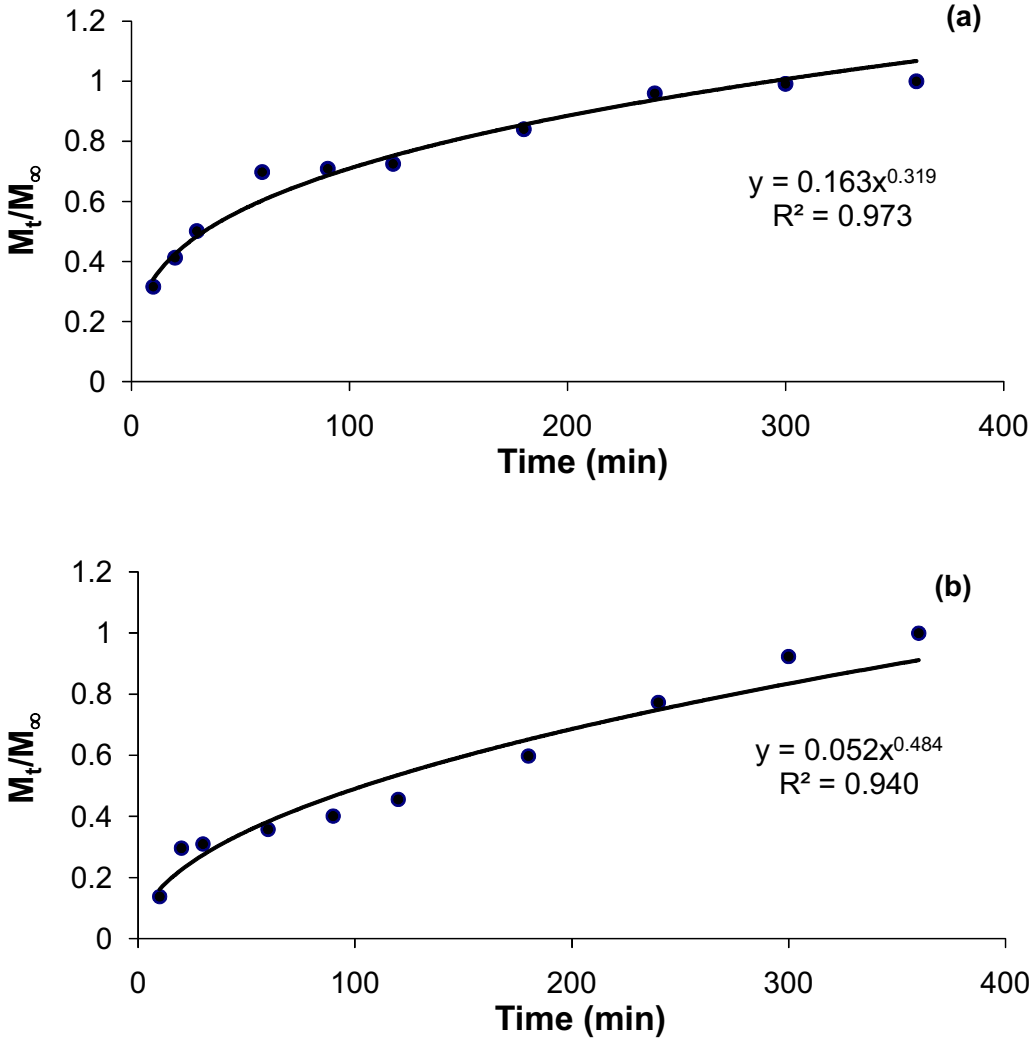

Figure 1.6 Release profile of α-TOC from (a) BLG-encapsulated α-TOC and (b) HEW-encapsulated α-TOC.

1.4 Summary

β-Lactoglobulin (BLG) and hen egg white protein (HEW) could be used as protein-based materials for encapsulation of α-tocopherol (α-TOC) after salt-induced gelation of the proteins. Concentrations of protein and α-TOC influenced on the encapsulation efficiency. To protect α-TOC from release in the gastric condition, alginate was used for coating of these encapsulated particles. With the alginate coat, the release of α-TOC was retarded till intestinal stage and the encapsulation efficiencies of α-TOC by BLG and HEW were enhanced.

1.5 References

1. Alting, A. C., Hamer, R. J., Kruif, C. G. & Visschers, R. W. (2003). Cold-set globular protein gels: interactions, structure and rheology as a function of protein concentration. *Journal of Agricultural and Food Chemistry*, *51*, 3150–3156.
2. Alzagtat, A. A. & Alli, I. (2002). Protein–lipid interactions in food systems: a review. *International Journal of Food Sciences and Nutrition*, *53*, 249-260.
3. Azzam, M. O. J. & Omari, R. M. (2002). Stability of egg white-stabilized edible oil emulsions using conductivity technique. *Food Hydrocolloids, 16*, 105-110.
4. Beaulieu, L., Savoie, L., Paquin, P. & Subirade, M. (2002). Elaboration and characterization of whey protein beads by an emulsification/cold gelation process: application for the protection of retinol. *Biomacromolecules*, *3*, 239-248.
5. Blatt, D. H., Pryor, W. A., Mata, J. E. & Proteau, R. R. (2004). Re-evaluation of the relative potency of synthetic and natural α-tocopherol: experimental and clinical observations. *The Journal of nutritional biochemistry, 15*, 380-395.
6. Borel, P. (2003). Factors affecting intestinal absorption of highly lipophilic food microconstituents (fat-soluble vitamins, carotenoids and phytosterols). *Clinical Chemistry and Laboratory Medicine*, *41*, 979-994.
7. Borel, P., Pasquier, B., Armand, M., Tyssandier, V., Grolier, P., Andre, M., Senft, M., Peyrot, J., Juassan, V., Lairon, D. & Azais-Braesco, V. (2001). Processing of vitamin A and E in the human gastrointestinal tract. *American Journal of Physiology - Gastrointestinal and Liver Physiology*, *280*, 95-103.
8. Brigelius-Flohé, R. & Traber, M. G. (1999). Vitamin E: function and metabolism. *FASEB Journal*, *13*, 1145-1155.
9. Bryant, C. M. & McClements, D. J. (1998). Molecular basis of protein functionality with special consideration of cold-set gels derived from heat-denatured whey. *Trends in Food Science & Technology, 9*, 143-151.
10. Bryant, C. M. & McClements, D. J. (2000). Influence of NaCl and $CaCl_2$ on cold-set gelation of heat-denatured whey protein. *Journal of Food Science*, *65*, 801-804.
11. Cheeseman, K. H., Holley, A. E., Kelly, F. J., Wasil, M., Hughes, L. & Burton, G. (1995). Biokinetics in humans of RRR-α-tocopherol: the free phenol, acetate ester, and succinate ester forms of vitamin E. *Free Radical Biology and Medicine*, *19*, 591-598.
12. Chen, L. & Subirade, M. (2006). Alginate-whey protein granular microspheres as oral delivery vehicles for bioactive compounds. *Biomaterials*, *27*, 4646-4654.

13. Chen, L. & Subirade, M. (2007). Effect of preparation conditions on the nutrient release properties of alginate–whey protein granular microspheres. *European Journal of Pharmaceutics and Biopharmaceutics*, *65*, 354-362.

14. Chen, L., Remondetto, G. E. & Subirade, M. (2006). Food protein-based materials as nutraceutical delivery systems. *Trends in Food Science & Technology, 17*, 272-283.

15. Croguennec, T., Nua, E. & Brulé, G. (2002). Influence of pH and salts on egg white gelation. *Journal of Food Science*, *67*, 608-614.

16. Dumay, E., Laligant, A., Zasypkin, D. & Cheftel, J. C. (1999). Pressure- and heat-induced gelation of mixed β-lactoglobulin/polysaccharide solutions: scanning electron microscopy of gels. *Food Hydrocolloids*, *13*, 339-351.

17. FDA (2008). EAFUS: A food additive database, (http://vm.cfsan.fda.gov/~dms/eafus.html), December 4, 2008.

18. Foegeding, E. A., Kuhn, P. R. & Hardin, C. C. (1992). Specific divalent cation-induced changes during gelation of β-lactoglobulin. *Journal of Agricultural Food Chemistry*, *40*, 2092-2097.

19. Gunasekaran, S., Ko, S. & Xiao, L. (2007). Use of whey proteins for encapsulation and controlled delivery applications. *Journal of Food Engineering*, *83*, 31-40.

20. Lefévre, T. & Subirade, M. (2003). Formation of intermolecular β-sheet structures: a phenomenon relevant to protein film structure at oil–water interfaces of emulsions. *Journal of Colloid and Interface Science*, *263*, 59-67.

21. Lin, C-C. & Metters, A. T. (2006). Hydrogels in controlled release formulations: Network design and mathematical modeling. *Advanced Drug Delivery Reviews, 58*, 1379-1408.

22. Line, V. L. S., Remondetto, G. E. & Subirade, M. (2005). Cold gelation of β-lactoglobulin oil-in-water emulsions. *Food Hydrocolloids*, *19*, 269-278.

23. Majhi, P. R., Vanam, R. P., Ganta, R. R., Seyrek, E., Giger, K. & Dubin, P. L. (2006). Electrostatically driven protein aggregation: β-lactoglobulin at low ionic strength. *Langmuir*, *22*, 9150-9159.

24. Maltais, A., Remondetto, G. E. & Subirade, M. (2008). Mechanisms involved in the formation and structure of soya protein cold-set gels: a molecular and supramolecular investigation. *Food Hydrocolloids*, *22*, 550-559.

25. Mardones, P. & Rigotti, A. (2004). Cellular mechanisms of vitamin E uptake: relevance in α-tocopherol metabolism and potential implications for disease. *The Journal of Nutritional Biochemistry, 15*, 252-260.

26. Mine, Y. (1995). Recent advances in the understanding of egg white protein functionality. *Trends in Food Science & Technology, 6*, 225-232.

27. Peppas, N.A. & Sahlin, J. J. (1989). A simple equation for the description of solute release. 3. Coupling of diffusion and relaxation. *International Journal of Pharmaceutics, 57*, 169-172.

28. Pérez, M. D. & Calvo, M. (1995). Interaction of β-lactoglobulin with retinol and fatty acids and its role as a possible biological function for this protein: a review. *Journal of Dairy Science*, *78*, 978-988.

29. Pongsawatmanit, R., Harnsilawat, T. & McClements, D. J. (2006). Influence of alginate, pH and ultrasound treatment on palm oil-in-water emulsions stabilized by β-lactoglobulin. *Colloids and Surfaces A: Physicochemical and Engineering Aspects*, *287*, 59-67.

30. Pryor, W. A. (2000). Vitamin E and heart disease: basic science to clinical intervention trials. *Free Radical Biology and Medicine*, *28*, 141-164.

31. Saeseaw, S., Shiowatana, J. & Siripinyanond, A. (2006). Observation of salt-induced β-lactoglobulin aggregation using sedimentation field-flow fractionation. *Analytical and Bioanalytical Chemistry*, *386*, 1681–1688.

32. Samontha, S., Nipattamanon, C., Shiowatana, J. & Siripinyanond, A. (2008). Toward Better Understanding of Salt-Induced Hen Egg White Protein Aggregation Using Field-Flow Fractionation. *Journal of Agricultural Food Chemistry*, *56*, 8809-8814.

33. Simons, J. W. F. A., Kosters, H. A., Visschers, R. W. & Jongh, H. H. J. (2002). Role of calcium as trigger in thermal β-lactoglobulin aggregation. *Archives of Biochemistry and Biophysics, 406*, 143-152.

34. Sriamornsak, P. & Kennedy, R. A. (2007). Effect of drug solubility on release behavior of calcium polysaccharide gel-coated pellets. *European Journal of Pharmaceutical Sciences*, *32*, 231-239.

35. Swaisgood, H. E., Wang, Q. & Allen, J. C. (2001). Protein ingredient for carrying lipophilic nutrients. *US Patent No, 6,290,974 B1.*

36. Totosaus, A., Montejano, J. G., Salazar, J. A. & Guerrero, I. (2002). A review of physical and chemical protein-gel induction. *International Journal of Food Science and Technology*, *37*, 589-601.

37. Tucker, J. M. & Townsend, D. M. (2005). Alpha-tocopherol: roles in prevention and therapy of human disease. *Biomedicine and Pharmacotherapy, 59*, 380–387.

38. Ubbink, J. & Krüger, J. (2006). Physical approaches for the delivery of active ingredients in foods. *Trends in Food Science & Technology*, *17*, 244-254.

39. Voth, O. L. & Miller, R. C. (1958). Interaction of tocopherol with proteins and amino acids. *Archives of Biochemistry and Biophys*ics, *77*, 191-205.

40. Wang, Q., Allen, J. C. & Swaisgood, H. E. (1997). Binding of vitamin D and cholesterol to β-lactoglobulin. *Journal of Dairy Science*, *80*, 1054-1059.

41. Wu, S.Y., Pérez, M. D., Puyol, P. & Sawyer, L. (1999). β-Lactoglobulin binds palmitate within its central cavity. *The Journal of Biological Chemistry*, *274*, 170-174.

Chapter 2

Flow Field-Flow Fractionation: A Versatile Approach for Size Characterization of α-Tocopherol Induced Gold Nanoparticles Enlargement

2.1 Introduction

Gold nanoparticles have gained considerable interest in different research fields, owing to their attractive properties such as high stability, biocompatibility, and optical properties [1]. Gold nanoparticles can be prepared by various ways [2], and the mildest way is relied on the reduction of gold salts in the presence of suitable stabilizing agents that prevent particle aggregation [2]. Many researchers have demonstrated the use of gold nanoparticles for optical labeling and sensing purposes [3,4]. Scampicchio et al. have used gold nanoparticles for estimating the antioxidant activity of phenolic acids in different beverage samples [5]. This assay was based on the capability of phenolic acid as reducing agent to catalyze the growth of gold nanoparticles in the reduction of $AuCl_4^-$ by sodium citrate. Considering the antioxidant activity, vitamin E, a group of tocopherols and tocotrienols, of which α-tocopherol has the highest biological activity, shows to be the most potent natural lipophilic antioxidant [6]. Therefore, we hypothesize that α-tocopherol should also exhibit catalytic activity on the growth of gold nanoparticles, and various α-tocopherol concentrations should result in different sizes of gold nanoparticles. A closer inspection on the influence of α-tocopherol on the size of gold nanoparticles should then be carried out because of the strong correlation between the size and their optical, electrical, and catalytic properties [7].

Size characterization of nanoparticles has been performed by conventional techniques such as scanning electron microscopy (SEM), transmission electron microscopy (TEM), and dynamic light scattering (DLS). A flow-assisted technique, field-flow fractionation (FFF), for size characterization of nanoparticles has also been reported [8, 9]. This technique allows fractionation of particles in the nanometer to sub-micrometer scale and the fractionated particles can be further characterized by various detection methods [10,11]. The principle [12-14] and applications [15,16] of FFF have been described elsewhere. Rameshwar et al. illustrated the use of field-flow fractionation (FFF) for size characterization of water-soluble nanoparticles and quantum dots [17]. In their study, the particle size results of core particles obtained from FFF measurements were in good agreement with those obtained from other conventional techniques. Nonetheless, for the particles which showed extensive aggregation, FFF was shown to be more convenient and easier method for the determination of the average particle size of the gold nanoparticles. Recently, Contado and Argazzi reported the use of sedimentation FFF to investigate the role of citrate concentrations on the gold nanoparticles size distribution [18]. In their study, the size of gold nanoparticles as small as 12 nm could be observed.

The aims of this investigation were to examine the capability of FFF as a size characterization of gold nanoparticles and to examine the capability of α-tocopherol to induce the enlargement of gold

nanoparticles. Flow field-flow fractionation (FlFFF) was exploited to observe the effects of α-tocopherol concentrations and the incubation time on the gold nanoparticles enlargement.

2.2 Experimental

2.2.1 Instrumentation

A symmetrical flow field-flow fractionation (FlFFF) system (Model PN-1021-FO, Postnova Analytics, Landsberg, Germany) equipped with a 1000 Da molecular weight cut-off regenerated cellulose acetate membrane (Postnova Analytics) was used for size characterization of gold nanoparticles. The FlFFF channel was rectangular shape with the following dimensions: 27 cm long, 2.0 cm wide, and 0.0254 cm thick. A high-pressure liquid chromatography (HPLC) pump (Model PN 2101, Postnova Analytics) was employed to deliver the channel and the forward flows. Another HPLC pump of the same model was employed to regulate the cross and the focusing (backward) flows. A UV detector (Model S3210 UV/Vis Detector, Postnova Analytics) was set at 254 nm to monitor light attenuation of gold nanoparticles samples. Conventional sample introduction method with a sample volume of 20 μL was applied for size characterization of commercial gold nanoparticles and those prepared by the modified Turkevich method.

To examine the particle size and the enlargement of gold nanoparticles induced by α-tocopherol, opposing flow large volume sample introduction (500 μL) for an on-channel FlFFF preconcentration and separation was performed. The system set up was similar to what reported by Hassellöv et al. [19] and Amarasiriwardena et al. [20]. This approach consists of two steps: (a) sample loading and focusing and (b) fractionation. In sample loading and focusing step, the sample was introduced into FlFFF channel and two opposing flow streams were applied to focus the sample zone into a narrow band near the inlet of FlFFF channel. After suitable focusing time, the sample was then fractionated by applying cross and channel flows. The optimum operating FlFFF conditions are listed in Table 2.1. For comparison purpose, a transmission electron microscope (TEM, JEM-2100, 200 KV, JEOL) was employed to observe the particle size of gold nanoparticles. The TEM operating condition is also listed in Table 2.1. A UV-Visible spectrometer (JASCO V530 UV-Visible Spectrometer, JASCO, Inc., Tokyo, Japan) was used for recording absorbance spectra of gold nanoparticles.

Table 2.1 FlFFF and TEM operating conditions

FlFFF with conventional sample introduction method	
Carrier liquid	0.02% (v/v) FL-70
Channel flow rate/ mL min^{-1}	1.5
Cross flow rate/ mL min^{-1}	1.0
Equilibration time/ min	1.0
FlFFF with opposing flow large volume sample introduction method	
Carrier liquid	0.02% (v/v) FL-70
Forward flow rate/ mL min^{-1}	0.24
Backward flow rate/ mL min^{-1}	3.0
Channel flow rate/ mL min^{-1}	1.5
Cross flow rate/ mL min^{-1}	1.0
Focusing time/ min	7.0
TEM	
Beam current/ μA	82.5
Temperature/ °C	25
Humidity/ %	25
Acceleration voltage/ kV	160

2.2.2 Chemicals

All chemicals used in this work were of analytical reagent grade. De-ionized water (18.2 MΩ cm^{-1}) obtained from a water purification system (Barnstead International, Dubuque, IA, USA) was used to prepare all chemical reagents. A commercial gold nanoparticle of 10 nm was purchased from Sigma, St. Louis, MO, USA. A 50 mM $AuCl_4^-$ solution was prepared by dissolving hydrogen tetrachloroaurate, $HAuCl_4.3H_2O$ (Sigma, St. Louis, MO, USA), in deionized water. A 1 mM sodium citrate (Riedel-deHaën®, Germany) was prepared in phosphate buffer, pH 8.0; 1×10^{-2} M. A 1 mM α-tocopherol was prepared by dissolving (±)-α-tocopherol (Fluka Chemie GmbH., Switzerland) in 95% ethanol (Merck, Darmstadt, Germany) and used as a stock solution for further dilution.

FL-70, a mixture of anionic and non-ionic compounds containing the following active components: oleic acid; sodium carbonate; tergitol; tetrasodium EDTA; polyethylene glycol; and triethanolamine [21], was purchased from Fisher Scientific Co., Ltd.

(Pittsburgh, PA). A 0.1% (v/v) of FL-70 was prepared by diluting concentrated FL-70 with de-ionized water and used as a carrier liquid.

2.2.3 Preparation of gold nanoparticles

To prepare gold nanoparticles, the modified Turkevich method [22] was used. A 20-mL of 0.01% (w/w) hydrogen tetrachloroaurate was heated for 15 min at 65 ^{o}C in a waterbath. A 1% sodium citrate was also heated for 5 min. Consequently, a 1.5-mL of the pre-heated sodium citrate was pipetted into the 20-mL solution of the pre-heated hydrogen tetrachloroaurate. The mixture was then stirred and heated till reflux for 30 min, while the solution turned from pale yellow to pale blue and changed into brilliant red upon completion. The obtained gold nanoparticles solution was sonicated for 15 min, cooled to room temperature and stored at 4 ^{o}C.

2.2.4 α-Tocopherol-induced gold nanoparticle enlargement

To observe the enlargement of gold nanoparticles induced by α-tocopherol, $AuCl_4^-$ (1×10^{-3} M) was mixed with FL-70 (0.01%) and sodium citrate (2×10^{-4} M) in phosphate buffer (pH 8.0; 1×10^{-2} M) with various concentrations of α-tocopherol (2.5×10^{-6}, 7.5×10^{-6}, and 10.0×10^{-6} M). All samples were heated for 10 min at 45 ºC. The effects of α-tocopherol and incubation time on enlargement of gold nanoparticles were examined. The obtained gold nanoparticles were introduced into a FlFFF using large volume sample introduction (500 μL) for size characterization.

2.2.5 Data transformation and information obtained from FlFFF experiment

Raw fractograms were translated into mass size distribution profiles [23] using Microsoft Excel (Microsoft® Excel 2007) spreadsheet software. Peak evaluation, baseline adjustment, and cumulative area distribution plotting were performed by using PeakFit (SPSS, Chicago, IL, USA). From a FlFFF experiment, a raw fractogram of separated particle, a plot between detector response (y-axis) versus retention time (x-axis), was obtained as shown in Figure 2.1a. The raw fractogram was translated into particle size distribution [23] as shown in Figure 2.1b. With this plot, the particle size at peak maximum (d_p) was measured. To measure a breadth of size distribution, particle size range at half maximum height ($\Delta d_{0.5}$) from distribution profile was calculated [23, 24]. Further,

the particle size distribution was converted into a cumulative area plot as shown in Figure 2.1c. With this plot, particle size in term of a mean diameter (d_{mean}) was measured by considering the particle size which gives 50% cumulative area.

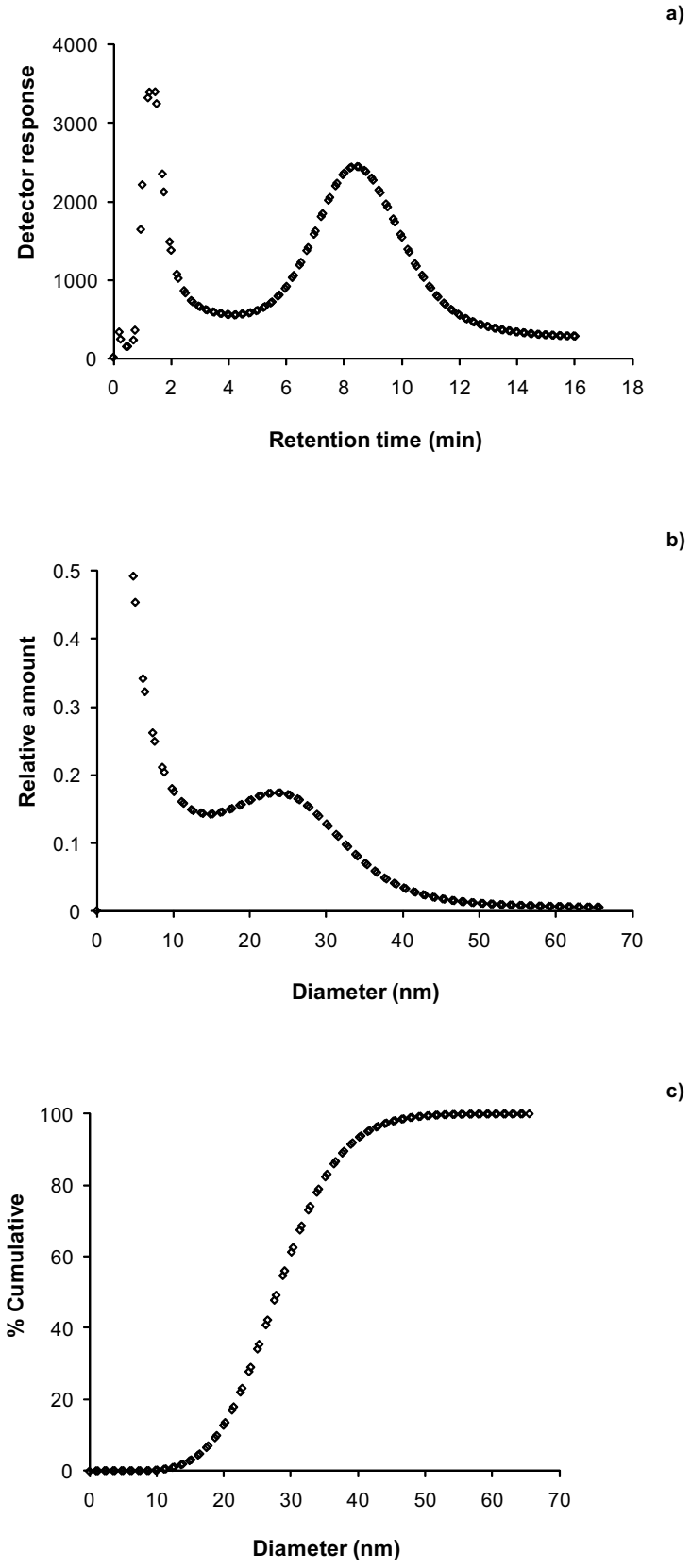

Figure 2.1 a) Raw fractogram of gold nanoparticles; b) the corresponding particle size distribution; c) the corresponding cumulative area distribution.

2.3 Results and Discussion

2.3.1 FlFFF size characterization of gold nanoparticles

To develop FlFFF method for size characterization of gold nanoparticles, an appropriate carrier liquid must be chosen. The carrier liquid must be compatible with the membrane and able to disperse particles without causing any interaction with the particles or changing the particle size characteristics. As gold nanoparticles are negatively charged [25], anionic surfactants should be used to disperse the gold nanoparticles. The nonpolar part of an anionic surfactant adsorbs to the hydrophobic solid, and the polar group is oriented towards the aqueous phase [26]. The resulting net negative charge on the particle surface prevents particles from agglomeration. In this work, FL-70 was selected as a carrier liquid. Therefore, the effect of carrier liquid concentrations (0.004, 0.02, and 0.1% (v/v) FL-70) for size characterization of gold nanoparticles was examined and summarized in Table 2.2. These concentrations were much lower than the critical micelle concentration of FL-70, which was reported to be 5.1% (v/v) [27]. At the concentration ranges much lower than the critical micelle concentration, increasing in the FL-70 concentrations resulted in increasing in the surfactant concentration on the gold nanoparticles surface and could affect on the retention time. Transmission electron microscopy was applied to investigate the particle sizes of the commercial gold nanoparticles and the gold nanoparticles prepared by the modified Turkevich method [22], as displayed in Figure 2.2. With 0.004% (v/v) FL-70 carrier liquid, gold nanoparticles were not eluted from the FlFFF channel. This might be due to the fact that too low concentration of carrier liquid is not effective for prevention of nanoparticles adsorption on the membrane surface. With higher concentrations of carrier liquid, i.e., 0.02% and 0.1% (v/v) FL-70, the particle size information obtained from TEM and FlFFF was not significantly different (Table 2.2). Therefore, FlFFF was proven to provide reliable particle size information for gold nanoparticles and 0.02% (v/v) FL-70 was selected as a suitable carrier liquid for FlFFF size characterization of gold nanoparticles.

Table 2.2 Mean particle size (d_{mean}) of gold nanoparticles measured by FlFFF at various FL-70 carrier liquid concentrations and by TEM

Measurement method	d_{mean} ± s.d. (n = 3)	
	Commercial gold nanoparticle (10 nm)	**Gold nanoparticles prepared in the laboratory**
FlFFF with 0.004% FL-70	n.d.*	n.d.*
FlFFF with 0.02% FL-70	7.9 ± 0.3	28.6 ± 0.2
FlFFF with 0.10% FL-70	6.9 ± 0.2	20.6 ± 0.4
TEM	8.3 ± 1.4	23.9 ± 2.0

* not determined – with 0.004% FL-70, gold nanoparticles were not eluted.

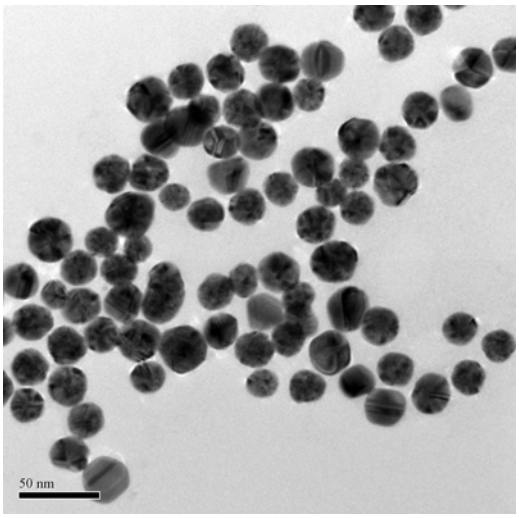

Figure 2.2 TEM photograph of gold nanoparticles prepared by the modified Turkevich method.

2.3.2 Use of an on FlFFF channel preconcentration for size characterization of very diluted gold nanoparticles

For a very diluted sample, the signal of fractionated gold nanoparticles is quite low as shown in Figure 2.3(◇). In order to improve the signal of gold nanoparticles, sample preconcentration is necessary. According to Hassellöv et al. [19] and Amarasiriwardena et al. [20], FlFFF allows an on-channel preconcentration of particulate samples exploiting the fact that FlFFF is similar to a membrane filtration unit. In principle, the sample is introduced to the FlFFF channel, focused and concentrated by using an opposed-flow

sample concentration [28]. Large volume of samples are introduced into the FlFFF channel and focused at a certain point. The particles, whose sizes are larger than the membrane pore size, can be retained in the channel. To improve the detection of gold nanoparticles, an aliquot of 500 μL sample was introduced into the FlFFF channel instead of the regular injection volume (20 μL) used in the conventional FlFFF separation. The sample was loaded through the back end of the channel with a flow ratio of 1:12.5 between the forward (0.24 mL min^{-1}) and backward (3 mL min^{-1}) focusing flows. Once the whole sample volume was loaded and focused in the FlFFF channel, the forward and backward flow pumps were disengaged while the cross flow stream was introduced, so that the sample could reach steady state equilibrium. Figure 2.3(□) displays the signal of gold nanoparticles obtained from the on-channel preconcentration system. The signal was extremely improved, when compared with the signal obtained from the conventional sample introduction (20 μL). Therefore, on-channel preconcentration FlFFF sample introduction was then applied to investigate size and enlargement of gold nanoparticles induced by α-tocopherol.

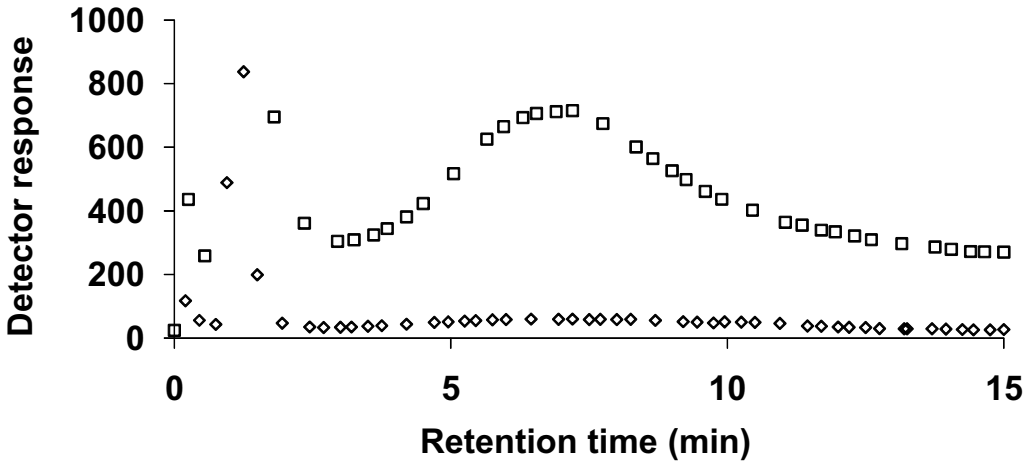

Figure 2.3 Fractograms of gold nanoparticles prepared by α-tocopherol catalyzing citric acid reduction of $AuCl_4^-$ obtained by conventional sample introduction (◇, 20 μL) and large volume sample introduction (□, 500 μL) FlFFF separation.

2.3.3 Parameters affecting the enlargement of gold nanoparticles induced by α-tocopherol

According to Scampicchio et al. [5], antioxidant activity could be estimated through the absorbance monitoring (at 555 nm) of the gold nanoparticles formation catalyzed by phenolic compounds in the presence of citric acid reducing agent. The increase in absorbance signals at 555 nm was linearly dependent upon the concentration of phenolic compounds. Nonetheless, the change in particle size of gold nanoparticles was not systematically examined. As α-tocopherol is the effective natural liphophilic antioxidant, it was our interest to investigate the potential of α-tocopherol to induce the formation and enlargement of gold nanoparticles. The role of α-tocopherol on the formation of gold nanoparticles was observed from the absorption spectra as illustrated in Figure 2.4. In the presence of sodium citrate, addition of α-tocopherol led to the enhanced absorbance signal at the characteristic absorption band at 555 nm. Without α-tocopherol, only small absorption signal was observed as a result of gold nanoparticles obtained purely from sodium citrate reduction (Figure 2.4a). In the absence of sodium citrate, α-tocopherol alone could not instantaneously induce gold nanoparticles formation (Figure 2.4b). Upon overnight incubation, however, gold nanoparticles formation was observed as evidenced by the occurrence of absorption band at 555 nm (Figure 2.4b). This observation suggested that the gold nanoparticles produced by sodium citrate reduction acted as a seed for the reduction of $AuCl_4^-$ by α-tocopherol and resulting in the enlargement of the particles, similar to what observed by Zayats et al. [29] for the catalytic growth of gold nanoparticles with addition of H_2O_2 as a reducing agent.

Further, the effects of α-tocopherol concentration and incubation time on the enlargement of gold nanoparticles were investigated using an on-channel FlFFF preconcentration for size characterization. At fixed incubation time of 0 hr (immediately analyzed), three different concentrations of α-tocopherol (2.5×10^{-6}, 7.5×10^{-6}, and 10.0×10^{-6} M) were examined for their effects on the enlargement of gold nanoparticles. At fixed incubation time of 0 hr, particle size distributions of gold nanoparticles at various α-tocopherol concentrations are illustrated in Figure 2.5. With increased α-tocopherol concentration, gold nanoparticles were enlarged as the d_{mean} value increased from 17 to 33 nm when the α-tocopherol concentrations increased from 2.5×10^{-6} to 10×10^{-6} M (Table 2.3). At fixed α-tocopherol of 7.5×10^{-6} M, various incubation times including 0, 2, and 4 hr were examined for their effects on the enlargement of gold nanoparticles as illustrated in Figure 2.6 and summarized in Table 2.3. With different incubation times, gold

nanoparticles were shown to exhibit monomodal distribution. The d_{mean} value increased from 19 (at 0 hr) to 23 nm (at 4 hr, demonstrating that incubation time showed an influence on the enlargement of gold nanoparticles. It is interesting to note that under each condition investigated, the values of d_{mean} and d_p were almost equal suggesting that the particle size distribution profiles of gold nanoparticles were ideally monomodal and of Gaussian characteristic. Moreover, the breadths of size distributions obtained from all experimental conditions were nearly the same, suggesting that the enlargement of gold nanoparticles induced by α-tocopherol would not affect on the polydispersity of the resulting particles.

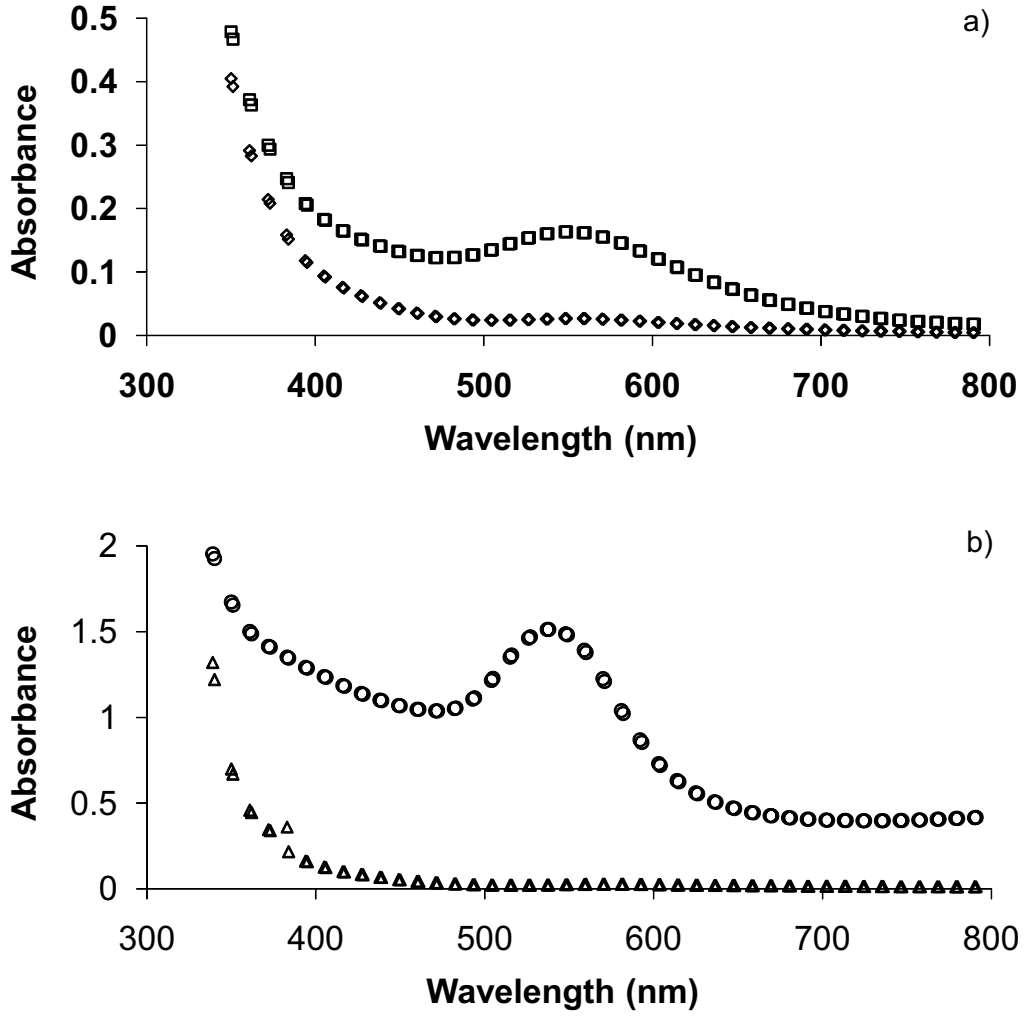

Figure 2.4 Absorption spectra of gold nanoparticles: a) prepared by sodium citrate reduction of $AuCl_4^-$ in the absence (◇) and presence (□) of α-tocopherol ($1x10^{-5}$ M); b) prepared in the presence of ($1x10^{-5}$ M) α-tocopherol without addition of sodium citrate, observed immediately (△) and after overnight incubation (○).

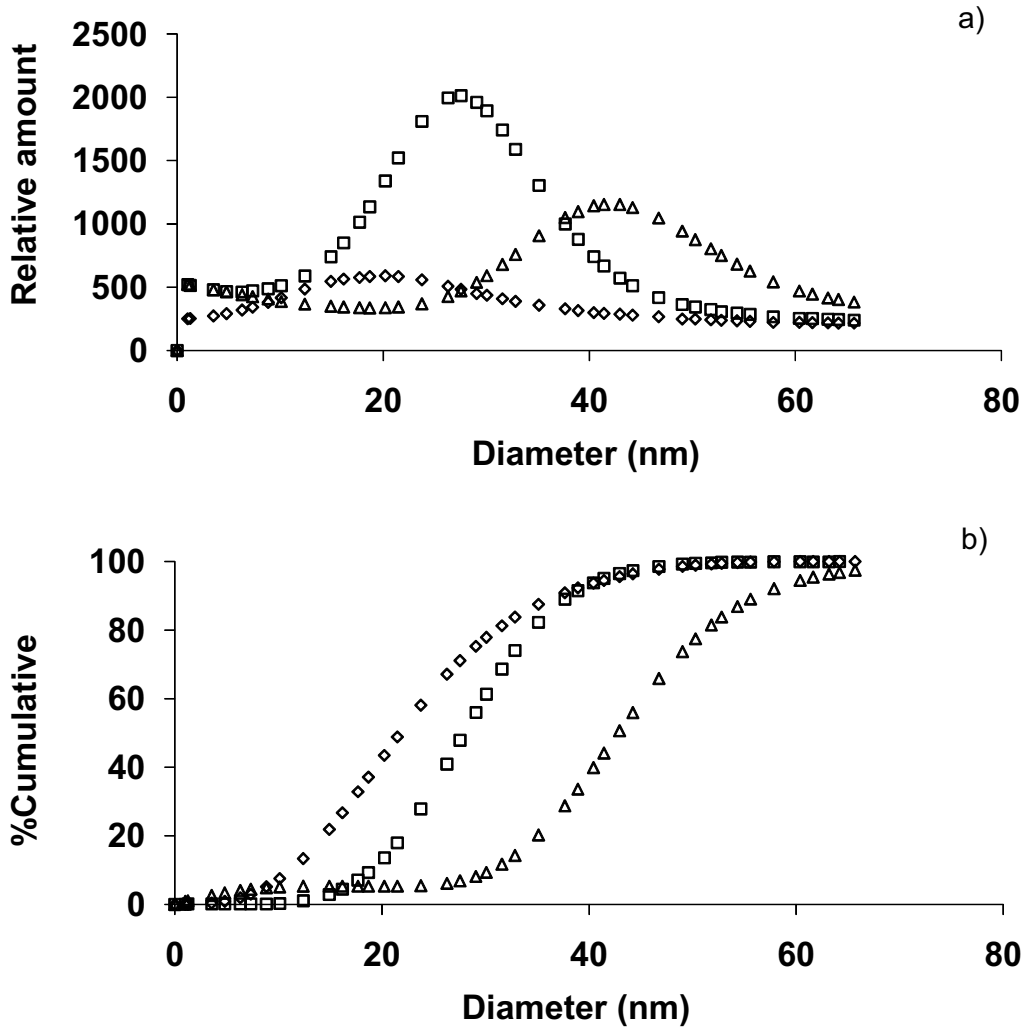

Figure 2.5 Effect of α-tocopherol concentration on the α-tocopherol induced enlargement of gold nanoparticles at 0 hr incubation time: a) particle size distributions; b) cumulative area distribution; where (◇), (□),and (△) represent 2.5, 7.5, and 10.0 x 10^{-6} M α-tocopherol, respectively.

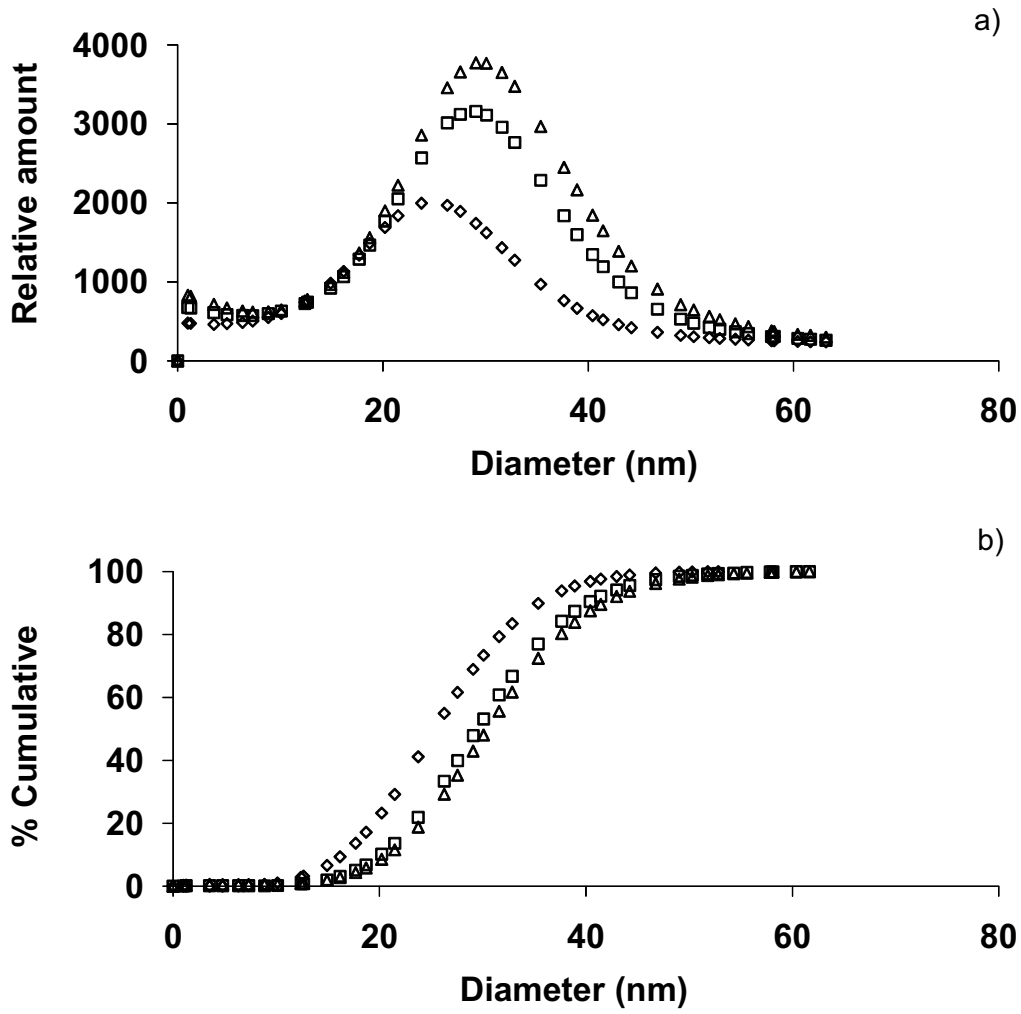

Figure 2.6 Effect of incubation time on the α-tocopherol induced enlargement of gold nanoparticles at fixed 7.5 x10^{-6} M α-tocopherol: a) particle size distributions; b) cumulative area distribution; where (◇), (□),and (△) represent 0, 2, and 4 hr incubation time, respectively.

Table 2.3 Particle size information of α-tocopherol induced enlargement of gold nanoparticles obtained from various experimental conditions

Effect of α-tocopherol concentration (at 0 hr incubation time)

α-tocopherol (10^{-6} M)	**d_p (nm)**	**d_{mean} (nm)**	**$\Delta d_{0.5}$ (nm)**
2.5	16 ± 3	17 ± 3	12
7.5	18 ± 1	19 ± 1	11
10.0	32 ± 4	33 ± 4	13

Effect of incubation time (at 7.5 x 10^{-6} M α-tocopherol)

incubation time (hr)	**d_p (nm)**	**d_{mean} (nm)**	**$\Delta d_{0.5}$ (nm)**
0	18 ± 1	19 ± 1	11
2	20 ± 2	21 ± 2	10
4	22 ± 2	23 ± 1	11

2.4 Summary

α-Tocopherol was shown to be capable of inducing the enlargement of gold nanoparticles obtained from the reduction reaction of $AuCl_4^-$ by sodium citrate. From the analytical viewpoint, an on-channel FlFFF preconcentration method was proven suitable for size characterization of diluted gold nanoparticles. Concentration of α-tocopherol and incubation time affected on the enlargement of gold nanoparticles. Flow FFF can be used to monitor the dynamic changes in size distribution of gold nanoparticles. The information obtained from FlFFF experiment can be used for guiding how to prepare the desired gold nanoparticles size for required applications.

2.5 References

1. Philip D (2008) Spectrochim Acta Mol Biomol Spectros 71**:**80-85
2. Ghosh P, Han G, De M, Kim CK, Rotello VM (2008) Adv Drug Deliv Rev 60**:**1307-1315
3. Thanh N, Vernhet A, Rosenzweig Z (2005) Frontiers in Chemical Sensors, Springer:261-277
4. Baron R, Zayats M, Willner I (2005) Anal Chem 77: 1566-1571
5. Scampicchio M, Wang J, Blasco AJ, Sanchez Arribas A, Mannino S, Escarpa A (2006) Anal Chem 78:2060-2063

6. Brigelius-Flohe R, Traber MG (1999) FASEB 13:1145-1155
7. Sun Y, Xia Y (2002) Science 298:2176-2179
8. Jungmann N, Schmidt M, Maskos M (2001) Macromolecules 34:8347-8353
9. Benincasa MA, Mazzoni V (2007) J Liq Chrom Relat Tech 30:453 – 462
10. Shin DY, Hwang E, Cho IH, Moon MH (2007) J Chrom A 1160:270-275
11. Jackson BP, Ranville JF, Neal AL (2005) Anal Chem 77:1393-1397
12. Giddings JC (1984) Sep Sci Technol 19:831-847
13. Giddings JC, Yang FJ, Myers MN (1976) Science 193:1244-1245
14. Giddings JC (1988) Chem Eng News 66:34-45
15. Roda B, Zattoni A, Reschiglian P, Moon MH, Mirasoli M, Michelini E, Roda A (2009) Anal Chim Acta 635:132-143
16. Ratanathanawongs Williams SK, Lee D (2006) J Sep Science 29:1720-1732
17. Rameshwar T, Samal S, Lee S, Kim S, Cho J, Kim IS (2006) J Nanosci Nanotechnol 6:2461-2467
18. Contado C, Argazzi R (2009) J Chromatogr A 1216:9088-9098
19. Hassellöv M, Lyven B, Haraldsson C, Sirinawin W (1999) Anal Chem 71:3497-3502
20. Amarasiriwardena D, Siripinyanond A, Barnes, RM (2001) J Anal At Spectrom 16:978-986
21. http://fscimage.fishersci.com/msds/06352.htm
22. Kimling J, Maier M, Okenve B, Kotaidis V, Ballot H, Plech A (2006) J Phys Chem B 110:15700-15707
23. Dondi F, Martin M. Physicochemical measurements and distributions from field-flow fractionation, in Schimpf ME, Caldwell JC, Giddings JC (2000) (eds) Field-flow fractionation handbook. Wiley, New York, pp 103-132
24. Siripinyanond A, Barnes RM (2002) Spectrochim Acta Part B 57:1885-1896
25. Yáñez-Sedeño P, Pingarrón JM (2005) Anal Bioanal Chem 382:884-886
26. Barman BN, Moon MH. Sample preparation and choice of carrier liquid in field-flow fractionation, in Schimpf ME, Caldwell JC, Giddings JC (2000) (eds) Field-flow fractionation handbook. Wiley, New York, pp 189-198
27. Atta KR, Gavril D, Loukopoulos V, Karaiskakis G (2004) J Chromatogr A 1023:287-296
28. Al-Ammar A, Siripinyanond A, Barnes RM (2001) Spectrochim Acta Part B 56:1951-1962
29. Zayats M, Baron R, Popov I, Willner I (2004) Nano Lett 5:21-25
30. Yin H (2007) Free Radic Biol Med 43:1229-1230
31. Nie Z, Liu KJ, Zhong CJ, Wang LF, Yang Y, Tian Q, Liu Y (2007) Free Radic Biol Med 43:1243-1254

Chapter 3

Particle Size Characterization of Titanium Dioxide in Sunscreen Products Using Sedimentation Field-Flow Fractionation-Inductively Coupled Plasma Mass Spectrometry

3.1 Introduction

Ultraviolet (UV) radiation including UV-A (320-400 nm) and UV-B (290-320 nm) can cause skin cancer and other harmful effects to humans [1-4]. It is necessary to avoid unwanted skin effects of the sun with the use of sunscreen filters. Titanium dioxide (TiO_2), which is a physical UV filter, can reflect and scatter UV radiation very efficiently [5] and it is therefore often used to formulate the sunscreen products with high sun protection factor (SPF) value [6]. According to the European legislation, titanium dioxide is the only inorganic UV filter permitted to be used in the sunscreen products with the maximum allowable concentration of 25% (w/w) [7]. The radiation reflection and scattering efficiencies of titanium dioxide depends on its concentrations and particle sizes, by which the particle size should be approximately 60 – 120 nm to be most effective in UV reflection and scattering ability [5]. Therefore, the analysis of sunscreen cosmetics in terms of the concentrations and particle sizes of titanium dioxide should be considered.

Although the official methods for determining titanium dioxide particles in sunscreen cosmetics, either in terms of quantitative element content or the particle size distribution, have never been documented, several analytical techniques have been reported for determination of titanium dioxide in sunscreen. These techniques include the classical volumetric method [8], atomic absorption spectrometry [9], inductively coupled plasma optical emission spectrometry [8, 10], and X-ray fluorescence spectrometry [11, 12]. For particle size characterization, flow field-flow fractionation (FlFFF) has been reported for titanium dioxide particles in a commercial sunscreen product [13] and titanium dioxide nanoparticles imprinted for tyrosine [14].

Field-flow fractionation (FFF) is a flow-assisted technique for size characterization of particles in the nanometer to sub-micrometer scale. The fractionated particles can be further characterized by various detection methods [15, 16]. The principle [16, 17] and applications [18, 19] of FFF have been described elsewhere. Depending on the type and the particle size of samples, various types of external field forces may be applied. These external fields give rise to an assortment of FFFsub-techniques, including gravitational, sedimentation, flow, electrical, and thermal FFF. Sedimentation (SdFFF) and flow FFF (FlFFF) are most commonly used. As the particle size of titanium dioxide in sunscreen products is in the sub-micrometer size range, SdFFF may be used [18]. Previous works indicated that sedimentation FFF was successfully used to separate titanium dioxide microparticles [18-20].

An on-line coupling between SdFFF and inductively coupled plasma-mass spectrometry (SdFFF-ICP-MS) was proposed to provide the quantitative information of titanium dioxide concentrations across particle size distribution profiles of the sunscreen samples. The necessity for sample preparation before SdFFF particle size characterization was evaluated. Various initial field strengths were employed in

SdFFF fractionation to check for the reliability of the resulting particle size distribution information. The ability of ICP-MS as an on-line detector for the fractionated titanium dioxide particles was examined. The developed SdFFF-ICP-MS method was applied to investigate size distribution of titanium dioxide particles in various sunscreen products of various SPF values.

3.2 Experimental

3.2.1 Chemicals and samples

Polystyrene latex standards having diameters of 0.35, 0.53, and 0.72 μm from Postnova Analytik (Landsberg, Germany) were used for SdFFF calibration. A carrier liquid was 0.02% (v/v) FL-70 detergent (Fisher Scientific, PA, U.S.A) containing 0.02% (w/v) NaN_3 (Merck, Darmstadt, Germany) to prevent bacterial growth. FL-70 is a mixture of anionic and non-ionic compounds containing the following active components: oleic acid; sodium carbonate; tergitol; tetrasodium EDTA; polyethylene glycol; and triethanolamine [21].

Three brands of commercial sunscreen cream products of various SPF values (0 and 50 SPF for brand A; 0, 15, and 30 SPF for brand B; and 0 and 15 SPF for brand C) were purchased from a local supermarket. Hexane, which was employed to remove some organic components, was purchased from Labscan (Bangkok, Thailand). Ti elemental standard solution of 100 μg mL^{-1} (AccuStandard, New Haven, CT, U.S.A.) was used to prepare the ICP-MS calibration solution.

3.2.2 Preparation of sunscreen sample

An SdFFF system (Model S-101 Particle/Colloid Fractionator, Postnova Analytik, Landsberg, Germany) was used to characterize the particle size distributions of BLG-encapsulated α-TOC. The elution of particles was monitored by a UV absorption detector operating at the fixed wavelength of 280 nm (UV-2000 Spectra System, Thermo Electron Corporation, Waltham, MA, USA). Samples were introduced into a Rheodyne (Rohnert Park, CA, USA) injector at a fixed loop of 50 μL.

3.2.3 Preparation of β-lactoglobulin solutions

0.01 g of sunscreen cream products of various brands and SPF values were weighed and diluted in 1 mL of deionized water to obtain the sunscreen sample of 1% (w/v). Before injection into SdFFF, a 50 μL-volume of 1% (w/v) of sunscreen cream sample in deionized water was mixed thoroughly by vortex.

3.2.4 Preparation of defatted sunscreen sample

To defat or remove some organic components from sunscreen cream products, 1 mL of hexane was applied to soak 0.01 g of sunscreen cream samples for 12 hr at room temperature. Hexane containing organic components was removed and the defatted part was diluted with deionized water to 1% (w/v). To study particle size distribution in sunscreen cream samples, a 50 μL-volume of 1% (w/v) of defatted sunscreen cream sample in deionized water was mixed thoroughly by vortex before SdFFF analysis.

3.2.5 Acid digestion of sunscreen sample

0.05 g of sunscreen cream products were weighed and digested at approximately 350°C with 10 mL of H_2SO_4 in the presence of 4 g of $(NH_4)SO_4$. Then, 25 mL of HCl and 30 mL of deionized water were added to the mixture and heated until the clear solution was obtained. Subsequently, the digested solution was diluted with deionized water before ICP-MS determination of Ti concentration.

3.2.6 Instrumentation

The SdFFF system (Model S-101 Particle/Colloid Fractionator, Postnova Analytik, Landsberg, Germany) was used in this study. The SdFFF channel was 89.5 cm long, 2.0 cm wide, and 0.0254 cm thick, with a rotor radius of 15.1 cm. The channel volume was calculated to be 4.45 mL. The carrier solution was introduced into the SdFFF channel by an HPLC pump (model PN1122, Postnova Analytik). A UV detector (model UV2075, Jasco, Essex, UK) was set at 254 nm to monitor light attenuation of the eluted particles. Samples of 50 μL were injected into SdFFF via a Rheodyne injector.

An ICP-MS instrument (model Sciex/ELAN 6000, Perkin Elmer, CT, U.S.A.) was used as an element detector sequentially after the UV absorption detector. Owing to the similarity of the SdFFF channel and ICP-MS sample flow rates typically used for

analysis, the ICP-MS cross-flow nebulizer was connected directly to the UV detector outlet with a 30-cm length of poly(tetrafluoroethylene) tubing (PTFE, 0.58 mm id). The operating conditions of SdFFF and ICP-MS measurements are summarized in Table 3.1.

Table 3.1 SdFFF and ICP-MS operating conditions

SdFFF operating conditions	
SdFFF channel dimensions/cm^3	89.5 x 2.0 x 0.0254
SdFFF rotor radius/cm	15.1
Carrier liquid	0.02% (v/v) FL-70 containing 0.02% (w/v) sodium azide
Channel flow rate/ mL min^{-1}	1.0
Equilibration time/ min	10
Power field programming	initial applied field, 400 rpm [obtained field, 397 rpm or 26.6 *g*] for 8 min; field decay parameter, -64; final field, 50 rpm [obtained field, 49 rpm]
ICP-MS operating conditions	
Rf generator frequency/ MHz	40
Rf power/ W	1150
Nebulizer gas flow rate/ L min^{-1}	0.99
Coolant gas flow rate/ L min^{-1}	15
Auxiliary gas flow rate/ L min^{-1}	1.0
Isotopes monitored (m/z)	^{47}Ti and ^{49}Ti

3.2.7 Data treatment

Raw fractograms were translated into size distribution profiles using the Postnova FFF Analysis software version 2.0 (Postnova Analytik, Landsberg, Germany). Peak evaluation, baseline adjustment, and integration were performed using PeakFit™ (SPSS, Illinois, U.S.A.).

3.3 Results and Discussion

3.3.1 The need for sample preparation before particle size characterization of titanium dioxide in cosmetics by using SdFFF

By knowing the exact geometry of the SdFFF channel, the field, flow rate, and the density difference between particle and carrier liquid, diameter of the separated particle can be calculated directly from the experimental retention time [22]. The average density of titanium dioxide particles was 4.05 g mL^{-1}[23], and therefore the density difference between the particles and the carrier liquid ($\Delta\rho$) was 3.05 g mL^{-1}. To apply SdFFF for particle size characterization of titanium dioxide in sunscreen samples, various experimental conditions were examined to demonstrate the reproducibility and reliability of SdFFF for particle size characterization of titanium dioxide in sunscreen products. Various initial field strengths (500, 600, and 800 RPM) were applied to fractionate titanium dioxide particles in a 30 SPF sunscreen as illustrated in Figure 3.1. Fractograms of 1% (w/v) 30 SPF sunscreen (brand B) showed two separated peaks at different retention times. With higher field strength, the peaks shifted towards longer retention times (Figure 3.1a). Nonetheless, the particle size distributions obtained from various experimental conditions did not agree well with each other, indicating the erroneous results in particle size determination by the SdFFF technique. This error might be due to the fact that the cosmetic sample contains not only the titanium dioxide particles, but also some other types of particles. Alternatively, it might be due to the fact that the titanium dioxide particles were coated by some organic components in the sunscreen sample, which could make the approximation of the particles density of 4.05 g mL^{-1} to be incorrect.

Therefore, it was necessary to carry out sample preparation before introduction of sunscreen samples into SdFFF channel. To remove the organic components from the titanium dioxide particles, hexane extraction was performed [13]. Hexane removes the organic compounds contained in the sunscreen products, which could cause some interaction between organic component and SdFFF channel and affected on particle size fractionation of sunscreen sample. With hexane removal of organic components from the sunscreen samples, the resulting samples were called “defatted sunscreen samples”. Various initial field strengths (400, 500, and 600 RPM) were applied to fractionate

titanium dioxide particles in the defatted sunscreen as illustrated in Figure 3.2a with the resulting particle size distributions shown in Figure 3.2b. The particle size distributions in Figure 3.2b obtained from various experimental conditions were all similar showing the particle size range of 0.1 – 0.6 μm with the peak maximum at around 0.52 μm. This suggests that the particle size determination of titanium dioxide in sunscreen products is possible with SdFFF with the necessity of sample preparation before analysis, and hexane extraction is considered effective for such purpose. The initial field strength of 400 RPM was selected for further use as it was sufficient to separate the particles from the void fraction with minimized analysis time.

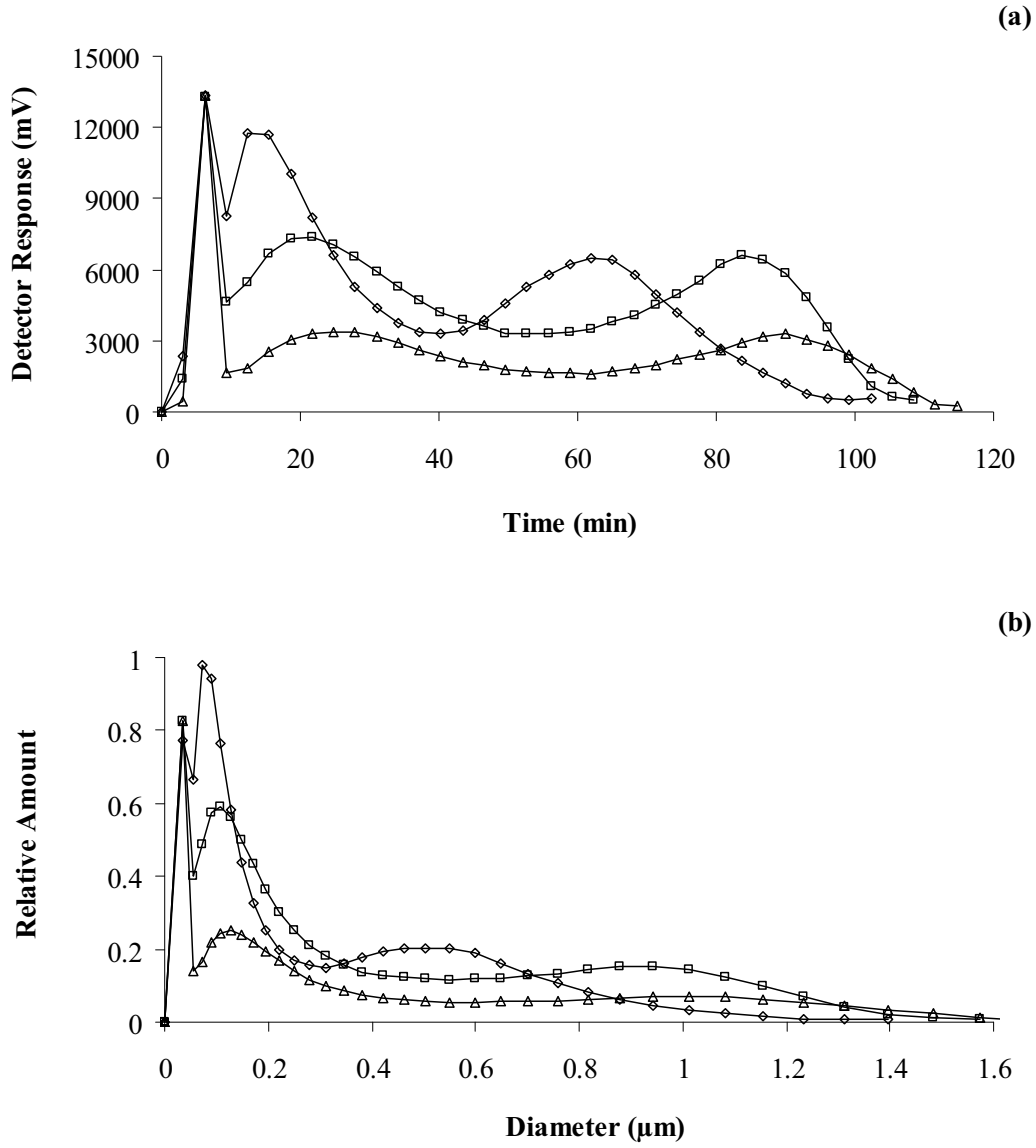

Figure 3.1 Effect of field strength on fractionation of 30 SPF sunscreen (brand B). (a) Raw fractograms; and (b) particle size distributions of 30 SPF sunscreen (brand B), obtained from various initial fields as 500 (◊), 600 (□), and 800 RPM (Δ). The SdFFF operating condition was as follows: initial field hold time 8 min; field decay parameter -64; final field 50 rpm, and $\Delta\rho$ = 3.05 g mL^{-1}. The channel flow rate was constant at 1 mL min^{-1}.

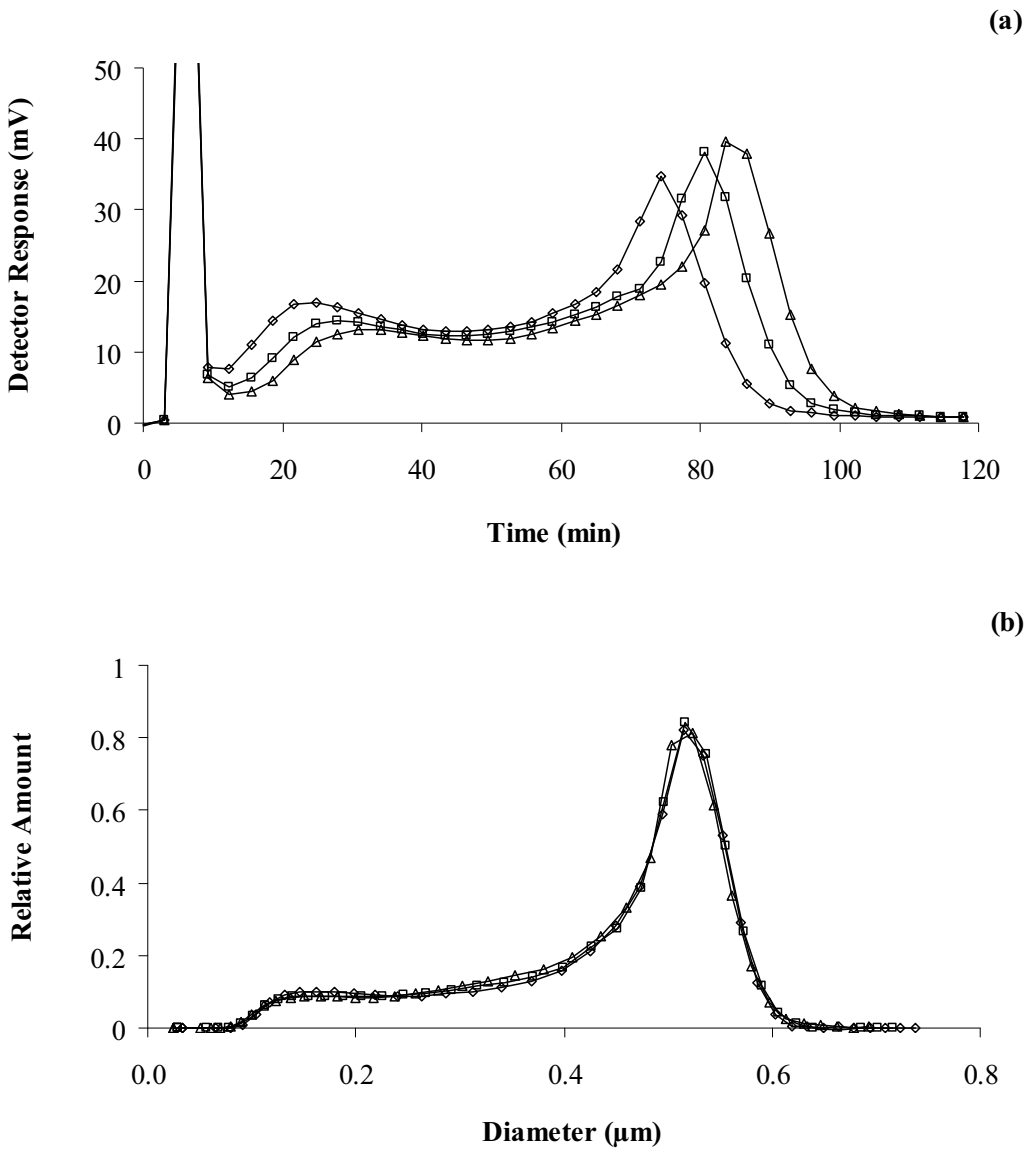

Figure 3.2 Effect of field strength on fractionation of the defatted 30 SPF sunscreen (brand B). (a) Raw fractograms; and (b) particle size distributions of 30 SPF sunscreen (brand B), obtained from various initial fields as 400 (◊), 500 (□), and 600 RPM (Δ). The SdFFF operating condition was as follows: initial field hold time 8 min; field decay parameter -64; final field 50 rpm, and $\Delta\rho$ = 3.05 g mL^{-1}. The channel flow rate was constant at 1 mL min^{-1}.

3.3.2 Particle size distribution of titanium dioxide in sunscreen products of various brands and SPF values

With the selected SdFFF operating conditions, particle size distributions of titanium dioxide in the defatted sunscreen products of various brands and SPF values were investigated by using SdFFF-ICP-MS. With the UV detector, the particle size distributions of sunscreen samples are shown in Figure 3.3. It can be seen that different brands of sunscreen products showed different particle size distribution patterns. For a particular brand of sunscreen products, the sample with higher SPF values showed larger particle size than that of the smaller SPF values. With the ICP-MS detector, the particle size distributions of titanium dioxide in sunscreen samples were obtained as illustrated in Figure 3.4. For brand A, the signal of titanium was only slightly observed for sunscreen of 0 SPF value whereas the distribution of titanium was found in the range of 0.1 – 0.5 μm for the sunscreen of 50 SPF value. For brand B, the distribution of titanium in sunscreen of various SPF values were different, but ranging between 0.1– 0.4 μm. Titanium was found to present in a smaller particle size for the sunscreen of 15 SPF values as compared to that of 0 and 30 SPF values, suggesting that the manufacturer might have different strategies to formulate the products of different SPF values within the same brand. The manufacturer of brand B might not use the same titanium dioxide particle size for the products of different SPF values. For brand C, the distribution of titanium in sunscreen of 0 and 15 SPF values were found in the range of 0.2 – 0.6 μm. Higher titanium content was found in the product of higher SPF value.

Particle size distributions of titanium dioxide in all sunscreen samples investigated in this work were larger than 100 nm size range, except for the brand B of 15 SPF value. The particle size distributions of titanium dioxide in the defatted sunscreen samples (Figure 3.4) were not well corresponded with the particle size distribution profiles (Figure 3.3) except for the sunscreen brand A. For brand B, titanium (Figure 3.4b) was found to associate with the small particle size range of the particles found in the defatted sunscreen samples (Figure 3.3b). For brand C, titanium (Figure 3.4c) was found to associate with the large particle size range of the particles found in the defatted sunscreen samples (Figure 3.3c). These data suggest that the manufacturer of brand A might use titanium dioxide solely to adjust the SPF values of their products, whereas the

manufacturers of brands B and C might adjust the SPF values of their products by adding both organic and inorganic components other than titanium dioxide as UV filters.

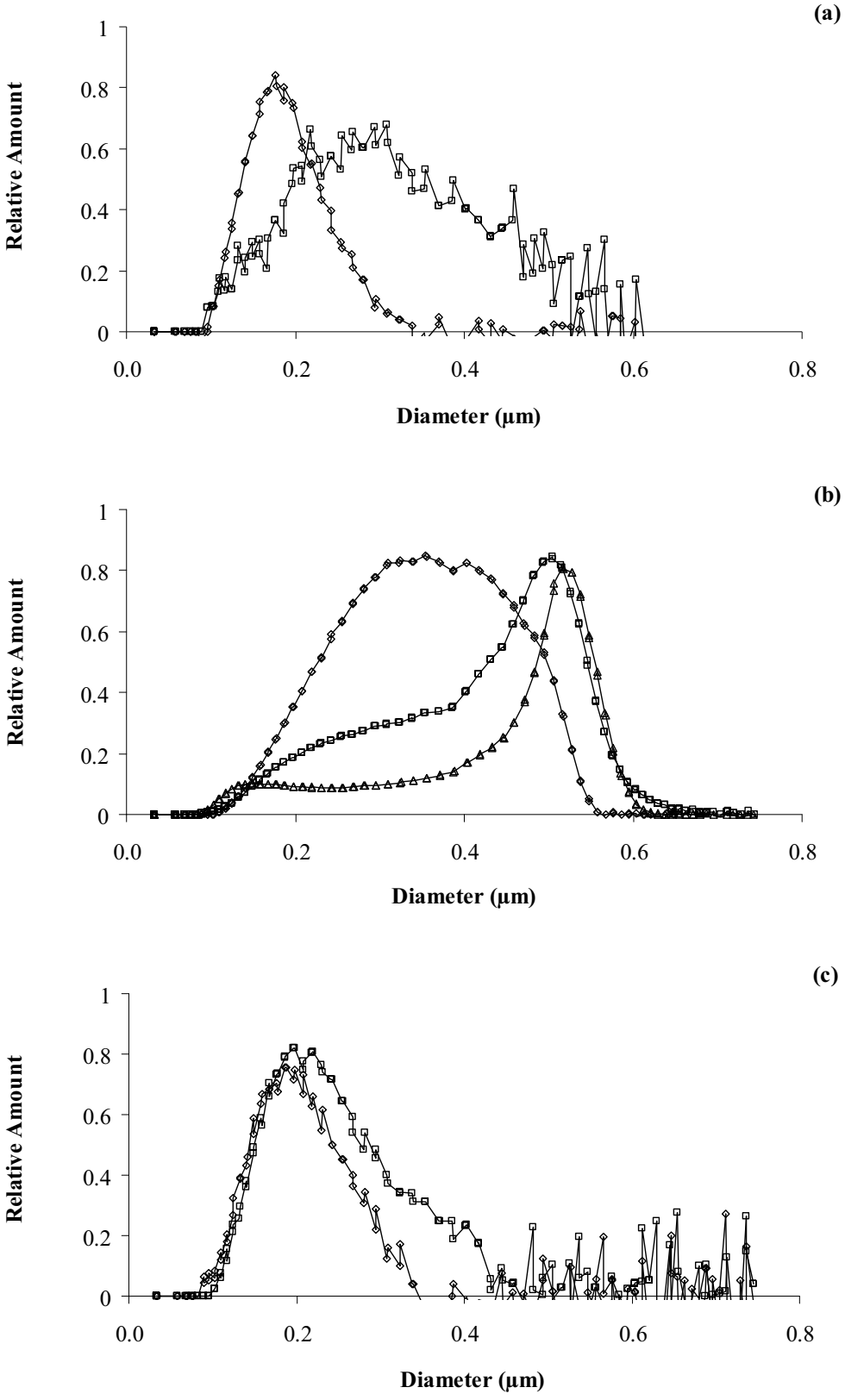

Figure 3.3 Particle size distributions of defatted sunscreen samples: (a) brand A, where (◊) and (□) represent 0 and 50 SPF, respectively; (b) brand B, where (◊), (□), and (Δ) represent 0, 15, and 30 SPF, respectively; and (c) brand C, where (◊) and (□) represent 0 and 15 SPF, respectively.

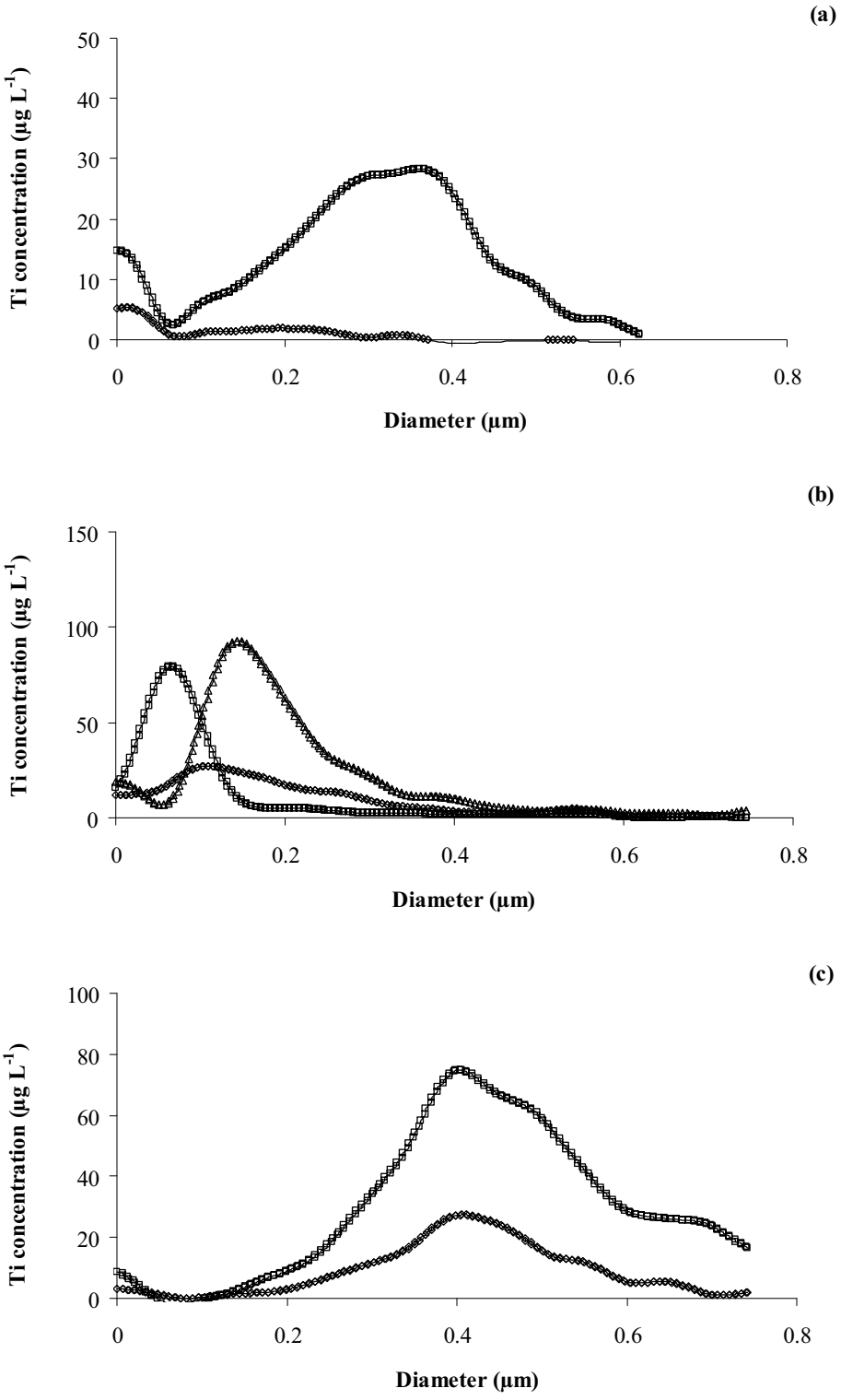

Figure 3.4 Particle size distributions of titanium dioxide in defatted sunscreen samples: (a) brand A, where (◊) and (□) represent 0 and 50 SPF respectively; (b) brand B, where (◊), (□), and (Δ) represent 0, 15, and 30 SPF, respectively; and (c) brand C, where (◊) and (□) represent 0 and 15 SPF, respectively. Data were smoothed with Savitzsky–Golay function (PeakFit@, SPSS, Chicago, IL, USA) with a smoothing level of 10%.

3.3.3 Titanium dioxide concentrations in sunscreen samples

Not only the particle size information, but it is also important to provide quantitative information on the titanium dioxide concentration in the sunscreen products, as its maximum allowable concentration in the sunscreen products has been declared by many countries such as European Union, Japan, and USA. In the European Union legislation, titanium dioxide is the only inorganic UV filter which is allowed at 25% maximum concentration [7]. The determination of titanium dioxide content (%w/w) in sunscreen products of various brands and SPF values was carried out using ICP-MS detection of titanium.

In this study, ICP-MS determination of titanium concentrations was performed with various approaches as follows: as an on-line detector for SdFFF; off-line detection of the collected fraction from SdFFF after acid digestion; and direct detection of the acid digested samples. The titanium dioxide concentrations in all sunscreen samples from various approaches are summarized in Table 3.2, which illustrates that the concentrations found from all approaches were similar. The closeness in the titanium dioxide concentrations obtained from the collected fraction from SdFFF after acid digestion with those directly determined after acid digestion of the samples indicates that titanium dioxide was not loss during the SdFFF fractionation of samples. The closeness in the titanium dioxide concentrations obtained from the on-line SdFFF-ICP-MS with those from the SdFFF fraction after acid digestion suggests that the ICP-MS could effectively atomize and ionize the titanium dioxide particle without the need for acid digestion. Therefore, the on-line coupling between SdFFF and ICP-MS could be effectively used to provide the quantitative information of titanium dioxide concentrations across particle size distribution profiles.

For all sunscreen samples in this study, the titanium dioxide contents were below the maximum allowable concentration (25 %) as set by the European legislation. Different brands of sunscreen products showed different titanium dioxide contents. Nevertheless higher titanium dioxide contents were observed for the sunscreen of the same brand but with increasing SPF values.

Table 3.2 TiO_2 concentrations in sunscreen samples of various brands and SPF values

Samples	TiO_2 concentration (% w/w) [average ± SD], n = 3		
	Method A	Method B	Method C
0 SPF brand A	n.d.	n.d.	< 0.04
50 SPF brand A	n.d.	n.d.	3.84 ± 0.28
0 SPF brand B	n.d.	n.d.	0.09 ± 0.02
15 SPF brand B	n.d.	n.d.	0.37 ± 0.05
30 SPF brand B	0.84 ± 0.10	0.74 ± 0.10	0.82 ± 0.20
0 SPF brand C	n.d.	n.d.	0.12 ± 0.02
15 SPF brand C	1.16 ± 0.16	0.94 ± 0.06	0.93 ± 0.05
LOQ	< 0.06	< 0.03	< 0.04

The concentration of titanium is represented as TiO_2 percentage in the sample (% w/w).

n.d. – not determined

- *Method A is an on-line SdFFF-ICP-MS. The concentration of titanium dioxide in the samples was obtained by on-line Sd-FFF-ICP-MS measurement with external calibration using standard solutions prepared in the SdFFF carrier liquid. Total titanium dioxide concentration was determined by integration of the signal through the whole fractionation time using a PeakFit™ program (SPSS, Illinois, U.S.A.).*
- *Method B is an off-line SdFFF and ICP-MS determination of titanium dioxide in the fractionated samples.*
- *Method C is ICP-MS determination of titanium after acid digestion of samples.*

3.4 Summary

Sedimentation field-flow fractionation-inductively coupled plasma-mass spectrometry (SdFFF-ICP-MS) was demonstrated feasible to provide quantitative information of titanium dioxide concentrations across particle size distribution profiles. Nonetheless, sample preparation was necessary prior to SdFFF particle size characterization. Various brands and SPF values of sunscreen products showed different

particle size distributions and different titanium dioxide contents. The information obtained from SdFFF-ICP-MS can be useful for quality control of the finished sunscreen products.

3.5 References

1. De Fabo EC, Noonan EP (1983) J Exp Med 158: 84-98
2. Heck DE, Vetrano AM, Mariano TM, Laskin JD (2003) J Biol Chem 278: 22432-22436
3. Agar NS, Halliday GM, Barnetson RS, Ananthaswamy HN, Wheeler M, Jones AM (2004) Proc Natl Acad Sci USA 101: 4954-4959
4. Krutmann J (2000) J Dermatol Sci 23: S22-S26
5. Popov AP, Lademann J, Priezzhev AV, Myllylä R (2005) J Biomed Optics 10: 1-9
6. Anderson MW, Hewitt JP, Spruce SR, (1997) in: Lowe NJ, Shaath NA, Pathak MA (Eds.), Broad-spectrum Physical Sunscreens: Titanium Dioxide and Zinc Dioxide, Marcel Dekker Inc., New York, 353-398
7. Salvador A, Chisvert A (2005) Anal Chim Acta 537: 1-14
8. Kim YS, Kim BM, Park SC, Jeong HJ, Chang JS (2006) J Cosmet Sci 57: 377-381
9. Mason JT (1980) J Pharm Sci 69: 101-102
10. Salvador A, Pascual-Martí MC, Adell JR, Requeni A, March JG (2000) J Pharm Biomed Anal 22: 301-306
11. Kawauchi A, Ishida M, Saitoh I (1996) Spectrosc Lett 29: 345-366
12. Melquiades FL, Ferreira DD, Appoloni CR, Lpoes F, Lonni AG, Oliveira FM, Duarte JC (2008) Anal Chim Acta 613: I35-I43
13. Contado C, Pagnoni A (2008) Anal Chem 80: 7594-7608
14. Zattoni A, Reschiglian P, Montalti M, Zaccheroni N, Prodi L, Picca RA, Malitesta C (2007) Inorg Chim Acta 360: 1063-1071
15. Contado C, Blo G, Fagioli F, Dondi F, Beckett R (1997) Colloid Surface A 120: 47-59
16. Saeseaw S, Shiowatana J, Siripinyanond A (2006) Anal Bioanal Chem 386: 1681-1688
17. Saeseaw S, Shiowatana J, Siripinyanond A (2005) Food Res Int 34: 777-786
18. Cardot PJP, Rasouli S, Blanchart P (2001) J Chromatogr A 905: 163-173
19. Rasouli S, Blanchart P, Cle´dat D, Cardot P J P (2001) J Chromatogr A 923: 119–126
20. Koliadima A, Gavril D, Karaiskakis G (1999) J Liq Chromatogr Rela. Technol 22: 2779–2793
21. http://fscimage.fishersci.com/msds/06352.htm
22. Kirkland JJ, Rementer SW, Yau WW (1981) Anal Chem 53: 1730-1736

23. The Merck Index: An Encyclopedia of Chemicals, Drugs, and Biological (2006) 14th ed.; Ó Neil , M.J.,.Ed.; Merck Research Laboratories: Whitehouse Station, NJ

Chapter 4

Flow Field-Flow Fractionation with Off-Line Electrothermal Atomic Absorption Spectrometry for Size Characterization of Silver Nanoparticles

4.1 Introduction

Silver nanoparticles (Ag NPs) are one of common engineered nanoparticles (ENPs) with at least one dimension within the size from approximately 1 nm to 100 nm [1]. Owing to their antibacterial properties, Ag NPs have been used in various consumer products including textiles, personal care products, food storage containers, and laundry additives. The release of Ag NPs into water and their mobilities in water should therefore be investigated. Silver ions (Ag^{+}) can release from consumer products by oxidation of metallic silver (Ag^{0}) in contact with water [2-3]. Blaser et al. studied the model of total silver in the form of Ag^{+} ions or AgNPs released from plastic and textile into water and indicated that up to 15% of the total Ag discharged into the environment [4]. Moreover, recent studies by Benn et al. confirmed that Ag NPs were easily released from nanosilver-coated socks during the washing process [5].

Recently, the issue of mobility and toxicity of Ag NPs has gained significant attention. In general, the smaller size can transport faster and has much higher toxicity than the larger size. Moreover, smaller size Ag NPs (<5 nm) are more toxic than any other forms of silver [6]. The aggregation is also one of the primary controls on both transport and toxicity of Ag NPs in the aquatic environment. Not only temperature, pH, ionic strength of environmental water, and concentration of Ag NPs show significant effect on the aggregation process, but also the surface property of Ag NPs is important [7]. The surface property of Ag NPs depends on how Ag NPs are synthesized. Ag NPs can be synthesized using various methods resulting in different shapes, sizes, and surface properties for numerous applications [8]. Normally, Ag NPs are synthesized via reduction of silver nitrate in water using reductants and stabilizing agent or capping agent for control of particle size to ensure a stable suspension [9-10]. The reductant and stabilizing agents commonly used are sodium borohydride and sodium citrate, respectively. Greener processes for the production of greener nanomaterials were reported by use of nontoxic chemicals [11].

As the particle size of Ag NPs plays important roles to their mobility and hence toxicity, particle size characterization of Ag NPs is necessary. Size characterization techniques for Ag NPs include dynamic light scattering (DLS) [12], transmission electron microscopy (TEM) [7, 13], atomic force microscopy (AMF) [14], size exclusion chromatography (SEC) [15], hydrodynamic chromatography (HDC) [15], and flow field-flow fractionation (FlFFF) [13]. The use of FlFFF coupled off-line with AFM to observe the structure of the smaller size fraction of aquatic colloids was reported to fractionate citrate-stabilized Ag NPs at environmentally relevant conditions [14]. In this study, the use of ETAAS as an off-line detector for the Ag NPs fractionated by FlFFF was evaluated. FlFFF with ETAAS detection was employed for size characterization of Ag NPs in environmental water. The aggregation phenomenon of Ag NPs from different synthesis methods including common method (citrate stabilized) and green synthesis

(polysaccharide stabilized) in various types of water was investigated. The effect of humic acid on the aggregation of Ag NPs was also examined.

4.2 Experimental

4.2.1 Chemicals and samples

Silver nitrate was purchased from Carlo Erba (Rodano, MI, Italy). Sodium borohydride, sodium hydroxide, and sodium azide were purchased from Merck (Darmstadt, Germany). Humic acid and sodium citrate tribasic dihydrate were purchased from Sigma Aldrich (Steinheim, Germany). Pectin and alginate were from Fluka (Buchs, Switzerland). Gold nanoparticle standard (Au NPs) of 10 nm diameter (Sigma Aldrich) was used to calibrate the FlFFF channel. The humic acid stock solution (2000 mg/L) was made by dissolving 0.050 g of humic acid in 25 mL of deionized water.

Water samples were collected from three different sites including sea water from the Jausumran beach (Phetchaburi, Thailand), ground water from the Lopburi farm (Lopburi, Thailand), and tap water (Bangkok, Thailand). The samples were stored in a refrigerator and filtered through 0.45 μm membrane filters before use.

4.2.2 Silver nanoparticles synthesis

Citrate stabilized-Ag NPs were prepared as described previously by Yang *et.al.* [16]. Briefly, 100 mL of 0.3 M silver nitrate and 8 mL of 12.6 M sodium citrate were mixed together in a conical flask, and then stirred at 50 rpm. Stirring was continued and 2 mL of 37 mM $NaBH_4$ were added into solution. The yellow solution was then observed.

For polysaccharide stabilized-Ag NPs, Ag NPs were prepared by the reduction of silver ion using ascorbic acid. Polysaccharide, i.e.,pectin and alginate, were used to stabilize nanoparticles. Briefly, 100 mL of 0.1% w/v polysaccharide solution (pectin or alginate) were mixed together with freshly prepared ascorbic acid of 1 mM (50 mL) and vigorously stirred. Fifty milliliters of 2 mM silver nitrate solution were added into the solution and 0.3 M NaOH (0.1 mL) was added quickly. Stirring was continued and the final yellow solution was observed.

4.2.3 Instrumentation

The FlFFF system is a PN-1201-FO model (Postnova Analytics, Landsberg, Germany). The FlFFF channel dimensions are 27.7 cm length, 2.0 cm wide, and 254 μm thick. A 1-kDa regenerated cellulose membrane (Postnova) was used. The carrier liquid was 0.02% FL-70 and 0.02% NaN_3 diluted in deionized water and adjusted to pH 9.2-10. Sample volume of 20 μL was introduced into FlFFF via the Rheodyne injector valve. A high pressure liquid chromatography (HPLC) pump (Model PN 2101, Postnova Analytics, Germany) was used to deliver the channel flow at 1 mL min^{-1}. The cross flow rate fixed at 1 mL min^{-1} was delivered by another HPLC pump of the same model. After fractionation, the effluent was directed through a UV detector (Model S3210 UV-visible detector; Postnova Analytics) and the detector was set at 400 nm for detection of the Ag NPs. The automatic fraction collector (Waters, Milford, Massachusetts, USA) was used to collect fraction from UV detector outlet. The FlFFF operating conditions are shown in Table 4.1.

Table 4.1 FlFFF operating condition

FlFFF: Model PN-1021-FO	
Channel dimension/cm×cm×cm	27.7 long x 2.0 wide x 0.02 thick
Carrier liquid	0.02% -FL-70 and 0.02 NaN_3 (pH 9.5)
Channel flow rate/ mL min^{-1}	1.0
Cross flow rate/ mL min^{-1}	1.0
Equilibration time/ min	2.2
Membrane	1 kDa MWCO poly(regenerated cellulose acetate)

A Perkin Elmer Model AAnalyst 100 (Norwalk, CT, USA) with deuterium background corrector was used for detection of silver after the UV absorption detector. The Perkin Elmer Model AS-72 autosampler was used to introduce solution into a graphite tube. The furnace operating condition for silver and silver nanoparticles measurement is summarized in Table 4.2.

Table 4.2 Electrothermal atomic absorption spectrometer operating condition for silver detection

ETAAS: Perkin Elmer Analyst 100-HGA-800				
Step		Temperature (°C)	Ramp time (sec)	Hold time (sec)
1	Drying	130	20	30
2	Ashing	800	20	30
3	Atomization	1800	0	8
4	Clean up	2600	1	5

The UV-visible absorption spectra of Ag NPs were observed by using UV-visible spectrophotometer (Model V-530, Jasco, Easton, Maryland, USA). Zeta potential measurements were carried out using the Zetasizer Nano ZS (Malvern Instruments Zetasizer1000 Hs, Malvern, UK). A transmission electron microscope (TEM), JEOL JEM-1230 (Peabody, MA, USA), was used to acquire images of the Ag NPs. The TEM was operated at 25°C and 80 kV.

4.3 Results and Discussion

4.3.1 Particle size characterization of the synthesized silver nanoparticles

Particle size characterization of three types of Ag NPs was performed by using FlFFF as illustrated in Figure 4.1. Particle size at peaks were 9 nm, 19 nm, and 45 nm for citrate stabilized-Ag NPs, pectin stabilized-Ag NPs, and alginate stabilized-Ag NPs, respectively. The particle size values obtained from FlFFF were in good agreement with those from TEM (Figure 4.2) and zetasizer as summarized in Table 4.3, by which the particle size of alginate stabilized-Ag NPs was larger than pectin stabilized-, and citrate stabilized-Ag NPs, respectively. With UV-visible absorption spectrometry, the surface plasmon resonance peaks were observed at 390 nm, 400 nm, and 412 nm for citrate stabilized-, pectin stabilized-, and alginate stabilized-Ag NPs, respectively, as shown in Figure 4.3, suggesting the same trend as those observed by the FlFFF, TEM, and zetasizer, as the smaller particles exhibit plasmon resonance band as shorter wavelength and the larger particles exhibit the plasmon band at longer wavelength [17]. Nonetheless,

the particle sizes of Ag NPs obtained from different techniques were slightly different owing to the fact that different techniques provide different particle size information. TEM measures a number based size distribution of the core particle excluding the stabilizing agent, while FlFFF and zetasizer measure a mass based size distribution or hydrodynamic volume [13].

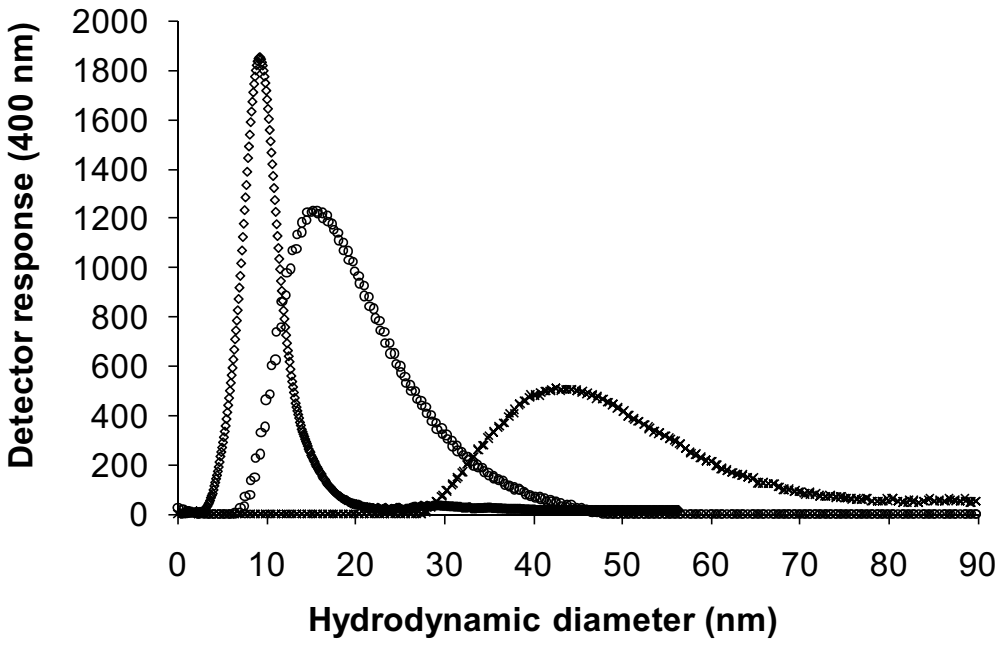

Figure 4.1 Hydrodynamic diameter distributions of Ag NPs: (◊) citrate stabilized Ag-NPs; (**O**) pectin stabilized-Ag NPs; and (×) alginate stabilized-Ag NPs. The FlFFF conditions were as follows: channel flow 1 mL min^{-1}, cross flow 1 mL min^{-1}, RC membrane (1 kDa), 0.02% FL-70 and 0.02% NaN_3 as carrier liquid. UV-Vis was used as FlFFF detector.

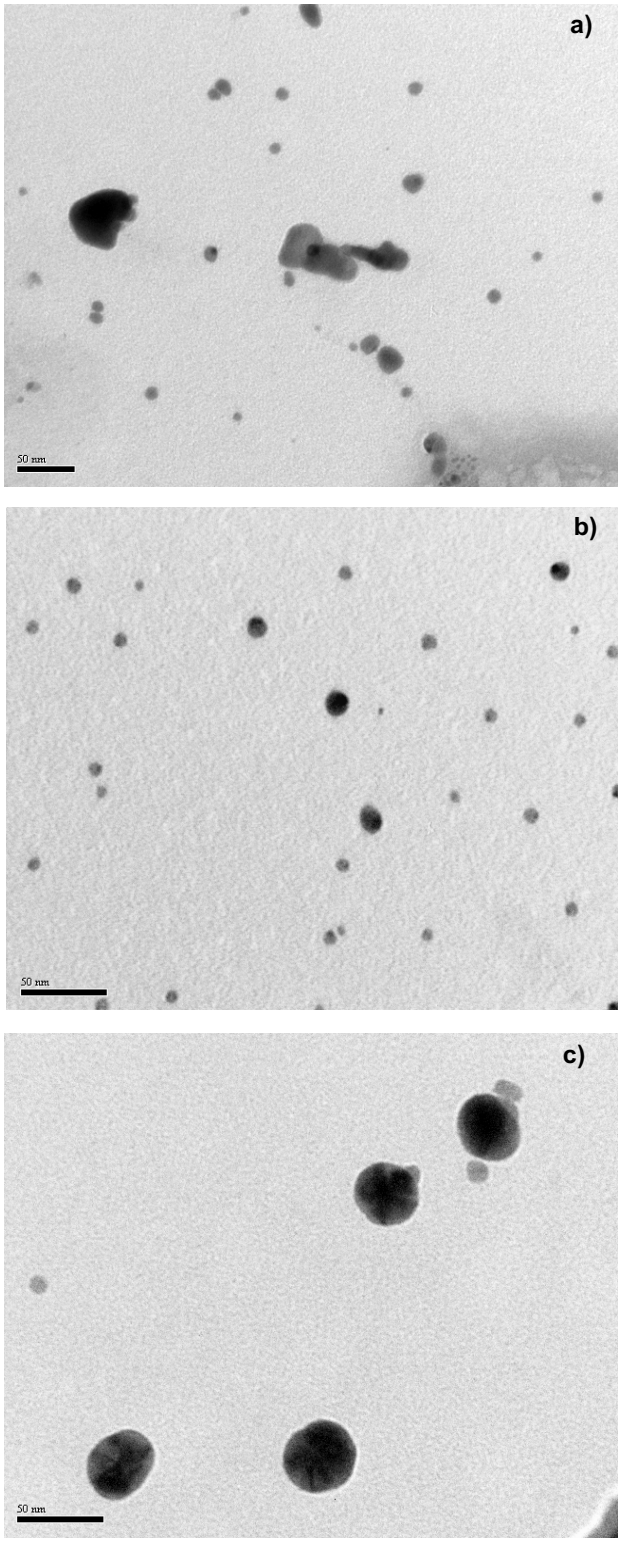

Figure 4.2 TEM images of a) citrate stabilized-Ag NPs, b) pectin stabilized-Ag NPs, and c) alginate stabilized-Ag NPs.

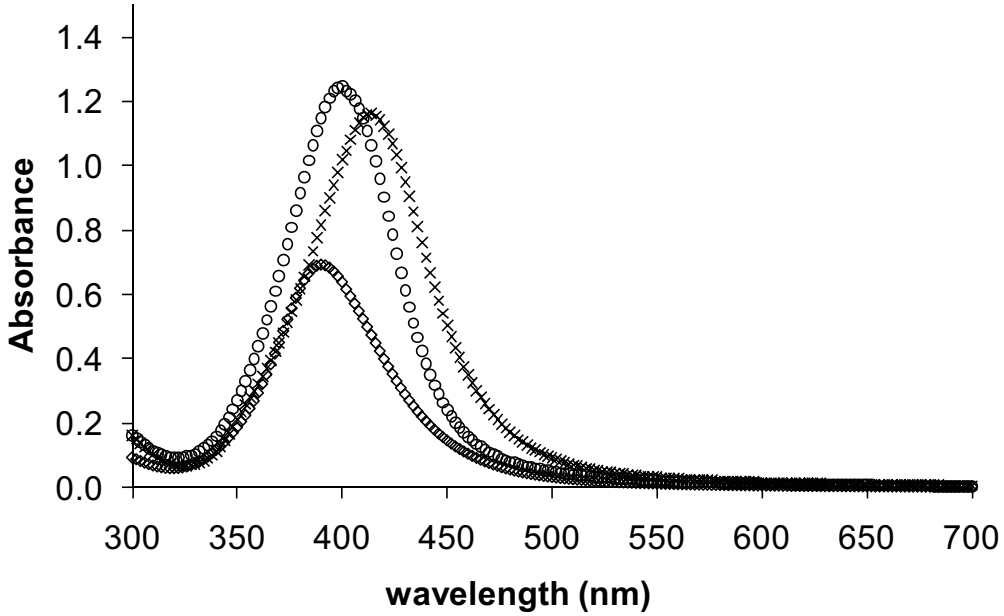

Figure 4.3 UV-visible absorption spectra of silver nanoparticles prepared by different stabilizer agents: (◊) citrate stabilized-Ag NPs; (O) pectin stabilized-Ag NPs; and (×) alginate stabilized-Ag NPs.

Table 4.3 Particle size of silver nanoparticles (Ag NPs) as determined by various techniques

Ag NPs	Particle diameter (nm)			
	TEM	Zetasizer	FlFFF with UV-Vis[a]	FlFFF with ETAAS[a]
Citrate-stabilized	11.3±3.5	13.6±3.1	9.50±0.0	10.5±0.5
Pectin-stabilized	10.5±5.1	18.3±9.4	19.1±0.1	18.2±0.7
Alginate-stabilized	37.5±2.3	48.8±11	45.5±0.1	40.1±0.4

a: the mean particles size (d_{mean}) and associated standard deviation (n=3).

4.3.2 FlFFF with off-line ETAAS detection of silver

Electrothermal atomic absorption spectrometer (ETAAS) was investigated as an off-line detector for FlFFF, as it was previously illustrated possible for SdFFF [18-19]. With the ashing temperature of 800°C and atomization temperature of 1800°C for ETAAS determination of silver, it was possible to completely atomize the fractionated particulate

sample thus avoiding complex and lengthy sample digestion steps [20]. Nonetheless, to confirm the similarity between the atomization behaviors of the Ag NPs and silver ions, calibration experiments were performed for Ag NPs of various types and silver ions. Calibration curves obtained from all silver types indicate that the slopes were not significantly different, suggesting that the analytical sensitivities were the same for silver of all types. It was 0.0227, 0.0214, 0.0235, and 0.0210 for silver ion, citrate stabilized-, pectin stabilized-, and alginate stabilized-Ag NPs, respectively. The standard *t* tests with a significance value of 0.05 were performed for data comparison and indicated that the calibration slopes were not significantly different. Table 4.4 summarizes the characteristic masses, the limits of detection (LOD), and the limits of quantification (LOQ) obtained for silver determination for various types of silver. As the analytical sensitivities obtained for all types of silver examined in this work were not significantly different, it was possible to use the standard calibration prepared from silver ions for determination of silver in the fractionated silver nanoparticles.

Table 4.4 The characteristic mass (m_o), slope, the limit of detection (LOD) and the limit of quantification (LOQ) for silver determination by ETAAS for various types of Ag NPs and silver ion

Sample	Slope	m_o (pg)	LOD (μg L^{-1})	LOQ (μg L^{-1})
Ag ion	0.0227	0.8	2.6	8.7
Citrate stabilized-Ag NPs	0.0214	0.9	2.8	9.3
Pectin stabilized-Ag NPs	0.0235	1.0	2.5	8.4
Alginate stabilized-Ag NPs	0.0210	0.9	2.8	9.4

4.3.3 Ag NPs stability in environmental waters

The stability of Ag NPs in various environmental waters including tap, sea, and ground water was investigated. UV-visible spectrophotometry and FlFFF with ETAAS detection were employed for such investigation. As reported earlier, the shift of the plasmon resonance band of Ag NPs towards the red end or the blue end depends upon the particle size, shape, state of aggregation, and the surrounding dielectric medium [17, 21-

22] . The blue shift is observed when the particles are smaller, and vice versa the red shift is observed when the particles grow larger. Therefore, UV-visible absorption spectrum can be used to examine the stability and the aggregation behavior of citrate stabilized-Ag NPs, as illustrated in Figure 4.4. The maximum absorption of Ag NPs occurred at approximately 400 nm. Upon incubation of Ag NPs in various types of water for 180 min, two bands were observed suggesting that the nanoparticles formed aggregation or deviated from spherical symmetry [17]. Among the three types of Ag NPs synthesized in this study, the stability of alginate stabilized-Ag NPs was higher than that of pectin stabilized- and citrate stabilized-Ag NPs, respectively.

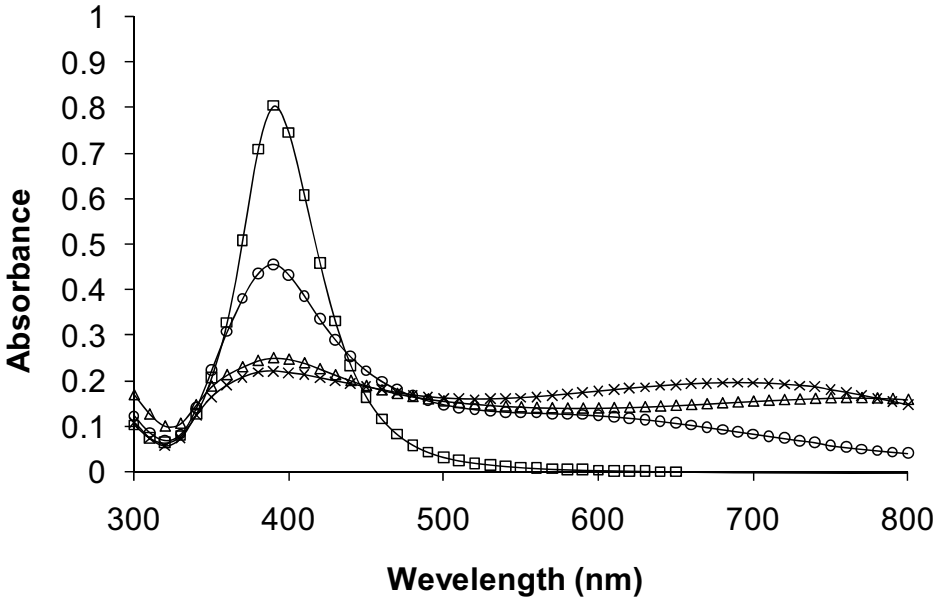

Figure 4.4 UV-visible absorption spectra obtained for citrate stabilized-Ag NPs in different types of environmental water: ( ) deionized water; ( ) tap water; (r) ground water; and (×) sea water, at contact time of 180 min.

Flow FFF with ETAAS detection was also employed to observe the changes in particle size distribution of various types of Ag NPs upon incubation in various types of water for 180 min as summarized in Table 4.5. No peak was observed for Ag NPs dispersed in seawater, suggesting that seawater caused change in Ag NPs into free Ag ion or other non-detectable forms. Changes in particle size of Ag NPs were very significant when dispersed in ground water, as compared to those in tap water. In ground water, no peak was observed for citrate stabilized-Ag NPs, whereas it was detectable for other types of Ag NPs, suggesting that the stability of citrate stabilized-Ag NPs was poorer

than that of other types of Ag NPs. Figure 4.5 illustrates the hydrodynamic diameter distribution of citrate stabilized-Ag NPs dispersed in various types of water. Further experiments are necessary to investigate parameters affecting changes in particle size of Ag NPs. Tap water was selected to be investigated.

Table 4.5 The particles size of Ag NPs dispersed in various environmental waters

	Particle size (nm) of Ag NPs in various types of water as determined by FlFFF-ETAAS		
Ag NPs	Deionized water	Tap water	Ground water
Citrate stabilized-	10.5	16.7	n.d.
Pectin stabilized-	18.2	19.7	21.2
Alginate stabilized-	40.9	40.9	36.7

n.d. – not detectable

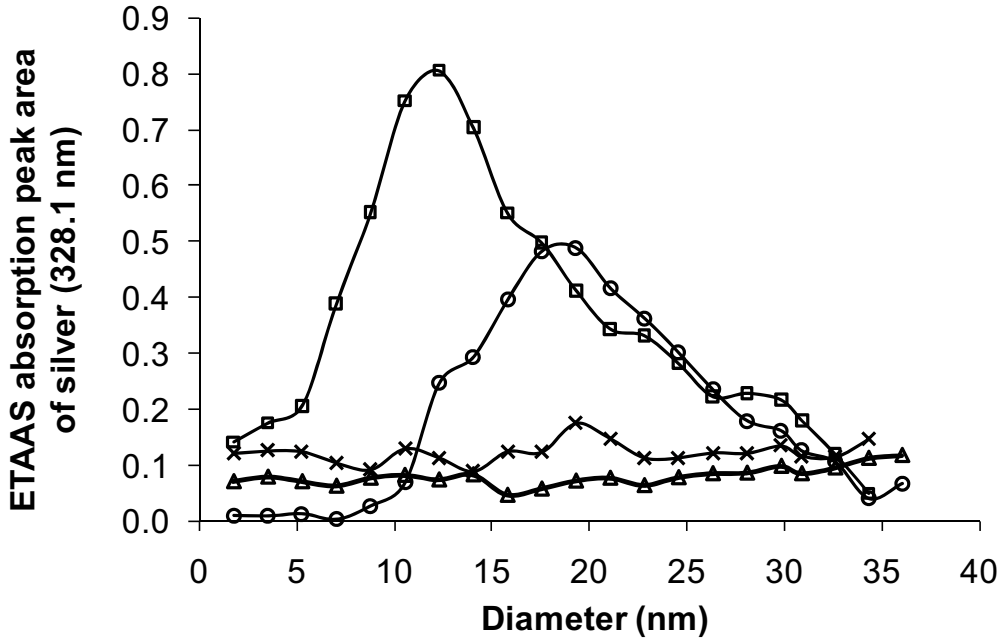

Figure 4.5 Hydrodynamic diameter distributions of citrate stabilized-Ag NPs in different types of environmental water: (□) deionized water; (O) tap water; (△) ground water; and (×) sea water, at contact time of 180 min. ETAAS was used as FlFFF detector.

4.3.4 Parameters affecting particle size of Ag NPs in tap water

In environmental waters, the stability of Ag NPs depends on their surface properties, pH, ionic strength, and the presence of natural organic macromolecules and their concentrations [1,7,13,23]. The stability of the colloidal systems in natural water can be governed by two fundamental mechanisms, which are steric repulsion and charge stabilization or electrostatic interaction [24-25]. The steric repulsion refers to the adsorption of polymers or macromolecules onto the particle surface preventing the particle surfaces coming into close contact with each other. Charge stabilization or electrostatic interaction refers to the distribution of charge species in the system.

For this reason, stabilizing agent was added in the Ag NPs synthesis process to prevent nanoparticles from aggregation and control the particle size of the Ag NPs. Various stabilizing agents, including alginate, citrate, and pectin, were used in the synthesis of Ag NPs. The stability of Ag NPs prepared from different stabilizing agents in environmental waters including tap, sea, and ground water was examined.

4.3.4.1 Types of stabilizing agent

Ag NPs were dispersed in tap water and UV-visible spectrophotometer was employed to investigate the stability of Ag NPs prepared from various stabilizing agents as shown in Figure 4.6. Among the three types of Ag NPs synthesized in this study, the stability of Ag NPs stabilized by alginate was found higher than those stabilized by pectin and citrate, respectively. This information is in good agreement with the zeta potential value (mV) of each Ag NPs as -51.3 ± 1.6, -35.6 ± 2.3 and -34.7 ± 2.4 for alginate, pectin, and citrate stabilized Ag NPs, respectively. The nanoparticles with zeta potential more negative than -30 mV or more positive than +30 mV are electrically stabilized while nanoparticles with low zeta potentials tend to form aggregates [25].

These findings can be described by steric repulsion. The structure of stabilizing agent is the key factor to control Ag NPs stability; larger steric structure offers higher stability than the smaller steric structure [17]. Therefore, alginate stabilized Ag NPs should have higher stability than pectin and citrate stabilized Ag NPs, respectively, according to the molecular weight of citrate, pectin, and alginate as 258, 30,000-100,000, and 100,000-200,000 g mol^{-1}, respectively.

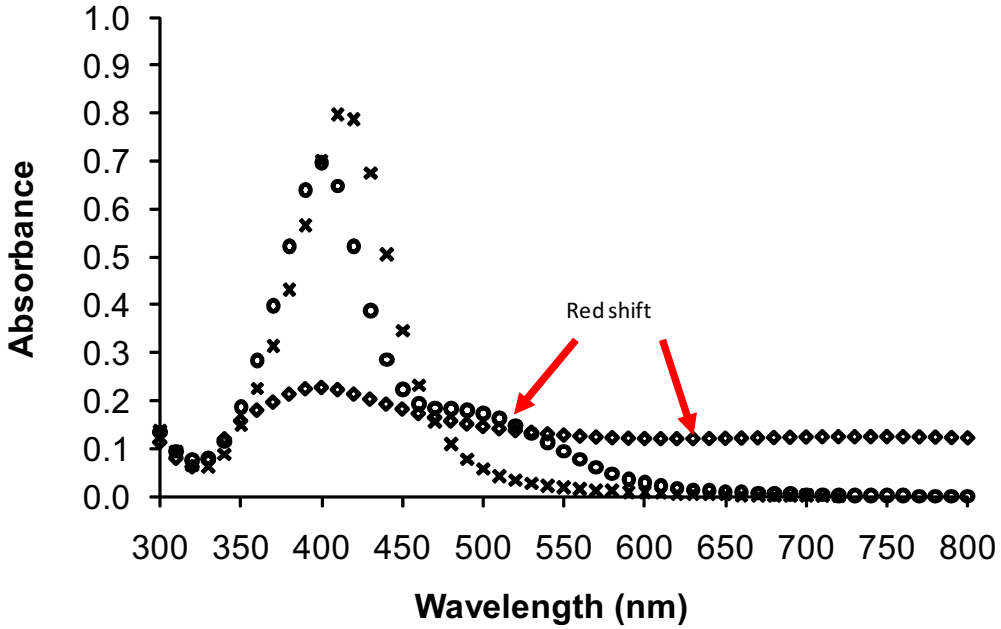

Figure 4.6 UV-visible absorption spectra obtained for Ag NPs prepared from different stabilizing agents: (◊) citrate stabilized-Ag NPs; (O) pectin stabilized-Ag NPs;, and (×) alginate stabilized-Ag NPs in tap water, at contact time of 180 min.

4.3.4.2 Effect of contact time

The particle size information obtained from FlFFF with ETAAS detection and zeta potential value from zeta potentiometer were used to provide evidence on Ag NPs aggregation. The aggregation of 20 mg L^{-1} citrate-stabilized Ag NPs in tap water was temporally investigated as demonstrated by shifts in size distributions with increasing contact time. With increasing contact time, the size distributions slightly broadened. The peak maximum appeared at larger diameter size, showing clear evidence of Ag NPs aggregation. The particle size at peak maximum (d_p) and the mean particle size (d_{mean}) increased with increasing contact time (Figure 4.7a), suggesting that the aggregation process gradually occurred. The aggregation of Ag NPs was confirmed by zeta potentiometer, and the results are shown in Figure 4.7b. The zeta potential values were less negative with increasing contact time, suggesting that the nanoparticles became less stable.

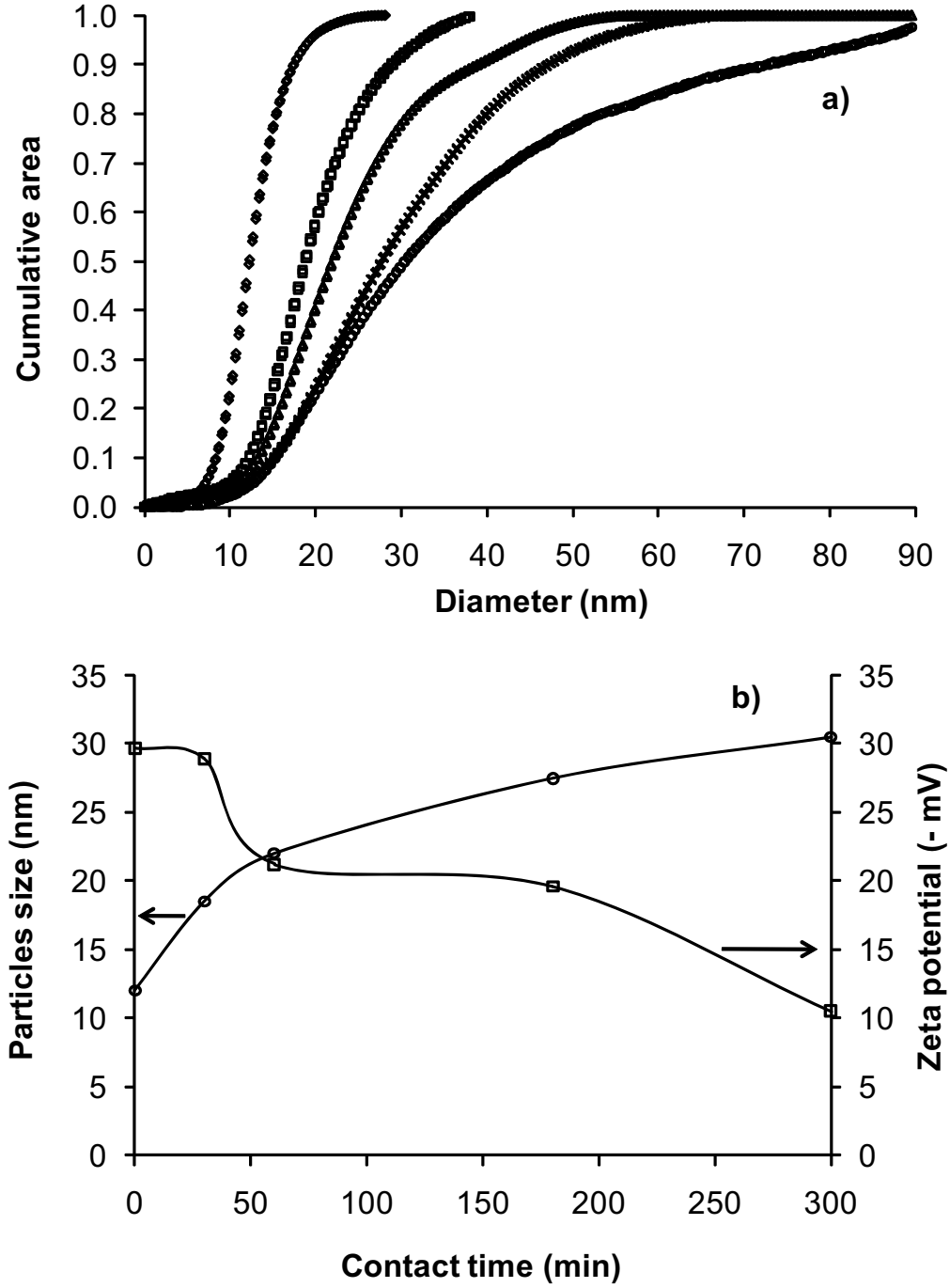

Figure 4.7 a) The cumulative area plot of 20 mg L^{-1} citrate stabilized-Ag NPs in tap water at various contact times: (◊) 0 min; (□) 30 min; (△) 60 min; (×) 180 min; (o) 300 min. b) Diagram showing the particles size and zeta potential value at various contact times.

4.3.4.3. Effect of Ag NPs concentration

The concentration of silver nanoparticles also affects on stability of nanoparticles in water. Therefore, the effect of Ag NPs concentration was examined, as

shown in Figure 4.8. The mean particle size (d_{mean}) increased when the concentration of Ag NPs decreased. This might be explained by using the DLVO theory, by which the ions present in water cause charge shielding effect, reducing the diffuse layer size and thereby allowing NPs to come into contact sufficiently closely to produce aggregation [26-27]. The very low ion concentrations in tap water were not effective to shield charge of high amount of nanoparticles, but they were sufficient to shield charge of small amount of nanoparticles.

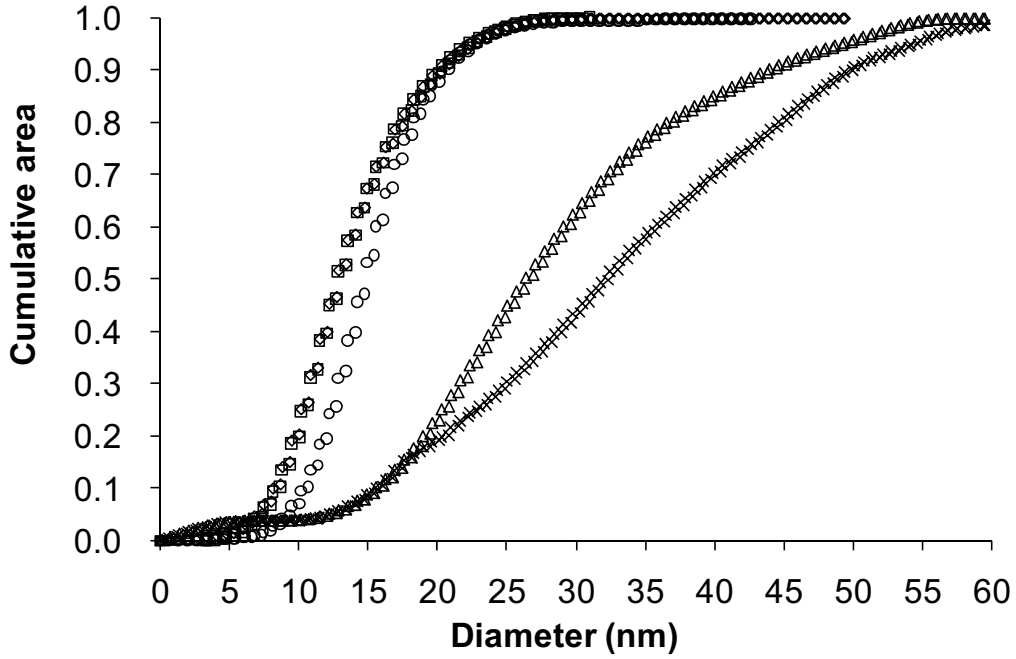

Figure 4.8 The cumulative area plot of particle size of citrate stabilized-Ag NPs in tap water at varying concentrations of Ag NPs: ( )53 ppm; ( ) 40 ppm; (○) 30 ppm; ( ) 20 ppm; and (×) 10 ppm.

4.3.4.4 Effect of humic acid

The dissolved organic matter and natural organic macromolecules (NOM) in natural water may react with Ag NPs, which influenced on the stability of Ag NPs. As humic substances are the most important class of NOM in aquatic environment, citrate stabilized-Ag NPs were investigated for their stability in tap water, both in the absence and presence of humic acid using FlFFF with ETAAS detection and zeta potential measurement, as illustrated in Figures 4.9 and 4.10, respectively. In the absence of humic acid, the particles sizes of citrate stabilized-Ag NPs increased with longer contact time, as shown in Figure 4.9 a) and the zeta potential values also became less negative with increasing contact time (Figure 4.10). In the presence of humic acid of 200 mg L^{-1},

the particles sizes remained unchanged in tap water even at 180 min contact time (Figure 4.9 b), suggesting that Ag NPs were stabilized with humic acid. This was further confirmed by the observation that the zeta potential values of Ag NPs in the presence of humic acid remained stable with increased contact time, as shown in Figure 4.10. These findings are related with the previous reports by Hahn and Stumm [28] who discussed about the effect of NOM to stabilize inorganic colloids in natural waters and Diegoli et al. [17] who reported that humic acid could stabilize the gold colloids in natural waters. Humic acid might cause aggregates to re-disperse or stabilize Ag NPs by steric repulsion [23, 29-30].

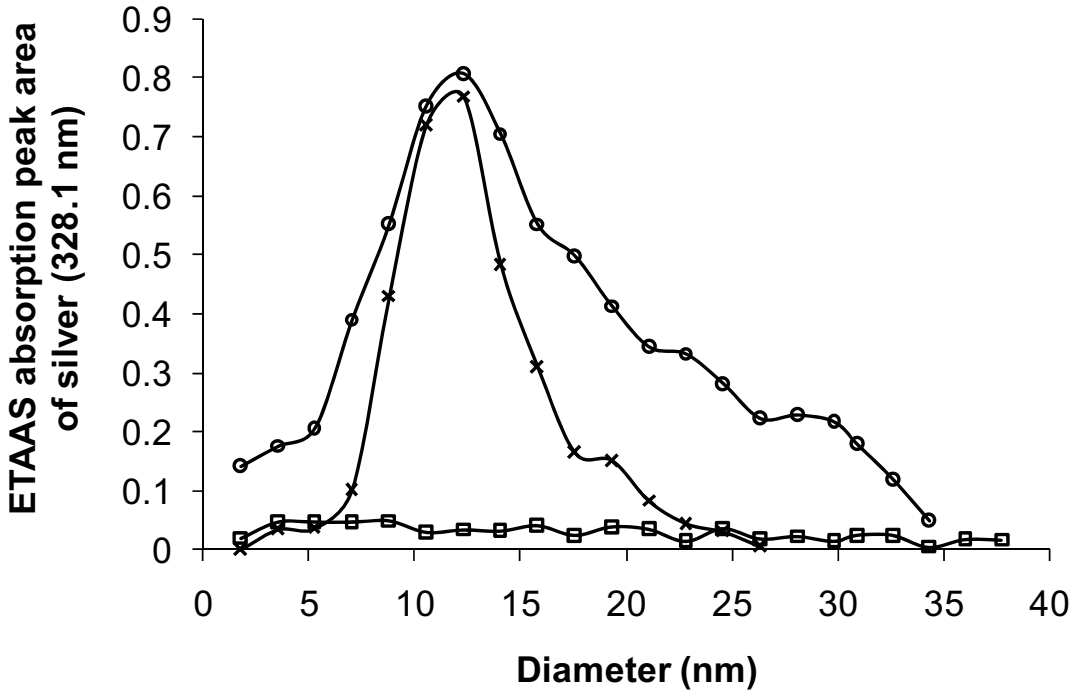

Figure 4.9 Particles size distribution of citrate stabilized-Ag NPs: (O) without humic acid in deionized water; (□) without humic acid in tap water; and (×) with 200 mg L^{-1} humic acid in tap water, at contact time of 180 min. ETAAS was used as FlFFF detector.

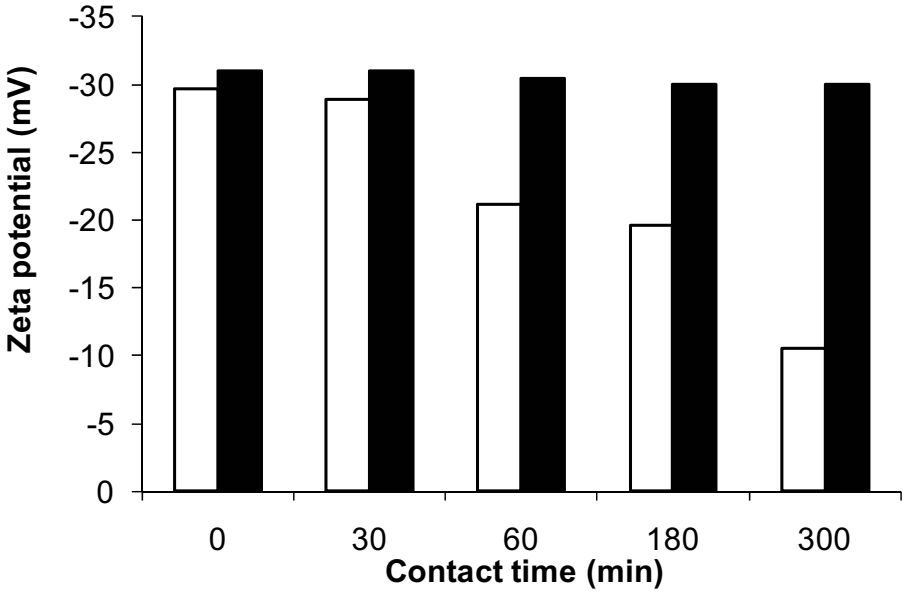

Figure 4.10 Zeta potential values of citrate stabilized-Ag NPs in tap water in the absence (□) and presence (■) of 200 mg L^{-1} humic acid.

4.4 Summary

Electrothermal atomic absorption spectrometry (ETAAS) was found efficient as an element specific detector for detection of silver in Ag NPs samples fractionated by FlFFF. In environmental water, citrate stabilized-Ag NPs undergo rapid aggregation than pectin and alginate stabilized-Ag NPs, suggesting that the surface property is the key factor that control the stability of Ag NPs in aquatic system. Humic acid affects on the stability of Ag NPs in the environment. In summary, the stability of Ag NPs in environmental water depends on the environment conditions such as types of stabilizing agent, contact time, Ag NPs concentration, and the presence of humic acid.

4.5 References

1. S.N. Luoma, PEN Report, Woodrow Wilson International Center for Scholars and The Pew Charitable Trusts, Washington, DC, US, 2008.
2. J. Liu, R.H. Hurt, Environ. Sci. Technol. 44 (2010) 2169.
3. L. Geranio, M. Heuberger, B. Nowack, Environ. Sci. Technol. 43 (2009) 8113.
4. S.A. Blaser, M. Scheringer, M. MacLeod, K. Hungerbühler, Sci. Total Environ. 390(2008) 396.
5. T.M. Benn, P. Westerhoff, Environ. Sci. Technol. 42(2008) 4133.

6. O. Choi, Z. Hu, Environ. Sci. Technol. 42(2008) 4583.
7. J. Fabrega, S.R. Fawcett, J.C. Renshaw, J.R. Lead, Environ. Sci. Technol. 43(2009) 7285.
8. T.M Tolaymat, A.M. EI Badawy, A. Genaidy, K. G. Scheckel, Sci. Total Environ. 48(2010) 999.
9. D.D. Evanoff Jr, G. Chumanov. Chem. Phys, 6(2005) 1221.
10. A. Panácek, L. Kvítek, R. Prucek, M. Kolár, R. Vecerova, N. Pizúrová, V.K. Sharma, T. Nevecna, R. Zboril, J. Phys. Chem. B 110(2006) 16248.
11. P. Raveendran, J. Fu, S.L. Wallen, J. Am. Chem. Soc. 125(2003) 13940.
12. R.F. Domingos, M.A. Baalousha, Y.J. Nam, M.M. Reid, N. Tufenkji, J.R. Lead, G.G. Leppard, K.J. Wilkinson, Environ. Sci. Technol. 43(2009) 7277.
13. S.A. Cumberland, J.R. Lead, J. Chromatogr. A 1216(2009) 9099.
14. M. Baalousha, J.R. Lead, Sci. Total Environ. 386(2007) 93.
15. K. Tiede, A.B.A. Boxall, S.P. Tear, J. Lewis, H. David, M. Hassellöv, Food Addit. Contam. A 25(2008) 795.
16. J. Yang, J.Y. Lee, L.X. Chen, H.P. Too, J. Phys. Chem. B 109(2005) 5468.
17. S. Diegoli, A.L. Manciulea, S. Begum, I.P. Jones, J.R. Lead, J.A. Preece, Sci. Total Environ. 402(2008) 51.
18. G. Blo, A. Ceccarini, C. Conato, C. Contado, F. Fagioli, R. Fuoco, A. Pagnoni, F. Dondi, Anal. Bioanal. Chem. 384(2006) 922.
19. C. Contado, G. Blo, F. Fagioli, F. Dondi, R. Beckett, Colloid Surface A 120(1997) 47.
20. P. Liang, L. Peng, Microchimica Acta, 168(2010) 45.
21. I.E. Sendroiu, S.F.L. Mertens, D.J. Schiffrin, Phys. Chem. Chem. Phys. 8(2006) 1430.
22. P. Mulvaney, , Langmuir, 12(1996) 788.
23. E.Navarro, A. Baun, R. Behra, N.B. Hartmann, J. Filser, A.J. Miao, A. Quigg, P.H. Santschi, L. Sigg, Ecotoxicology 17(2008) 372.
24. W. Kreyling, M. Semmler-Behnke, W. Möller, J. Nanopart. Res. 8(2006) 543.
25. Zeta Potential, An Introduction in 30 Minutes. Zetasizer Nano Series technical note, (MRK654-01), Malvern Instruments, Worcestershire, UK, 2006.
26. H. Christenson, J. Chem. Soc. 80(1984) 1933.
27. S.Elzey, V. Grassian, J. Nanopart. Res. 12(2009) 1945.
28. W. Stumm, Chemistry of the solid-water interface: processes at the mineral-water and particle-water interface in natural systems, New York, US, 1992.
29. M. Farré, K. Gajda-Schrantz, L. Kantiani, D. Barceló, Anal. Bioanal. Chem. 393(2009) 81.
30. J. Buffle, K.J. Wilkinson, S. Stoll, M. Filella, J. Zhang, Environ. Sci. Technol. 32(1998) 2887.

Output (RSA 5180009)

โครงการ การพัฒนาวิธีการเตรียมและวิธีการวิเคราะห์อนุภาคระดับนาโนเมตรและไมโครเมตร เพื่อประยุกต์ใช้เป็นอนุภาคนำส่งสำหรับสารเสริมสุขภาพ

ผลงานตีพิมพ์ในวารสารวิชาการนานาชาติ 4 เรื่อง

1. Somchue, W., Sermsri, W., Shiowatana, J. & Siripinyanond, A. 2009, "Encapsulation of α-Tocopherol in Protein-based Delivery Particles", *Food Res. Int.,* vol. 42, pp. 909–914. (impact factor = 2.414)
2. Sermsri, W., Jarujamras, P., Shiowatana, J. & Siripinyanond, A. 2010, "Flow Field-Flow Fractionation: A Versatile Approach for Size Characterization of α-Tocopherol-Induced Enlargement of Gold Nanoparticles", *Anal. Bioanal. Chem.,* vol. 396, pp. 3079–3085. (impact factor = 3.480)
3. Samontha, A., Shiowatana, J. & Siripinyanond, A. 2011, "Particle Size Characterization of Titanium Dioxide in Sunscreen Products Using Sedimentation Field-Flow Fractionation-Inductively Coupled Plasma Mass Spectrometry", *Anal. Bioanal. Chem.,* vol. 399, pp. 973–978. (impact factor = 3.480)
4. Songsilawat, K., Shiowatana, J. & Siripinyanond, A. 2011, "Flow Field-Flow Fractionation with Off-line Electrothermal Atomic Absorption Spectrometry for Size Characterization of Silver Nanoparticles", *J. Chromatogr. A,* vol. 1218, pp. 4213–4218. (impact factor = 4.101)

ผลงานเสนอในการประชุมวิชาการนานาชาติ 5 เรื่อง

1. Atitaya Samontha, Juwadee Shiowatana and Atitaya Siripinyanond, Ti Size Characterization in Sunscreen Products Using Sedimentation Field-Flow Fractionation-Inductively Coupled Plasma-Mass Spectrometry, **Pure and Applied Chemistry International Conference (PACCON 2010)**, January 21 – 23, 2010, Ubon Ratchathani, Thailand.
2. Kanchana Songsilawat, Juwadee Shiowatana and Atitaya Siripinyanond, Field-Flow Fractionation Coupled with GFAAS for Size Characterization of Silver Nanoparticles, **Pure and Applied Chemistry International Conference (PACCON 2010)**, January 21 – 23, 2010, Ubon Ratchathani, Thailand.
3. Kanchana Songsilawat, Manita Untang, Juwadee Shiowatana and Atitaya Siripinyanond, Field-Flow Fractionation Coupled with GFAAS for Size Characterization of Silver Nanoparticles, **16th**

International Conference on Flow Injection Analysis (ICFIA), April 25 – 30, 2010, Pattaya, Thailand.

4. Atitaya Samontha, Juwadee Shiowatana and Atitaya Siripinyanond, Investigation of Elemental Size Distribution of Nanoparticles in Household Products Using Sedimentation Field-Flow Fractionation-Inductively Coupled Plasma Mass Spectrometry (SdFFF-ICP-MS), **16th International Conference on Flow Injection Analysis (ICFIA),** April 25 – 30, 2010, Pattaya, Thailand.
5. Atitaya Siripinyanond, Kanchana Songsilawat, Supharart Sangsawong and Juwadee Shiowatana, Field-Flow Fractionation with Off-line Electrothermal Atomic Absorption Spectrometry for Size Characterization of Silver Nanoparticles, **15th International Symposium on Field- and Flow-Based Separations (FFF 2011)**, May 23 – 25, 2011, South San Francisco, California, U.S.A.

Food Research International 42 (2009) 909–914

Contents lists available at ScienceDirect

Food Research International

journal homepage: www.elsevier.com/locate/foodres

Encapsulation of α-tocopherol in protein-based delivery particles

W. Somchue, W. Sermsri, J. Shiowatana, A. Siripinyanond *

Department of Chemistry and Center for Innovation in Chemistry, Faculty of Science, Mahidol University, Rama VI Rd., Bangkok 10400, Thailand

ARTICLE INFO

Article history:
Received 5 December 2008
Accepted 26 April 2009

Keywords:
β-Lactoglobulin
Hen egg white
α-Tocopherol
Encapsulation
Nutraceutical delivery

ABSTRACT

Two types of proteins, including β-lactoglobulin (BLG) and hen egg white protein (HEW), were examined for their ability to encapsulate α-tocopherol (α-TOC) after salt-induced gelation of the proteins. Parameters affecting encapsulation efficiency were investigated including the type of salt, as well as concentrations of salt, protein, and α-TOC. Concentrations of protein and α-TOC revealed to have an influence on encapsulation efficiency. The optimum preparation condition of BLG-encapsulated α-TOC was as follows: BLG of 0.5% (w/v); α-TOC of 100 mM; and $CaCl_2$ of 25 mM. The optimum preparation condition of HEW-encapsulated α-TOC was as follows: HEW of 4.0% (w/v); α-TOC of 50 mM; and $ZnCl_2$ of 25 mM. With the selected preparation conditions, encapsulation efficiency by BLG aggregates was approx. 20% and that by HEW was approx. 32%. From the *in vitro* estimation, the release of α-TOC was nearly 100% in simulated gastric condition. Alginate was therefore used for coating of these encapsulated particles to prolong the release of α-TOC till simulated intestinal condition. The α-TOC of approx. 55% and 38% were retained and released in the simulated intestinal condition from BLG- and HEW-encapsulated particles, respectively.

1. Introduction

Vitamin E is an important antioxidant that can help reduce risk of diseases such as cardiovascular diseases (Blatt, Pryor, Mata, & Proteau, 2004; Brigelius-Flohé & Traber, 1999; Mardones & Rigotti, 2004; Pryor, 2000; Tucker & Townsend, 2005). Although vitamin E deficiency is rare in humans, absorption of vitamin E is reduced in the patients with some diseases including pancreatic diseases, biliary obstruction, coeliac disease, and abetalipoproteinaemia. Therefore, supplementation of vitamin E is needed in some cases. Vitamin E exists in eight different forms including four tocopherols (α, β, γ, and δ) and four tocotrienols (α, β, γ, and δ), but vitamin E supplements are usually available in forms of relatively stable all-rac α-tocopherol acetate and all-rac α-tocopherol succinate. Nonetheless, α-tocopherol was believed to be most absorbable in human intestine. Although it was believed that tocopherol esters were hydrolyzed to free tocopherol on the duodenum (Borel, 2003; Borel et al., 2001; Cheeseman et al., 1995) the need of hydrolytic enzyme to de-esterify the supplement cannot guarantee the efficient bioavailability. Consequently, it would be beneficial if vitamin E supplements can be prepared in the free phenol form of α-tocopherol (α-TOC). As it is relatively unstable and sensitive to temperature, oxygen, and light, encapsulation is needed for protection of α-tocopherol during shelf storage. Further, the release of vitamin E on the target digestive system should be controllable with the use of encapsulation technologies (Ubbink & Krüger, 2006).

Encapsulation technologies have gained increased interest to the food industry as they are used to increase stability of the bioactive compounds during processing and storage and also to prevent undesirable interactions with the food matrix. Further, a real benefit of encapsulation is due to the ability to control the release of the incorporated ingredients and deliver them to a specific target at a suitable time. Protein hydrogel has been used as a carrier particle because of its high nutritional value and generally recognized as safe. Various preparation techniques have been used to induce gelation of proteins (Totosaus, Montejano, Salazar, & Guerrero, 2002). These include acid-induced gelation (Alting, Hamer, Kruif, & Visschers, 2003), heat-induced gelation (Dumay, Laligant, Zasypkin, & Cheftel, 1999), and ion-induced gelation processes (Bryant & McClements, 1998, 2000; Croguennec, Nua, & Brulé, 2002; Maltais, Remondetto, & Subirade, 2008; Simons, Kosters, Visschers, & Jongh, 2002). The cold-set gelation has gained wide interest as it offers an advantage to maintain heat-sensitive ingredients (Beaulieu, Savoie, Paquin, & Subirade, 2002; Chen, Remondetto, & Subirade, 2006). Two steps were used to form cold-set gel. Initially, heat treatment was used to cause globular proteins to unfold and expose multiple functional groups within the protein which could create the interaction between the active ingredients and polypeptide chains. After cooling, salt was added to the protein solution to cause aggregation of protein by electrostatic interaction (Chen et al., 2006). Various kinds of globular proteins including soy and whey proteins, especially β-lactoglobulin (BLG), were

* Corresponding author. Tel.: +66 2 201 5195; fax: +66 2 354 7151.
E-mail address: scasp@mahidol.ac.th (A. Siripinyanond).

0963-9969/$ - see front matter © 2009 Elsevier Ltd. All rights reserved.
doi:10.1016/j.foodres.2009.04.021

examined for their gelation characteristics. Further, gelation behavior of hen egg white protein (HEW) has been described by many researchers.

Due to its amphiphilic nature, BLG was reported to bind with small lipid molecules such as cholesterol (Wang, Allen, & Swaisgood, 1997), fatty acid (Wu, Pérez, Puyol, & Sawyer, 1999), vitamin A (Pérez & Calvo, 1995), vitamin D (Wang et al., 1997), and vitamin E (Swaisgood, Wang, & Allen, 2001; Voth & Miller, 1958). It was illustrated that the globular proteins were adsorbed to the emulsion interface and formed continuous and homogeneous membrane around the oil droplets through β-sheet interaction (Beaulieu et al., 2002; Lefévre & Subirade, 2003; Line, Remondetto, & Subirade, 2005). Moreover, the hydrogel of BLG could entrap fat-soluble ingredients to keep them in the active form until the time of consumption (Chen et al., 2006).

Hen egg white protein, a low cost protein, has been widely used as ingredients in many food products as it possesses several excellent functional properties such as foaming, emulsification, heat setting, and binding adhesion. Hen egg white is composed of various types of proteins, including 54.0% ovalbumin (44.5 kDa), 12.0% ovotransferrin (77.7 kDa), 11.0% ovomucoid (28.0 kDa), 3.5% ovomucin (5500–8300 kDa), 3.4% lysozyme (14.3 kDa), and a few other proteins. Hen egg white protein was demonstrated to form stable intermolecular β-sheet structures during the thermal denaturation (Mine, 1995). Heat caused the protein molecules to partially unfold to expose their hydrophobic residues to allow adsorption of fat-soluble components forming continuous and homogeneous membrane around the oil droplets through β-sheet interaction.

In order to control the release of active ingredients at the intestinal tract, alginate coating was employed to prevent hydrolysis of protein hydrogel from proteolytic enzymatic digestion in gastric condition (Chen & Subirade, 2006, 2007; Pongsawatmanit, Harnsilawat, & McClements, 2006; Sriamornsak & Kennedy, 2007). In gastric condition, protonation converted sodium alginate to insoluble alginic acid that could protect diffusion of the active ingredients from the alginate-coated protein hydrogel. In intestinal condition, the alginate matrix swelled allowing the release of the active ingredients (Chen et al., 2006).

This study was carried out to evaluate the ability of BLG and hen egg white protein (HEW) aggregates induced by salt as protein-based particles for encapsulation of α-TOC in its free phenol form. Parameters affecting encapsulation efficiency including concentrations of proteins, α-TOC, and salt were examined. The release of α-TOC from the encapsulated particles was investigated. The use of alginate coating for protection of α-TOC release in the gastric condition was also explored. This study shows a successful attempt to use protein-based particles in combination with alginate to allow delivery of α-TOC to intestinal for bioavailability improvement.

2. Materials and methods

2.1. Chemicals

(±)-α-Tocopherol, sodium alginate, sodium phosphate monohydrate and sodium phosphate dibasic dodecahydrate were purchased from Fluka Chemie GmbH, Buchs, Germany. β-Lactoglobulin (from bovine milk, approx. 90% purified using polyacrylamide gel electrophoresis and lyophilized), pepsin 1:10,000 (from porcine stomach mucosa, crystallized and lyophilized), pancreatin (from porcine pancreas), 2,2′-bipyridyl and $ZnCl_2$ were purchased from Sigma, St. Louis, MO, USA. $FeCl_3$ and $CaCl_2$ were purchased from Riedel-de Haën, Seelze, Germany. α-Tocopherol stock solutions of the appropriate concentrations were diluted in ethanol (Lab Scan Asia Co., Ltd., Bangkok, Thailand).

2.2. Preparation of protein solutions

β-Lactoglobulin powder was dissolved in deionized water to obtain a stock solution of 6% (w/v). To cause BLG to unfold, the 6% (w/v) BLG solution (pH 7.5) was heated at 80 °C for 30 min and cooled to room temperature (27 °C) (Saeseaw, Shiowatana, & Siripinyanond, 2006). Hen egg white protein powder was prepared using the procedure described by Croguennec et al. (2002). Hen egg white protein powder was dissolved in deionized water to obtain a stock solution of 8% (w/v). To cause HEW to unfold, the 8% (w/v) HEW solution (pH 8.0) was heated at 40 °C for 30 min and cooled to room temperature (27 °C). The proteins solutions, BLG and HEW, were filtered through 0.45 m cellulose acetate syringe filter before use.

2.3. Preparation of protein based-encapsulated α-TOC

Salt-induced gelation technique was used for preparation of protein based-encapsulated α-TOC. To prepare BLG-encapsulated α-TOC, appropriate concentration of α-TOC was mixed with appropriate concentration of BLG solution and subsequently $CaCl_2$ was added to induce aggregation of BLG. The molar ratio of protein and α-TOC and salts was 2:1:1. A method to prepare HEW-encapsulated α-TOC was similar to that of the BLG-encapsulated α-TOC except that $ZnCl_2$ was added instead of $CaCl_2$ to induce aggregation. Parameters affecting encapsulation efficiency of protein-encapsulated α-TOC were examined as follows: 0.5–2% (w/v) BLG; 1–6% (w/v) HEW; 10–150 mM α-TOC; and 10–100 mM salt solutions. The incubation time was 5 h for BLG-encapsulated α-TOC and 30 min for HEW-encapsulated α-TOC.

2.4. Preparation of alginate coated-protein based-encapsulated α-TOC

To prepare alginate coated-BLG-encapsulated α-TOC, appropriate concentration of α-TOC was mixed with appropriate concentration of BLG solution and then appropriate concentration of sodium alginate was added to the mixture with subsequent addition of appropriate concentration of $CaCl_2$ to form gel. The molar ratio of protein and α-tocopherol and alginate and salts was 2:1:2:1. A method to prepare alginate coated-HEW-encapsulated α-TOC was similar to that of alginate coated-BLG-encapsulated α-TOC except that $ZnCl_2$ was added instead of $CaCl_2$ as a gelling and hardening agent. The incubation time was 5 h for alginate coated-BLG-encapsulated α-TOC and 30 min for alginate coated-HEW-encapsulated α-tocopherol.

2.5. Estimation of α-TOC loading

The protein based-encapsulated α-TOC was centrifuged at 12,000 rpm for 30 min (Beckman Allegra X-22R Centrifuge, Palo Alto, USA) to separate the unencapsulated α-TOC from the mixture. The concentration of unencapsulated α-TOC was determined by colorimetric method exploiting the ability of α-TOC to reduce Fe^{3+} into Fe^{2+} which could subsequently form red–orange color with 2,2′-bipyridyl. The absorbance of the resulting solution was measured at 521 nm. Subsequently, the precipitate part containing protein aggregates was dispersed in 30 ml of simulated gastric fluid (SGF) (HCl solution, pH 1.2) with 0.1% pepsin (w/v) at 37 °C under vigorous agitation for 2 h (Chen & Subirade, 2007). The resulting mixture was extracted by hexane solution and α-TOC concentration in the extract was determined by absorbance measurement at 297 nm with a UV–Visible Spectrophotometer (JASCO V530 UV–Visible Spectrophotometer, JASCO, Inc., Tokyo, Japan). The amount of α-TOC encapsulated was calculated by subtraction of the unencapsulated α-TOC from the total amount of α-TOC added. The encapsulation efficiency (EE) was calculated from the

ratio of the encapsulated α-TOC and the added α-TOC. All experiments were performed at least in five replicates ($n = 5$). Estimation of α-TOC loading and calculation of encapsulation efficiency of alginate coated-protein based-encapsulated α-TOC were performed in the same way as described for the protein based-encapsulated α-TOC. All experiments were performed at least in five replicates. Graphs were plotted with error bars showing the standard deviation of the results obtained.

2.6. Estimation of in vitro release of alginate coated-protein based-encapsulated α-TOC and evaluation of α-TOC release kinetics

The release of α-TOC from alginate coated-protein based-encapsulated α-TOC was determined by incubating the encapsulated particles in 30 ml of simulated gastric fluid (SGF) (HCl solution, pH 1.2) with 0.1% pepsin (w/v) at 37 °C under vigorous agitation by an incubator shaker (Grant Instrument, model SS40-D2, Cambridge, England) for 2 h and then the supernatant was separated from the swollen aggregates for further determination of α-TOC concentration. The release of α-TOC in SGF condition was determined by absorbance measurement at 297 nm after extraction of the released α-TOC from the supernatant part with hexane. Subsequently, the swollen aggregate was digested by 30 ml of simulated intestinal fluid (SIF) (phosphate buffer in saline solution, pH 7.4) with 1.0% pancreatin (w/v) at 37 °C under vigorous agitation for 4 h. The release of α-TOC in SIF condition was determined by absorbance measurement at 297 nm after extraction of the released α-TOC with hexane. The percentages of released amount of α-TOC in SGF and SIF conditions are presented as $\%R_{SGF}$ and $\%R_{SIF}$, respectively. These percentages were calculated from the ratio of the released amount from each digestion condition and the encapsulated amount in the aggregates, by which the resulting numbers were multiplied by 100.

To evaluate the release kinetics of α-TOC, the encapsulated particles were incubated in simulated gastric fluid for 2 h and subsequently in simulated intestinal fluid at various incubation times of 10, 20, 30, 60, 90, 120, 180, 240, 300, and 360 min. Hexane was added to allow extraction of the released α-TOC into the hexane portion followed by absorbance measurement at 297 nm.

3. Results and discussion

3.1. Selection of divalent cation for the preparation of protein based-encapsulated α-TOC by cold gelation

Cold gelation of protein can be achieved by adding salts including monovalent or divalent cations, e.g., Na^+; Ca^{2+}; or Zn^{2+} to the solution containing charged protein molecules (Foegeding, Kuhn, & Hardin, 1992; Saeseaw et al., 2006). To perform salt-induced gelation of proteins, $CaCl_2$ and $ZnCl_2$ were used as they are listed as generally recognized as safe (GRAS) by the United States of America Food and Drug Administration when used in accordance with good manufacturing practice (FDA, 2008). Our earlier investigations indicated that salt-induced gelation of BLG or HEW was best achieved by $CaCl_2$ or $ZnCl_2$, respectively (Saeseaw et al., 2006; Samontha, Nipattamanon, Shiowatana, & Siripinyanond, 2008). One might argue that aggregate formation could already be obtained by mixing BLG with α-TOC. Without addition of $CaCl_2$, however, the added α-TOC was mostly found in the supernatant part suggesting that they were not encapsulated in BLG aggregates. Conversely, without addition of $ZnCl_2$ to the mixture of HEW and α-TOC, the added α-TOC was found in the aggregate part suggesting that α-TOC was encapsulated in HEW particles. Nonetheless, addition of $ZnCl_2$ to the mixture was carried out as salt was used not only to induce gel formation, but the added $CaCl_2$ or $ZnCl_2$ also acted as a hardening agent for the alginate coating of the encapsulated products.

3.2. Parameters affecting encapsulation efficiency of BLG-encapsulated α-TOC

The concentrations of BLG and α-TOC showed combined influence on encapsulation efficiency of BLG-encapsulated α-TOC as illustrated in Fig. 1. At fixed concentration of BLG, the encapsulation efficiency decreased with increasing concentration of α-TOC for each BLG concentration (Fig. 1a–c). Nonetheless, the mole amount of α-TOC in the aggregate increased with increasing concentration of α-TOC added and reached a plateau at a certain concentration of α-TOC because of the limited amount of BLG. Fig. 1d shows the relationship between the added α-TOC concentration

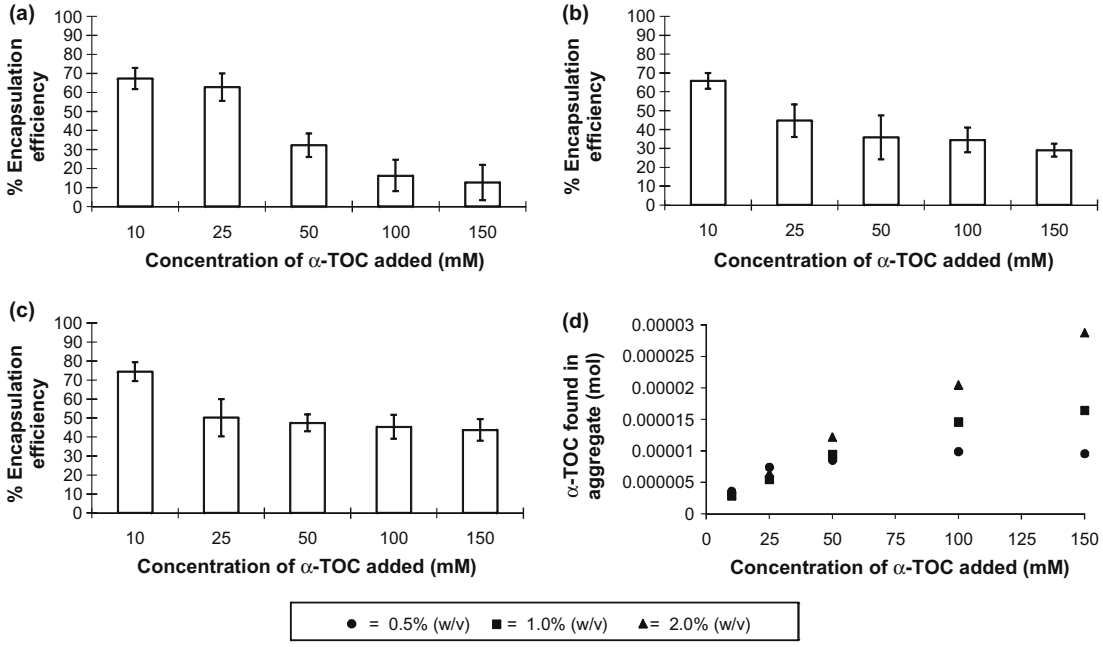

Fig. 1. Effect of α-TOC concentration on its encapsulation efficiency in BLG particles at various concentrations of BLG; (a) 0.5% (w/v), (b) 1.0% (w/v), (c) 2.0% (w/v), with 100 mM $CaCl_2$ as a gelling agent and (d) relationship between concentration of α-TOC added and mole amount of α-TOC encapsulated.

and the mole amount of α-TOC encapsulated at various BLG concentrations. In the excess of BLG at 2% (w/v), a straight line relationship was obtained. Deviation from the straight line was observed when BLG was not adequate for encapsulation of α-TOC. At the plateau, the mole ratio of α-TOC and BLG was calculated to be 140 and 104 for BLG of 0.5% (w/v) and 1% (w/v), respectively, suggesting that the average mole ratio of the two compounds might be at approx. 120. In general, higher protein concentrations can hold higher amount of α-TOC at the fixed concentrations of α-TOC and $CaCl_2$. This statement was confirmed by determining the encapsulation efficiency and the mole amount of α-TOC in the aggregate at various concentrations of BLG at fixed concentrations of α-TOC and $CaCl_2$. The amount of α-TOC encapsulated increased with increasing in BLG concentration (Fig. 1d). β-Lactoglobulin was reported to form continuous and homogeneous membranes around the α-TOC oil droplets through intermolecular β-sheets interaction because of its flexibility and amphiphilic nature (Alzagtat & Alli, 2002; Lefévre & Subirade, 2003). At fixed concentrations of BLG and α-TOC, the change in encapsulation efficiency was not so significant with the change in $CaCl_2$ concentrations (from 10 to 100 mM), as illustrated in Fig. 2. Therefore, only small amount of Ca^{2+} was needed for neutralization of the negatively charged BLG and lowering electrostatic repulsion with the subsequent aggregates formation through intermolecular bridges (Line et al., 2005; Majhi et al., 2006; Simons et al., 2002). Addition of $CaCl_2$ at concentrations higher than 100 mM was not tested, as too high concentration of salt weakened electrostatic interactions, which could suppress aggregate formation because of charge screening effects (Simons et al., 2002).

3.3. Parameters affecting encapsulation efficiency of HEW-encapsulated α-TOC

Similar to the case of BLG-encapsulated α-TOC, the concentrations of HEW and α-TOC showed combined influence on encapsulation efficiency of HEW-encapsulated α-TOC as illustrated in Fig. 3. The encapsulation efficiency decreased with increasing concentration of α-TOC for each HEW concentration (Fig. 3a–c). At fixed concentration of HEW at 1% (w/v), the mole amount of α-TOC in the aggregate was almost constant with increasing in the concentration of α-TOC added. At higher HEW concentrations, however, mole of α-TOC in the aggregate increased with increasing concentration of α-TOC and reached a plateau at a certain concentration of α-TOC because of the limited amount of HEW. Higher protein concentrations can hold higher amount of α-TOC at the fixed concentrations of α-TOC and $ZnCl_2$. This observation was confirmed by fixing the concentrations of α-TOC and $ZnCl_2$ and determining the encapsulation efficiency and the mole amount of α-TOC in the aggregate at various concentrations of HEW (Fig. 4). The amount of α-TOC encapsulated increased with increasing in HEW

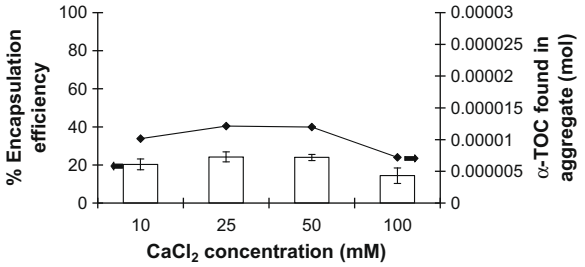

Fig. 2. Effect of $CaCl_2$ concentration on encapsulation efficiency of α-TOC (100 mM) in 0.5% (w/v) BLG particles.

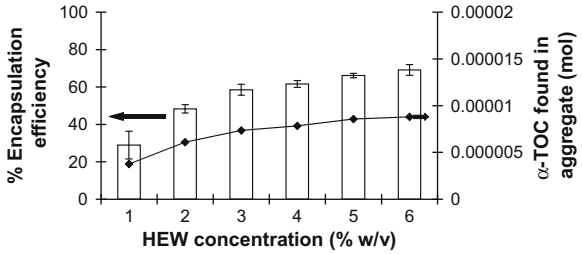

Fig. 4. Effect of HEW concentration on encapsulation efficiency of α-TOC (50 mM) in HEW particles with 25 mM $ZnCl_2$ as a gelling agent.

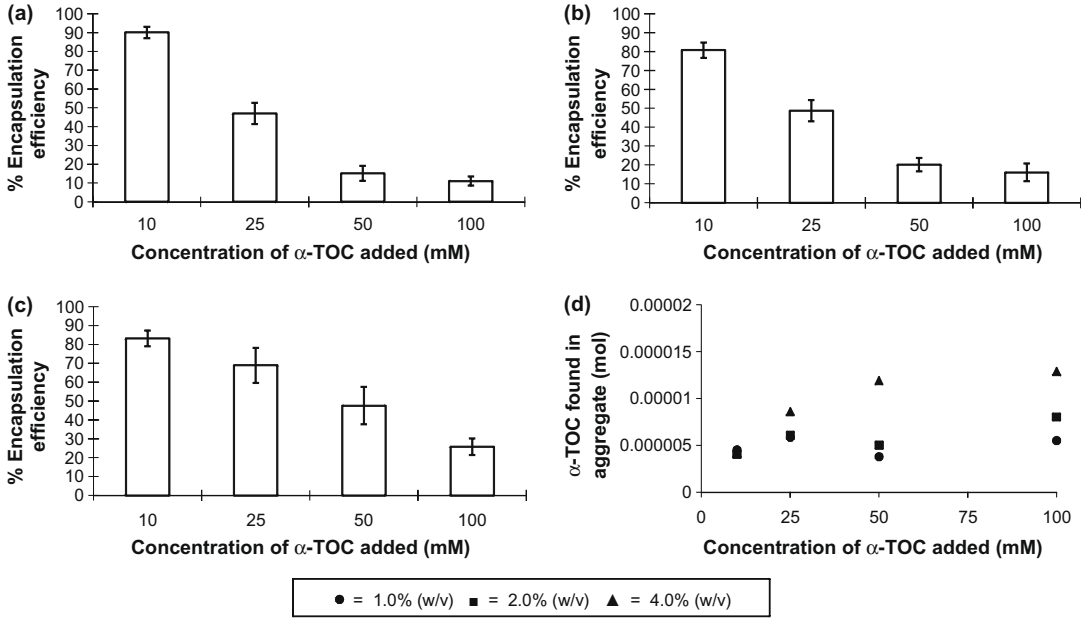

Fig. 3. Effect of α-TOC concentration on its encapsulation efficiency in HEW particles at various concentrations of HEW; (a) 1.0% (w/v), (b) 2.0% (w/v), and (c) 4.0% (w/v), with 25 mM $ZnCl_2$ as a gelling agent. (d) Relationship between concentration of α-TOC added and mole amount of α-TOC encapsulated.

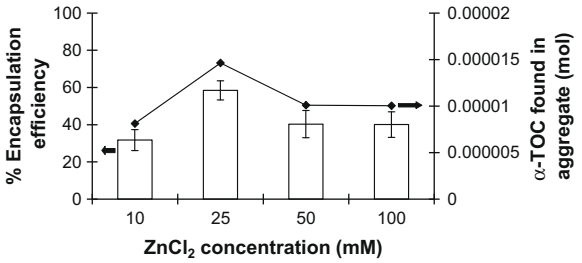

Fig. 5. Effect of $ZnCl_2$ concentration on encapsulation efficiency of α-TOC (50 mM) in 4.0% (w/v) HEW particles.

(Fig. 4). The mole ratio of α-TOC and HEW was not calculated because the composition of HEW was rather complex consisting of various proteins. At fixed concentrations of HEW and α-TOC, the encapsulation efficiency was found to be highest at $ZnCl_2$ concentration of 25 mM (Fig. 5). Therefore, a suitable encapsulation condition for HEW-encapsulated α-TOC was 4% (w/v) HEW with 50 mM α-TOC and 25 mM $ZnCl_2$.

3.4. Release of α-tocopherol from protein-based delivery particles: a comparison between BLG and HEW (with and without alginate coating)

To assess the suitability of BLG or HEW as a protein-based delivery particle for α-TOC, release of α-TOC from the protein particles were examined under simulated gastric and simulated intestinal digestion conditions. Table 1 shows that the α-TOC encapsulated was almost completely released (86.4 ± 9.9% for BLG-encapsulated α-TOC, and 93.4 ± 10.1% for HEW-encapsulated α-TOC) in SGF condition. Considering that most nutrients and vitamins are best absorbed in intestine for further utilization in the body, α-TOC should be protected in the encapsulated particles and should not release in the SGF condition. Therefore, encapsulation of α-TOC by salt induced protein aggregates only is not adequate for such purposes. Consequently, sodium alginate was used as a coating material for these encapsulated particles as it was widely used as stabilizers, thickening, or gelling agents in food products (Pongsawatmanit et al., 2006). Several reports showed that the alginate gel was very strong, rigid, and hard to swell in simulated gastric fluid (SGF) condition (Chen et al., 2006; Chen & Subirade, 2007; Gunasekaran, Ko, & Xiao, 2007). By coating with alginate, the release of α-TOC should occur in intestinal condition. Table 1 illustrates that the release of α-TOC in the SGF was retarded and the release was then observed in the SIF. For BLG- and HEW-encapsulated α-TOC, the released amount of α-TOC under SGF condition decreased whereas that under SIF condition increased with increasing in concentration of sodium alginate. Not only that the alginate could prolong the release of α-TOC till intestinal stage, but also it increased the encapsulation efficiency of α-TOC by BLG and HEW. The increase was prominent for HEW-encapsulated

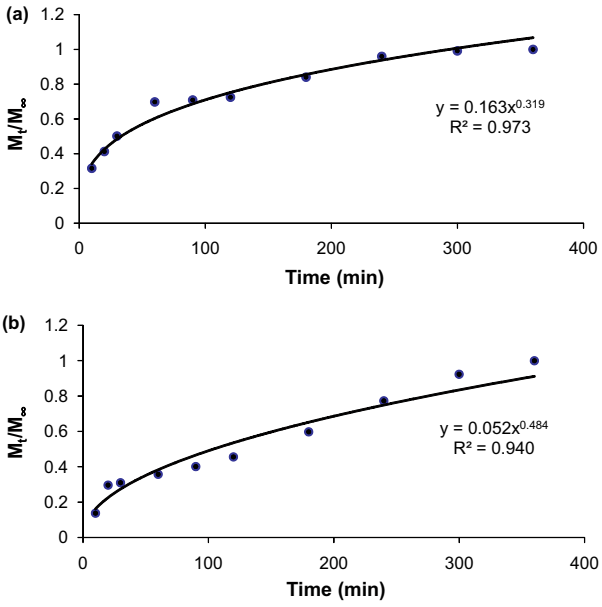

Fig. 6. Release profile of α-TOC from (a) BLG-encapsulated α-TOC and (b) HEW-encapsulated α-TOC.

α-TOC, as the encapsulation efficiency increased from approx. 32% (without alginate coat) to approx. 85% (with alginate coat). For BLG-encapsulated α-TOC, the encapsulation efficiency was increased with the increase in concentration of alginate because the emulsion stability was improved through the formation of interfacial complex between alginate and the protein (Azzam & Omari, 2002; Pongsawatmanit et al., 2006).

Considering at the selected preparation conditions, the encapsulation efficiency obtained for HEW-encapsulated α-TOC was higher than that for BLG-encapsulated α-TOC (Table 1). Although encapsulation by HEW requires higher concentration than that by BLG, the cost of HEW is much less than that of BLG. With the use of alginate coating, both BLG and HEW aggregates can be employed as protein-based materials for encapsulation of α-TOC.

The release profiles of α-TOC from BLG- and HEW-encapsulated α-TOC coated with 0.25% alginate at various incubation times in simulated intestinal fluid could fit well with the diffusion-controlled release model as illustrated in Fig. 6. This diffusion-controlled release model was considered from an empirical equation proposed by Peppas and Sahlin (1989), as described by the following equation.

$$\frac{M_t}{M_\infty} = kt^n$$

where M_t is the amount of α-TOC released up to any time t, M_∞ is the final amount of α-TOC released (the total amount of α-TOC released at 6 h in this study), k is a constant incorporating structural

Table 1
Encapsulation efficiency and release of α-tocopherol.

Samples	EE (% ± SD)	R_{SGF}[a] (% ± SD)	R_{SIF}[b] (% ± SD)
0.5% (w/v) BLG + 100 mM α-TOC + 25 mM $CaCl_2$			
Without alginate coat	18.8 ± 6.3	86.4 ± 9.9	
Coated with 0.125% (w/v) alginate	20.7 ± 6.1	4.2 ± 0.2	26.8 ± 1.0
Coated with 0.25% (w/v) alginate	51.4 ± 3.3	1.4 ± 0.5	54.8 ± 0.6
4% (w/v) HEW + 50 mM α-TOC + 25 mM $ZnCl_2$			
Without alginate coat	31.9 ± 8.3	93.4 ± 10.1	
Coated with 0.125% (w/v) alginate	82.1 ± 4.3	17.5 ± 9.5	21.8 ± 9.9
Coated with 0.25% (w/v) alginate	85.2 ± 2.1	7.3 ± 2.5	38.0 ± 3.9

[a] The percentages of released amount of α-TOC in simulated gastric fluid at 2 h.
[b] The percentages of released amount of α-TOC in simulated intestinal fluid at 4 h.

and geometrical characteristics, and n is a release exponent value. The α-TOC release from the two systems was therefore shown to mainly follow the diffusion-controlled model. However, other mechanisms might also involve. As the coefficients of determination (R^2) of the diffusion-controlled release profiles from the BLG- and HEW-encapsulated α-TOC coated with 0.25% alginate were 0.973 and 0.940, respectively, the release of α-TOC from BLG coated with 0.25% alginate fit with the diffusion-controlled model better than that from the HEW. Therefore, further investigation was performed for the release of α-TOC from HEW coated with 0.25% alginate. The final amount of α-TOC released from the HEW coated with 0.25% alginate was investigated at 24 h. The release profile was found to be biphasic showing a constant release with an almost instantaneous burst release. The total mole amount of α-TOC released increased from 0.000991 at 6 h to 0.005135 at 24 h. Therefore, gel erosion might also be taken place (Lin & Metters, 2006).

4. Conclusions

β-Lactoglobulin (BLG) and hen egg white protein (HEW) could be used as protein-based materials for encapsulation of α-tocopherol (α-TOC) after salt-induced gelation of the proteins. Concentrations of protein and α-TOC influence the encapsulation efficiency. To protect α-TOC from release in the gastric condition, alginate was used for coating of these encapsulated particles. With the alginate coat, the release of α-TOC was retarded till intestinal stage and the encapsulation efficiencies of α-TOC by BLG and HEW were enhanced.

Acknowledgements

The Thailand Research Fund is gratefully acknowledged for the research grants given to JS and AS. Thanks are also due to Center for Innovation in Chemistry: Postgraduate Education and Research Program in Chemistry (PERCH-CIC), Commission on Higher Education, Ministry of Education, for the scholarships given to W. Somchue and W. Sermsri.

References

Alting, A. C., Hamer, R. J., Kruif, C. G., & Visschers, R. W. (2003). Cold-set globular protein gels: Interactions, structure and rheology as a function of protein concentration. *Journal of Agricultural and Food Chemistry, 51*, 3150–3156.

Alzagtat, A. A., & Alli, I. (2002). Protein–lipid interactions in food systems: A review. *International Journal of Food Sciences and Nutrition, 53*, 249–260.

Azzam, M. O. J., & Omari, R. M. (2002). Stability of egg white-stabilized edible oil emulsions using conductivity technique. *Food Hydrocolloids, 16*, 105–110.

Beaulieu, L., Savoie, L., Paquin, P., & Subirade, M. (2002). Elaboration and characterization of whey protein beads by an emulsification/cold gelation process: Application for the protection of retinol. *Biomacromolecules, 3*, 239–248.

Blatt, D. H., Pryor, W. A., Mata, J. E., & Proteau, R. R. (2004). Re-evaluation of the relative potency of synthetic and natural α-tocopherol: Experimental and clinical observations. *The Journal of Nutritional Biochemistry, 15*, 380–395.

Borel, P. (2003). Factors affecting intestinal absorption of highly lipophilic food microconstituents (fat-soluble vitamins, carotenoids and phytosterols). *Clinical Chemistry and Laboratory Medicine, 41*, 979–994.

Borel, P., Pasquier, B., Armand, M., Tyssandier, V., Grolier, P., Andre, M., et al. (2001). Processing of vitamin A and E in the human gastrointestinal tract. *American Journal of Physiology – Gastrointestinal and Liver Physiology, 280*, 95–103.

Brigelius-Flohé, R., & Traber, M. G. (1999). Vitamin E: Function and metabolism. *FASEB Journal, 13*, 1145–1155.

Bryant, C. M., & McClements, D. J. (1998). Molecular basis of protein functionality with special consideration of cold-set gels derived from heat-denatured whey. *Trends in Food Science & Technology, 9*, 143–151.

Bryant, C. M., & McClements, D. J. (2000). Influence of NaCl and $CaCl_2$ on cold-set gelation of heat-denatured whey protein. *Journal of Food Science, 65*, 801–804.

Cheeseman, K. H., Holley, A. E., Kelly, F. J., Wasil, M., Hughes, L., & Burton, G. (1995). Biokinetics in humans of RRR-α-tocopherol: The free phenol, acetate ester, and succinate ester forms of vitamin E. *Free Radical Biology and Medicine, 19*, 591–598.

Chen, L., Remondetto, G. E., & Subirade, M. (2006). Food protein-based materials as nutraceutical delivery systems. *Trends in Food Science & Technology, 17*, 272–283.

Chen, L., & Subirade, M. (2006). Alginate–whey protein granular microspheres as oral delivery vehicles for bioactive compounds. *Biomaterials, 27*, 4646–4654.

Chen, L., & Subirade, M. (2007). Effect of preparation conditions on the nutrient release properties of alginate–whey protein granular microspheres. *European Journal of Pharmaceutics and Biopharmaceutics, 65*, 354–362.

Croguennec, T., Nua, E., & Brulé, G. (2002). Influence of pH and salts on egg white gelation. *Journal of Food Science, 67*, 608–614.

Dumay, E., Laligant, A., Zasypkin, D., & Cheftel, J. C. (1999). Pressure- and heat-induced gelation of mixed β-lactoglobulin/polysaccharide solutions: Scanning electron microscopy of gels. *Food Hydrocolloids, 13*, 339–351.

FDA (2008). EAFUS: A food additive database. <http://www.vm.cfsan.fda.gov/dms/eafus.html>, Accessed 04.12.08.

Foegeding, E. A., Kuhn, P. R., & Hardin, C. C. (1992). Specific divalent cation-induced changes during gelation of β-lactoglobulin. *Journal of Agricultural Food Chemistry, 40*, 2092–2097.

Gunasekaran, S., Ko, S., & Xiao, L. (2007). Use of whey proteins for encapsulation and controlled delivery applications. *Journal of Food Engineering, 83*, 31–40.

Lefévre, T., & Subirade, M. (2003). Formation of intermolecular β-sheet structures: A phenomenon relevant to protein film structure at oil–water interfaces of emulsions. *Journal of Colloid and Interface Science, 263*, 59–67.

Lin, C.-C., & Metters, A. T. (2006). Hydrogels in controlled release formulations: Network design and mathematical modeling. *Advanced Drug Delivery Reviews, 58*, 1379–1408.

Line, V. L. S., Remondetto, G. E., & Subirade, M. (2005). Cold gelation of β-lactoglobulin oil-in-water emulsions. *Food Hydrocolloids, 19*, 269–278.

Majhi, P. R., Vanam, R. P., Ganta, R. R., Seyrek, E., Giger, K., & Dubin, P. L. (2006). Electrostatically driven protein aggregation: β-Lactoglobulin at low ionic strength. *Langmuir, 22*, 9150–9159.

Maltais, A., Remondetto, G. E., & Subirade, M. (2008). Mechanisms involved in the formation and structure of soya protein cold-set gels: A molecular and supramolecular investigation. *Food Hydrocolloids, 22*, 550–559.

Mardones, P., & Rigotti, A. (2004). Cellular mechanisms of vitamin E uptake: Relevance in α-tocopherol metabolism and potential implications for disease. *The Journal of Nutritional Biochemistry, 15*, 252–260.

Mine, Y. (1995). Recent advances in the understanding of egg white protein functionality. *Trends in Food Science & Technology, 6*, 225–232.

Peppas, N. A., & Sahlin, J. J. (1989). A simple equation for the description of solute release. 3. Coupling of diffusion and relaxation. *International Journal of Pharmaceutics, 57*(16), 169–172.

Pérez, M. D., & Calvo, M. (1995). Interaction of β-lactoglobulin with retinol and fatty acids and its role as a possible biological function for this protein: A review. *Journal of Dairy Science, 78*, 978–988.

Pongsawatmanit, R., Harnsilawat, T., & McClements, D. J. (2006). Influence of alginate, pH and ultrasound treatment on palm oil-in-water emulsions stabilized by β-lactoglobulin. *Colloids and Surfaces A: Physicochemical and Engineering Aspects, 287*, 59–67.

Pryor, W. A. (2000). Vitamin E and heart disease: Basic science to clinical intervention trials. *Free Radical Biology and Medicine, 28*, 141–164.

Saeseaw, S., Shiowatana, J., & Siripinyanond, A. (2006). Observation of salt-induced β-lactoglobulin aggregation using sedimentation field-flow fractionation. *Analytical and Bioanalytical Chemistry, 386*, 1681–1688.

Samontha, S., Nipattamanon, C., Shiowatana, J., & Siripinyanond, A. (2008). Toward better understanding of salt-induced hen egg white protein aggregation using field-flow fractionation. *Journal of Agricultural Food Chemistry, 56*, 8809–8814.

Simons, J. W. F. A., Kosters, H. A., Visschers, R. W., & Jongh, H. H. J. (2002). Role of calcium as trigger in thermal β-lactoglobulin aggregation. *Archives of Biochemistry and Biophysics, 406*, 143–152.

Sriamornsak, P., & Kennedy, R. A. (2007). Effect of drug solubility on release behavior of calcium polysaccharide gel-coated pellets. *European Journal of Pharmaceutical Sciences, 32*, 231–239.

Swaisgood, H. E., Wang, Q., & Allen, J. C. (2001). Protein ingredient for carrying lipophilic nutrients. US Patent No. 6, 290, 974 B1.

Totosaus, A., Montejano, J. G., Salazar, J. A., & Guerrero, I. (2002). A review of physical and chemical protein–gel induction. *International Journal of Food Science and Technology, 37*, 589–601.

Tucker, J. M., & Townsend, D. M. (2005). Alpha-tocopherol: Roles in prevention and therapy of human disease. *Biomedicine and Pharmacotherapy, 59*, 380–387.

Ubbink, J., & Krüger, J. (2006). Physical approaches for the delivery of active ingredients in foods. *Trends in Food Science & Technology, 17*, 244–254.

Voth, O. L., & Miller, R. C. (1958). Interaction of tocopherol with proteins and amino acids. *Archives of Biochemistry and Biophysics, 77*, 191–205.

Wang, Q., Allen, J. C., & Swaisgood, H. E. (1997). Binding of vitamin D and cholesterol to β-lactoglobulin. *Journal of Dairy Science, 80*, 1054–1059.

Wu, S. Y., Pérez, M. D., Puyol, P., & Sawyer, L. (1999). β-Lactoglobulin binds palmitate within its central cavity. *The Journal of Biological Chemistry, 274*, 170–174.

Anal Bioanal Chem (2010) 396:3079–3085
DOI 10.1007/s00216-010-3511-4

ORIGINAL PAPER

Flow field-flow fractionation: a versatile approach for size characterization of α-tocopherol-induced enlargement of gold nanoparticles

Wimut Sermsri · Purim Jarujamrus · Juwadee Shiowatana · Atitaya Siripinyanond

Received: 2 November 2009 / Revised: 24 January 2010 / Accepted: 25 January 2010 / Published online: 23 February 2010

Abstract Flow field-flow fractionation (FlFFF) was used for size characterization of gold nanoparticles. The measured particle sizes obtained from FlFFF for the commercial 10 nm gold nanoparticle standard and the gold nanoparticles synthesized in the laboratory were in good agreement with those measured by transmission electron microscopy (TEM). Further, the capability of α-tocopherol to induce enlargement of gold nanoparticles by catalysis of the reduction of $AuCl_4^-$ by citrate was observed by monitoring the changes in particle size of gold nanoparticles using FlFFF. The effects of α-tocopherol and incubation time on enlargement of the gold nanoparticles were examined. Higher concentrations of α-tocopherol resulted in larger nanoparticles. At fixed α-tocopherol concentration, larger nanoparticles were formed at longer incubation times.

Keywords Gold nanoparticles · Field-flow fractionation · α-Tocopherol · Particle size

Introduction

Gold nanoparticles have gained considerable interest in different research fields, owing to their attractive properties such as high stability, biocompatibility, and optical properties [1]. Gold nanoparticles can be prepared in various ways [2]; the mildest rely on reduction of gold salts in the presence of suitable stabilizing agents that prevent particle aggregation [2]. Many researchers have demonstrated the use of gold nanoparticles for optical labeling and sensing purposes [3, 4]. Scampicchio et al. have used gold nanoparticles to estimate the antioxidant activity of phenolic acids in different beverages [5]. This assay was based on the capability of phenolic acid as reducing agent to catalyze the growth of gold nanoparticles in the reduction of $AuCl_4^-$ by sodium citrate. Considering the antioxidant activity, vitamin E, a group of tocopherols and tocotrienols, of which α-tocopherol has the highest biological activity, is found to be the most potent natural lipophilic antioxidant [6]. Therefore, we hypothesize that α-tocopherol should also exhibit catalytic activity on the growth of gold nanoparticles, and various α-tocopherol concentrations should result in different sizes of gold nanoparticles. Closer inspection of the effect of α-tocopherol on the size of gold nanoparticles should then be carried out because of the strong correlation between the size and their optical, electrical, and catalytic properties [7].

Size characterization of nanoparticles has been performed by conventional techniques such as scanning electron microscopy (SEM), transmission electron microscopy (TEM), and dynamic light scattering (DLS). A flow-assisted technique, field-flow fractionation (FFF), for size characterization of nanoparticles has also been reported [8, 9]. This technique enables fractionation of particles on the nanometer to sub-micrometer scales and the fractionated particles can be further characterized by various detection methods [10, 11]. The principle [12–14] and applications [15, 16] of FFF have been described elsewhere. Rameshwar et al. illustrated the use of field-flow fractionation (FFF) for size characterization of water-soluble nanoparticles and quantum dots [17]. In their study, the particle size results of core particles obtained from FFF measurements were in good agreement with

W. Sermsri · P. Jarujamrus · J. Shiowatana · A. Siripinyanond (✉)
Department of Chemistry and Center for Innovation in Chemistry,
Faculty of Science, Mahidol University,
Rama VI Road,
Bangkok 10400, Thailand
e-mail: scasp@mahidol.ac.th

those obtained from other conventional techniques. Nonetheless, for gold nanoparticles which showed extensive aggregation, FFF was shown to be a more convenient and easier method for determination of average particle size. Recently, Contado and Argazzi reported the use of sedimentation FFF to investigate the role of citrate concentrations on the size distribution of gold nanoparticles [18]. In their study, the size of gold nanoparticles as small as 12 nm could be observed.

The objectives of this investigation were to examine the capability of FFF for characterization of the size of gold nanoparticles and to examine the capability of α-tocopherol to induce enlargement of gold nanoparticles. Flow field-flow fractionation (FlFFF) was used to observe the effects of α-tocopherol concentrations and incubation time on enlargement of the gold nanoparticles.

Experimental

Instrumentation

A symmetrical flow field-flow fractionation (FlFFF) system (Model PN-1021-FO; Postnova Analytics, Landsberg, Germany) equipped with a 1000 Da molecular weight cut-off regenerated cellulose acetate membrane (Postnova Analytics) was used for size characterization of gold nanoparticles. The FlFFF channel was rectangular in shape with the dimensions: 27 cm long, 2.0 cm wide, and 0.0254 cm thick. A high-pressure liquid chromatography (HPLC) pump (Model PN 2101; Postnova Analytics) was used to deliver the channel and the forward flows. Another HPLC pump of the same model was used to regulate the cross and focusing (backward) flows. A UV detector (Model S3210 UV–visible detector; Postnova Analytics) was set at 254 nm to monitor light attenuation of gold nanoparticles samples. Conventional sample introduction with a sample volume of 20 μL was used for characterization of the size of commercial gold nanoparticles and those prepared by the modified Turkevich method.

To examine the particle size and enlargement of gold nanoparticles induced by α-tocopherol, opposing-flow large-volume sample introduction (500 μL) were used for on-channel FlFFF preconcentration and separation. The system set up was similar to that reported by Hassellöv et al. [19] and Amarasiriwardena et al. [20]. This approach consists of two steps:

1. sample loading and focusing, and
2. fractionation.

In the sample loading and focusing step, the sample was introduced into the FlFFF channel and two opposing flow streams were used to focus the sample zone into a narrow band near the inlet of FlFFF channel. After a suitable focusing time, the sample was fractionated by applying cross and channel flows. The optimum operating FlFFF conditions are listed in Table 1. For comparison purposes, a transmission electron microscope (TEM; JEM-2100, 200 kV; Jeol) was used to observe the size of gold nanoparticles. The TEM operating conditions are also listed in Table 1. A UV–visible spectrometer (V530 UV–visible spectrometer; Jasco, Tokyo, Japan) was used for recording the absorbance spectra of gold nanoparticles.

Chemicals

All chemicals used in this work were of analytical reagent grade. De-ionized water (18.2 MΩ cm^{-1}) obtained from a water-purification system (Barnstead International, Dubuque, IA, USA) was used to prepare all chemical reagents. Commercial 10-nm gold nanoparticles were purchased from Sigma (St Louis, MO, USA). A 50 mmol L^{-1} $AuCl_4^-$ solution was prepared by dissolving hydrogen tetrachloroaurate, $HAuCl_4.3H_2O$ (Sigma), in deionized water. A solution (1 mmol L^{-1}) of sodium citrate (Riedel-deHaën, Germany) was prepared in phosphate buffer (pH 8.0; 1×10^{-2} mol L^{-1}). A solution (1 mmol L^{-1}) of α-tocopherol was prepared by dissolving (±)-α-tocopherol (Fluka Chemie, Switzerland) in 95% ethanol (Merck, Darmstadt, Germany) and used as a stock solution for further dilution.

FL-70, a mixture of anionic and non-ionic compounds containing the active components oleic acid, sodium carbon-

Table 1 FlFFF and TEM operating conditions

FlFFF with conventional sample introduction	
Carrier liquid	0.02% (*v*/*v*) FL-70
Channel flow rate (mL min^{-1})	1.5
Cross flow rate (mL min^{-1})	1.0
Equilibration time (min)	1.0
FlFFF with opposing flow large-volume sample introduction	
Carrier liquid	0.02% (*v*/*v*) FL-70
Forward flow rate (mL min^{-1})	0.24
Backward flow rate (mL min^{-1})	3.0
Channel flow rate (mL min^{-1})	1.5
Cross flow rate (mL min^{-1})	1.0
Focusing time (min)	7.0
TEM	
Beam current (μA)	82.5
Temperature (°C)	25
Humidity (%)	25
Acceleration voltage (kV)	160

ate, tergitol, tetrasodium EDTA, poly(ethylene glycol), and triethanolamine [21] was purchased from Fisher Scientific (Pittsburgh, PA, USA). A 0.1% (*v*/*v*) solution of FL-70 was prepared by diluting concentrated FL-70 with de-ionized water and used as a carrier liquid.

Preparation of gold nanoparticles

To prepare gold nanoparticles, the modified Turkevich method [22] was used. A solution of hydrogen tetrachloroaurate (0.01% (*w*/*w*), 20 mL) was heated for 15 min at 65°C in a water bath. A 1% sodium citrate solution was also heated for 5 min. Subsequently, 1.5 mL of the pre-heated sodium citrate solution was pipetted into the 20 mL solution of the pre-heated hydrogen tetrachloroaurate . The mixture was then stirred and heated to reflux for 30 min, while the solution turned from pale yellow to pale blue then to brilliant red upon completion. The gold nanoparticles solution obtained was sonicated for 15 min, cooled to room temperature and stored at 4°C.

α-Tocopherol-induced gold nanoparticle enlargement

To observe the enlargement of gold nanoparticles induced by α-tocopherol, $AuCl_4^-$ (1×10^{-3} mol L^{-1}) was mixed with FL-70 (0.01%) and sodium citrate (2×10^{-4} mol L^{-1}) in phosphate buffer (pH 8.0; 1×10^{-2} mol L^{-1}) with different concentrations of α-tocopherol (2.5×10^{-6}, 7.5×10^{-6}, and 10.0×10^{-6} mol L^{-1}). All samples were heated for 10 min at 45°C. The effects of α-tocopherol and incubation time on enlargement of gold nanoparticles were examined. The gold nanoparticles obtained were introduced into a FlFFF using large-volume sample introduction (500 μL) for size characterization.

Data transformation and information obtained from FlFFF experiment

Raw fractograms were translated into mass size distribution profiles [23] by using Microsoft Excel (Microsoft Excel 2007) spreadsheet software. Peak evaluation, baseline adjustment, and cumulative area distribution plotting were performed by using PeakFit (SPSS, Chicago, IL, USA). From a FlFFF experiment, a raw fractogram of separated particles, a plot of detector response (*y*-axis) against retention time (*x*-axis), was obtained, as shown in Fig. 1a. The raw fractogram was translated into particle size distribution [23] as shown in Fig. 1b. With this plot, the particle size at peak maximum (d_p) was measured. To measure a breadth of size distribution, particle size range at half maximum height ($\Delta d_{0.5}$) was calculated from the distribution profile [23, 24]. Further, the particle size distribution was converted into a cumulative area plot as shown in Fig. 1c. With this plot, particle size in terms of mean diameter (d_{mean}) was measured by considering the particle size which gives 50% cumulative area.

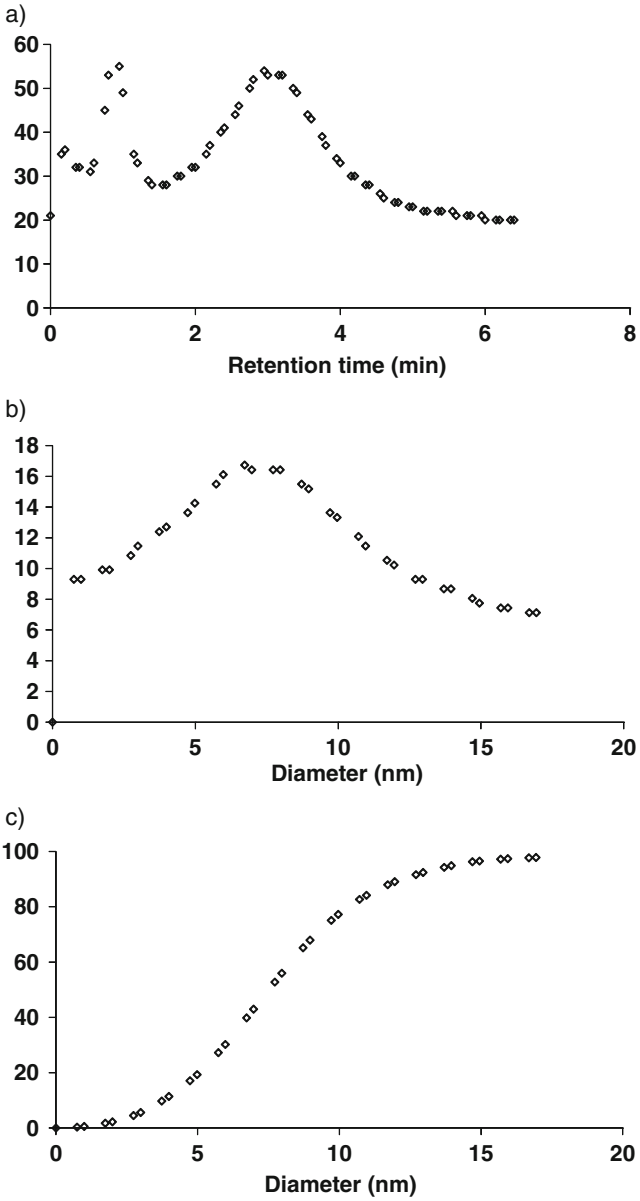

Fig. 1 (**a**) Raw fractogram of gold nanoparticles; (**b**) the corresponding particle-size distribution; (**c**) the corresponding cumulative area distribution

Results and discussion

FlFFF size characterization of gold nanoparticles

To develop an FlFFF method for size characterization of gold nanoparticles, an appropriate carrier liquid must be chosen. The carrier liquid must be compatible with the

Table 2 Mean particle size (d_{mean}±s.d.; n=3) of gold nanoparticles measured by FlFFF at various FL-70 carrier liquid concentrations and by TEM

Measurement method	Commercial gold nanoparticle (10nm)	Gold nanoparticles prepared in the laboratory
FlFFF with 0.004% FL-70	n.d.[a]	n.d.[a]
FlFFF with 0.02% FL-70	7.9±0.3	28.6±0.2
FlFFF with 0.10% FL-70	6.9±0.2	20.6±0.4
TEM	8.3±1.4	23.9±2.0

[a] Not determined – with 0.004% FL-70, gold nanoparticles were not eluted

membrane and able to disperse particles without interacting with them or changing the particle size characteristics. Because gold nanoparticles are negatively charged [25], anionic surfactants should be used to disperse the gold nanoparticles. The nonpolar part of an anionic surfactant is adsorbed by the hydrophobic solid, and the polar group is oriented towards the aqueous phase [26]. The resulting net negative charge on the particle surface prevents particles from agglomeration. In this work, FL-70 was selected as a carrier liquid. Therefore, the effect of carrier liquid concentrations (0.004, 0.02, and 0.1% (*v*/*v*) FL-70) for size characterization of gold nanoparticles was examined; the results are summarized in Table 2. These concentrations were much lower than the critical micelle concentration of FL-70, which was reported to be 5.1% (*v*/*v*) [27]. At concentrations much lower than the critical micelle concentration, increasing the FL-70 concentration resulted in an increase in the surfactant concentration on the gold nanoparticles surface, which could affect retention time. Transmission electron microscopy was used to investigate the particle sizes of the commercial gold nanoparticles and the gold nanoparticles prepared by the modified Turkevich method [22], as displayed in Fig. 2. With 0.004% (*v*/*v*) FL-70 carrier liquid, gold nanoparticles were not eluted from the FlFFF channel. This might be because concentrations of carrier liquid which are too low do not effectively prevent adsorption of the nanoparticles on the membrane surface. With higher concentrations of carrier liquid, i.e., 0.02% and 0.1% (*v*/*v*) FL-70, the particle size information obtained from TEM and FlFFF was not significantly different (Table 2). Therefore, FlFFF was proved to provide reliable particle size information for gold nanoparticles and 0.02% (*v*/*v*) FL-70 was selected as a suitable carrier liquid for FlFFF size characterization of gold nanoparticles.

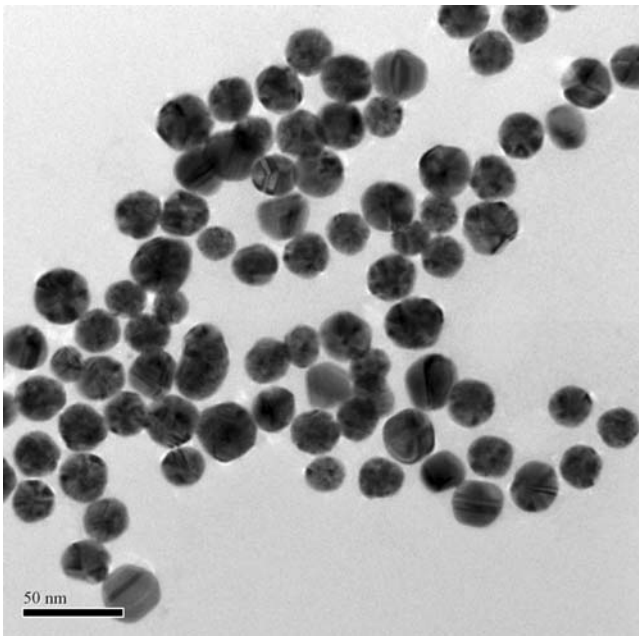

Fig. 2 TEM photograph of gold nanoparticles prepared by the modified Turkevich method

Use of an on FlFFF channel preconcentration for size characterization of very diluted gold nanoparticles

For a very dilute sample, the signal of the fractionated gold nanoparticles is quite low, as shown in Fig. 3 (*diamonds*). In order to improve the signal of gold nanoparticles, sample preconcentration is necessary. According to Hassellöv et al. [19] and Amarasiriwardena et al. [20], FlFFF allows on-channel preconcentration of particulate samples exploiting the fact that FlFFF is similar to a membrane filtration unit. In principle, the

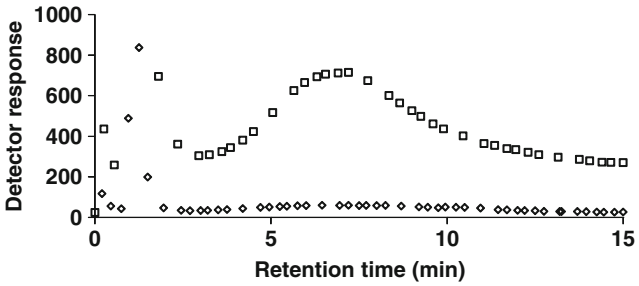

Fig. 3 Fractograms of gold nanoparticles prepared by α-tocopherol-catalyzed citric acid reduction of $AuCl_4^-$ obtained by conventional sample introduction (*diamonds*, 20 μL) and large-volume sample introduction (*squares*, 500 μL) FlFFF separation

sample is introduced to the FlFFF channel, focused and concentrated by using an opposed-flow sample concentration [28]. Large-volume samples are introduced into the FlFFF channel and focused at a certain point. The particles, whose sizes are larger than the membrane pore size, can be retained in the channel. To improve the detection of gold nanoparticles, 500 μL sample was introduced into the FlFFF channel instead of the regular injection volume (20 μL) used in the conventional FlFFF separation. The sample was loaded through the back end of the channel with a flow ratio of 1:12.5 between the forward (0.24 mL min^{-1}) and backward (3 mL min^{-1}) focusing flows. When the whole sample volume was loaded and focused in the FlFFF channel, the forward and backward flow pumps were disengaged and the cross flow stream was introduced, so that the sample could reach steady state equilibrium. Figure 3 (*squares*) displays the signal of gold nanoparticles obtained from the on-channel preconcentration system. The signal was substantially improved compared with that obtained from conventional sample introduction (20 μL). Therefore, on-channel preconcentration FlFFF sample introduction was then used to investigate size and enlargement of gold nanoparticles induced by α-tocopherol.

Conditions affecting enlargement of gold nanoparticles induced by α-tocopherol

According to Scampicchio et al. [5], antioxidant activity could be estimated by absorbance monitoring (at 555 nm) of the formation of gold nanoparticles catalyzed by phenolic compounds in the presence of citric acid reducing agent. The increase in absorbance at 555 nm was linearly dependent upon the concentration of phenolic compounds. Nonetheless, the change in particle size of gold nanoparticles was not systematically examined. As α-tocopherol is an effective natural lipophilic antioxidant, our interest was to investigate the potential of α-tocopherol to induce the formation and enlargement of gold nanoparticles. The role of α-tocopherol in the formation of gold nanoparticles was observed from the absorption spectra as illustrated in Fig. 4. In the presence of sodium citrate, addition of α-tocopherol led to an enhanced absorbance signal at the characteristic absorption band at 555 nm. Without α-tocopherol, only a small absorption signal was observed as a result of gold nanoparticles obtained purely from sodium citrate reduction (Fig. 4a). In the absence of sodium citrate, α-tocopherol alone could not instantaneously induce formation of gold nanoparticles (Fig. 4b). Upon overnight incubation, however, formation of gold nanoparticles was observed, as evidenced by the occurrence of an absorption band at 555 nm (Fig. 4b). This observation suggested that

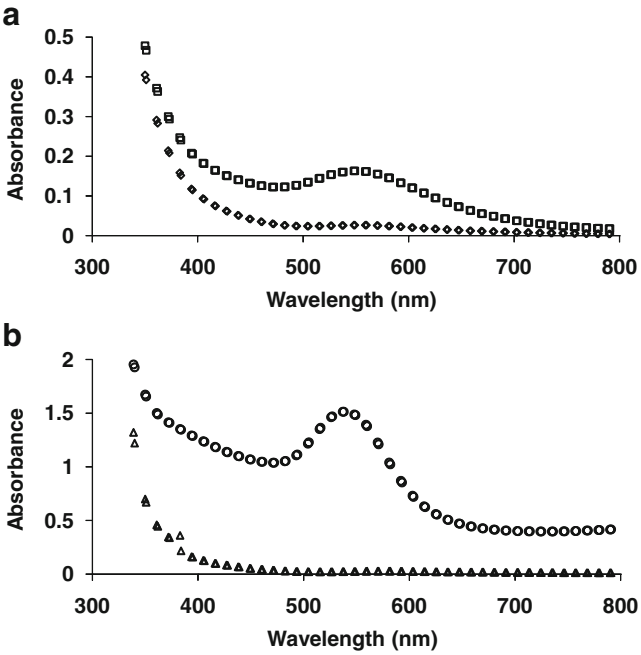

Fig. 4 Absorption spectra of gold nanoparticles: (**a**) prepared by sodium citrate reduction of $AuCl_4^-$ in the absence (*diamonds*) and presence (*squares*) of α-tocopherol (1×10^{-5} mol L^{-1}); (**b**) prepared in the presence of (1×10^{-5} mol L^{-1}) α-tocopherol without addition of sodium citrate, observed immediately (*triangles*) and after overnight incubation (*circles*)

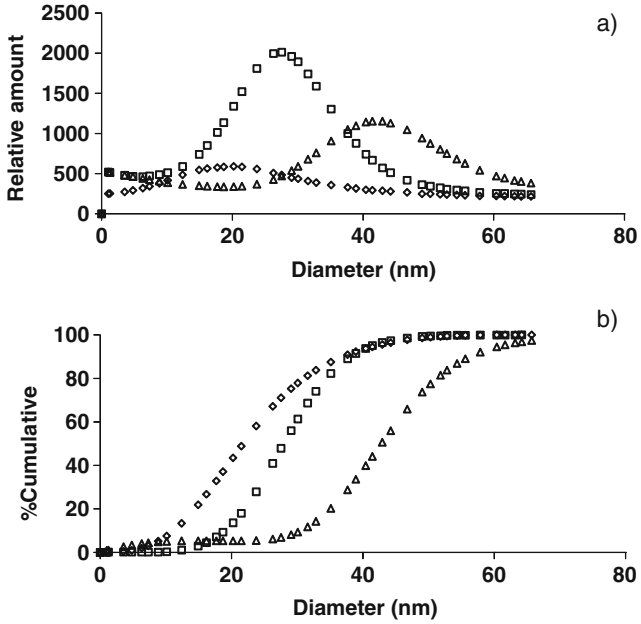

Fig. 5 Effect of α-tocopherol concentration on the α-tocopherol-induced enlargement of gold nanoparticles with 0 h incubation time: (**a**) particle size distributions; (**b**) cumulative area distribution. The *diamonds*, *squares*, and *triangles* represent 2.5, 7.5, and 10.0×10^{-6} mol L^{-1} α-tocopherol, respectively

Table 3 Particle size information for α-tocopherol-induced enlargement of gold nanoparticles obtained from various experimental conditions

Effect of α-tocopherol concentration (0h incubation time)			
α-Tocopherol (10^{-6}mol L^{-1})	d_p (nm)	d_{mean} (nm)	$\Delta d_{0.5}$ (nm)
2.5	16±3	17±3	12
7.5	18±1	19±1	11
10.0	32±4	33±4	13
Effect of incubation time (7.5×10^{-6}mol L^{-1} α-tocopherol)			
Incubation time (h)	d_p (nm)	d_{mean} (nm)	$\Delta d_{0.5}$ (nm)
0	18±1	19±1	11
2	20±2	21±2	10
4	22±2	23±1	11

the gold nanoparticles produced by sodium citrate reduction acted as a seed for the reduction of $AuCl_4^-$ by α-tocopherol and resulting in enlargement of the particles, similar to that observed by Zayats et al. [29] for the catalytic growth of gold nanoparticles on addition of H_2O_2 as a reducing agent.

Further, the effects of α-tocopherol concentration and incubation time on the enlargement of gold nanoparticles were investigated using on-channel FlFFF preconcentration for size characterization. At fixed incubation time of 0 h (immediately analyzed), three different concentrations of α-tocopherol (2.5×10^{-6}, 7.5×10^{-6}, and 10.0×10^{-6}mol L^{-1}) were examined for their effects on enlargement of the gold nanoparticles. For a fixed incubation time of 0 h, particle-size distributions of gold nanoparticles for various α-tocopherol concentrations are illustrated in Fig. 5. With increased α-tocopherol concentration, gold nanoparticles were enlarged, and the d_{mean} value increased from 17 to 33 nm when the α-tocopherol concentration was increased from 2.5×10^{-6} to 10×10^{-6}mol L^{-1} (Table 3). At a fixed α-tocopherol concentration of 7.5×10^{-6}mol L^{-1}, various incubation times including 0, 2, and 4 h were examined for their effects on enlargement of the gold nanoparticles; the results are illustrated in Fig. 6 and summarized in Table 3. With different incubation times, gold nanoparticles were shown to exhibit monomodal distribution. The d_{mean} value increased from 19 (at 0 h) to 23 nm (at 4 h), demonstrating that incubation time had an effect on enlargement of the gold nanoparticles. It is interesting to note that under each condition investigated the values of d_{mean} and d_p were almost equal, suggesting that the particle size distribution profiles of gold nanoparticles were ideally monomodal and of Gaussian characteristics. Moreover, the breadths of size distributions obtained from all experimental conditions were nearly the same, suggesting that the enlargement of the gold nanoparticles induced by α-tocopherol would not affect on the polydispersity of the resulting particles.

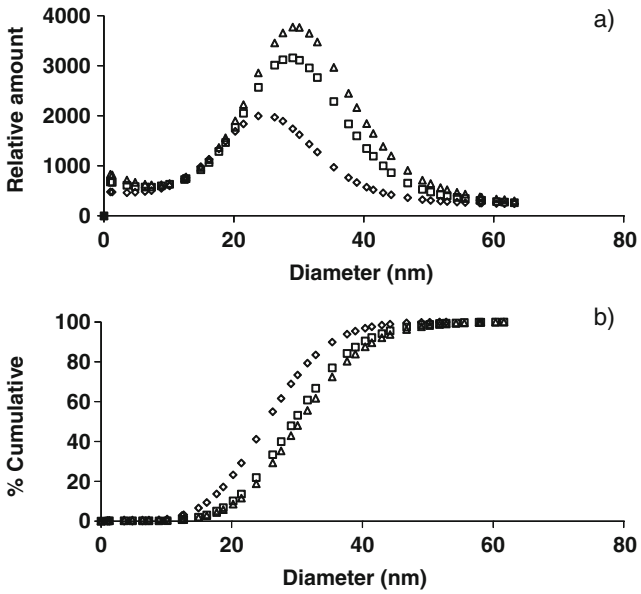

Fig. 6 Effect of incubation time on the α-tocopherol-induced enlargement of gold nanoparticles with fixed 7.5×10^{-6}mol L^{-1} α-tocopherol: (**a**) particle size distributions; (**b**) cumulative area distribution. The *diamonds*, *squares*, and *triangles* represent 0, 2, and 4 h incubation time, respectively

Conclusions

α-Tocopherol was shown to be capable of inducing enlargement of the gold nanoparticles obtained by reduction of $AuCl_4^-$ with sodium citrate. From the analytical viewpoint, an on-channel FlFFF preconcentration method was proved suitable for size characterization of diluted gold nanoparticles. Concentration of α-tocopherol and incubation time affected enlargement of the gold nanoparticles. Flow FFF can be used to monitor the dynamic changes in size distribution of gold nanoparticles. The information obtained from the FlFFF experiment can be used as a guide to the preparation of gold nanoparticles of the desired size for required applications.

Acknowledgements The authors are grateful for research grants from the Thailand Research Fund and support from the Center for Innovation in Chemistry: Postgraduate Education and Research Program in Chemistry (PERCH-CIC), Commission on Higher Education, Ministry of Education.

References

1. Philip D (2008) Spectrochim Acta Mol Biomol Spectrosc 71:80–85
2. Ghosh P, Han G, De M, Kim CK, Rotello VM (2008) Adv Drug Del Rev 60:1307–1315
3. Thanh N, Vernhet A, Rosenzweig Z (2005) Frontiers in chemical sensors. Springer, Berlin Heidelberg New York, pp 261–277
4. Baron R, Zayats M, Willner I (2005) Anal Chem 77:1566–1571
5. Scampicchio M, Wang J, Blasco AJ, Arribas AS, Mannino S, Escarpa A (2006) Anal Chem 78:2060–2063
6. Brigelius-Flohe R, Traber MG (1999) FASEB 13:1145–1155
7. Sun Y, Xia Y (2002) Science 298:2176–2179
8. Jungmann N, Schmidt M, Maskos M (2001) Macromolecules 34:8347–8353
9. Benincasa MA, Mazzoni V (2007) J Liq Chromatogr Related Technol 30:453–462
10. Shin DY, Hwang E, Cho IH, Moon MH (2007) J Chromatogr A 1160:270–275
11. Jackson BP, Ranville JF, Neal AL (2005) Anal Chem 77:1393–1397
12. Giddings JC (1984) Sep Sci Technol 19:831–847
13. Giddings JC, Yang FJ, Myers MN (1976) Science 193:1244–1245
14. Giddings JC (1988) Chem Eng News 66:34–45
15. Roda B, Zattoni A, Reschiglian P, Moon MH, Mirasoli M, Michelini E, Roda A (2009) Anal Chim Acta 635:132–143
16. Ratanathanawongs Williams SK, Lee D (2006) J Sep Sci 29:1720–1732
17. Rameshwar T, Samal S, Lee S, Kim S, Cho J, Kim IS (2006) J Nanosci Nanotechnol 6:2461–2467
18. Contado C, Argazzi R (2009) J Chromatogr A 1216:9088–9098
19. Hassellöv M, Lyven B, Haraldsson C, Sirinawin W (1999) Anal Chem 71:3497–3502
20. Amarasiriwardena D, Siripinyanond A, Barnes RM (2001) J Anal At Spectrom 16:978–986
21. http://fscimage.fishersci.com/msds/06352.htm
22. Kimling J, Maier M, Okenve B, Kotaidis V, Ballot H, Plech A (2006) J Phys Chem B 110:15700–15707
23. Dondi F, Martin M (2000) Physicochemical measurements and distributions from field–flow fractionation. In: Schimpf ME, Caldwell JC, Giddings JC (eds) Field-flow fractionation handbook. Wiley, New York, pp 103–132
24. Siripinyanond A, Barnes RM (2002) Spectrochim Acta B 57:1885–1896
25. Yáñez-Sedeño P, Pingarrón JM (2005) Anal Bioanal Chem 382:884–886
26. Barman BN, Moon MH (2000) Sample preparation and choice of carrier liquid in field-flow fractionation. In: Schimpf ME, Caldwell JC, Giddings JC (eds) Field-flow fractionation handbook. Wiley, New York, pp 189–198
27. Atta KR, Gavril D, Loukopoulos V, Karaiskakis G (2004) J Chromatogr A 1023:287–296
28. Al-Ammar A, Siripinyanond A, Barnes RM (2001) Spectrochim Acta B 56:1951–1962
29. Zayats M, Baron R, Popov I, Willner I (2004) Nano Lett 5:21–25

Particle size characterization of titanium dioxide in sunscreen products using sedimentation field-flow fractionation–inductively coupled plasma–mass spectrometry

Analytical and Bioanalytical Chemistry

ISSN 1618-2642
Volume 399
Number 2

Anal Bioanal Chem (2010)
399:973-978
DOI 10.1007/s00216-010-4298-z

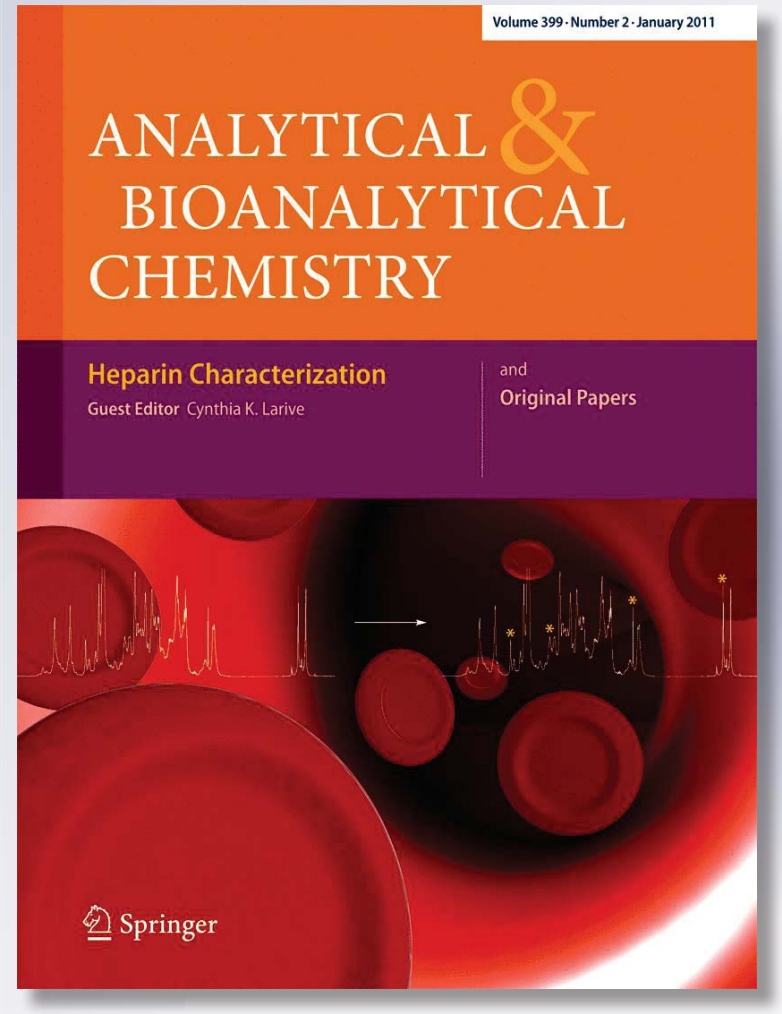

Springer

Anal Bioanal Chem (2011) 399:973–978
DOI 10.1007/s00216-010-4298-z

ORIGINAL PAPER

Particle size characterization of titanium dioxide in sunscreen products using sedimentation field-flow fractionation–inductively coupled plasma–mass spectrometry

Atitaya Samontha · Juwadee Shiowatana · Atitaya Siripinyanond

Received: 29 July 2010 / Revised: 2 October 2010 / Accepted: 4 October 2010 / Published online: 16 October 2010

Abstract Sedimentation field-flow fractionation–inductively coupled plasma–mass spectrometry (SdFFF-ICP-MS) was successfully applied to investigate particle size distribution of titanium dioxide (TiO_2) in sunscreen samples after hexane extraction to remove organic components from the samples. Three brands of sunscreen products of various sun protection factor (SPF) value were used as samples. Different particle size distribution profiles were observed for sunscreen samples of various brands and SPF values; however, the particle size distributions of titanium dioxide in most sunscreen samples investigated in this work were larger than 100 nm. The titanium dioxide concentrations were higher for the products of higher SPF values. By comparing the results obtained from online SdFFF-ICP-MS and those from the off-line ICP-MS determination of titanium after acid digestion, ICP-MS was found to effectively atomize and ionize the titanium dioxide particle without the need for acid digestion of the samples. Therefore, the online coupling between SdFFF and ICP-MS could be effectively used to provide quantitative information of titanium dioxide concentrations across particle size distribution profiles.

Keywords Titanium dioxide · Sunscreen · Particle size · Sedimentation field-flow fractionation · Inductively coupled plasma–mass spectrometry

A. Samontha · J. Shiowatana · A. Siripinyanond (✉)
Department of Chemistry and Center of Excellence for Innovation in Chemistry, Faculty of Science, Mahidol University,
Rama VI Road,
Bangkok 10400, Thailand
e-mail: scasp@mahidol.ac.th

Introduction

Ultraviolet (UV) radiation including UV-A (320–400 nm) and UV-B (290–320 nm) can cause skin cancer and other harmful effects to humans [1–4]. To avoid unwanted skin effects from the sun it is necessary to use sunscreen filters. Titanium dioxide (TiO_2), which is a physical UV filter, can reflect and scatter UV radiation very efficiently [5], and it is, therefore, often used to formulate sunscreen products with a high sun protection factor (SPF) value [6]. According to the European legislation, titanium dioxide is the only inorganic UV filter permitted to be used in sunscreen products with the maximum allowable concentration of 25% (*w*/*w*) [7]. The radiation reflection and scattering efficiencies of titanium dioxide depend on its concentration and particle size, with a particle size of approximately 60–120 nm the most effective in UV reflection and scattering ability [5]. Therefore, the analysis of sunscreen cosmetics in terms of the concentration and particle size of titanium dioxide should be considered.

Although the official methods for determining titanium dioxide particles in sunscreen cosmetics, either in terms of quantitative element content or the particle size distribution, have never been documented, several analytical techniques have been reported for determination of titanium dioxide in sunscreen. These techniques include the classical volumetric method [8], atomic absorption spectrometry [9], inductively coupled plasma optical emission spectrometry [8, 10], and X-ray fluorescence spectrometry [11, 12]. For particle size characterization, flow field-flow fractionation (FlFFF) has been reported for titanium dioxide particles in a commercial sunscreen product [13] and titanium dioxide nanoparticles imprinted for tyrosine [14].

Field-flow fractionation (FFF) is a flow-assisted technique for size characterization of particles in the nanometer to sub-micrometer scale. The fractionated particles can be further characterized by various detection methods [15, 16]. The principle [16, 17] and applications [18, 19] of FFF have been described elsewhere. Depending on the type and the particle size of samples, various types of external field forces may be applied. These external fields give rise to an assortment of FFF sub-techniques, including gravitational, sedimentation, flow, electrical, and thermal FFF. Sedimentation FFF (SdFFF) and FlFFF are most commonly used. As the particle size of titanium dioxide in sunscreen products is in the sub-micrometer size range, SdFFF may be used [18]. Previous works indicated that sedimentation FFF was successfully used to separate titanium dioxide microparticles [18–20].

An online coupling between SdFFF and inductively coupled plasma–mass spectrometry (SdFFF-ICP-MS) was proposed to provide the quantitative information of titanium dioxide concentrations across particle size distribution profiles of the sunscreen samples. The necessity for sample preparation before SdFFF particle size characterization was evaluated. Various initial field strengths were employed in SdFFF fractionation to check for the reliability of the resulting particle size distribution information. The ability of ICP-MS as an online detector for the fractionated titanium dioxide particles was examined. The developed SdFFF-ICP-MS method was applied to investigate size distribution of titanium dioxide particles in various sunscreen products of various SPF values.

Experimental

Chemicals and samples

Polystyrene latex standards having diameters of 0.35, 0.53, and 0.72 μm from Postnova Analytik (Landsberg, Germany) were used for SdFFF calibration. A carrier liquid was 0.02% (*v*/*v*) FL-70 detergent (Fisher Scientific, PA, USA) containing 0.02% (*w*/*v*) NaN_3 (Merck, Darmstadt, Germany) to prevent bacterial growth. FL-70 is a mixture of anionic and non-ionic compounds containing the following active components: oleic acid, sodium carbonate, tergitol, tetrasodium EDTA, polyethylene glycol, and triethanolamine [21].

Three brands of commercial sunscreen cream products of various SPF values (0 and 50 SPF for brand A; 0, 15, and 30 SPF for brand B; and 0 and 15 SPF for brand C) were purchased from a local supermarket. Hexane, which was employed to remove some organic components, was purchased from Labscan (Bangkok, Thailand). Ti elemental standard solution of 100 $\mu g\,mL^{-1}$ (AccuStandard, New Haven, CT, USA) was used to prepare the ICP-MS calibration solution.

Preparation of sunscreen sample

Sunscreen cream products (0.01 g) of various brands and SPF values were weighed and diluted in 1 mL of deionized water to obtain the sunscreen sample of 1% (*w*/*v*). Before injection into SdFFF, a 50-μL volume of 1% (*w*/*v*) of sunscreen cream sample in deionized water was mixed thoroughly by vortex.

Preparation of defatted sunscreen sample

To defat or remove some organic components from sunscreen cream products, 1 mL of hexane was applied to soak 0.01 g of sunscreen cream samples for 12 h at room temperature. Hexane containing organic components was removed and the defatted part was diluted with deionized water to 1% (*w*/*v*). To study particle size distribution in sunscreen cream samples, a 50-μL volume of 1% (*w*/*v*) of defatted sunscreen cream sample in deionized water was mixed thoroughly by vortex before SdFFF analysis.

Acid digestion of sunscreen sample

Sunscreen cream products (0.05 g) were weighed and digested at approximately 350 °C with 10 mL of H_2SO_4 in the presence of 4 g of $(NH_4)SO_4$. Then, 25 mL of HCl and 30 mL of deionized water were added to the mixture and heated until the clear solution was obtained. Subsequently, the digested solution was diluted with deionized water before ICP-MS determination of Ti concentration.

Instrumentation

The SdFFF system (Model S-101 Particle/Colloid Fractionator, Postnova Analytik, Landsberg, Germany) was used in this study. The SdFFF channel was 89.5 cm long, 2.0 cm wide, and 0.0254 cm thick, with a rotor radius of 15.1 cm. The channel volume was calculated to be 4.45 mL. The carrier solution was introduced into the SdFFF channel by an HPLC pump (model PN1122, Postnova Analytik). A UV detector (model UV2075, Jasco, Essex, UK) was set at 254 nm to monitor light attenuation of the eluted particles. Samples of 50 μL were injected into SdFFF via a Rheodyne injector.

An ICP-MS instrument (model Sciex/ELAN 6000, Perkin Elmer, CT, USA) was used as an element detector sequentially after the UV absorption detector. Owing to the similarity of the SdFFF channel and ICP-MS sample flow rates typically used for analysis, the ICP-MS cross-flow nebulizer was connected directly to the UV detector outlet with a 30-cm length of poly(tetrafluoroethylene) tubing

(0.58 mm id). The operating conditions of SdFFF and ICP-MS measurements are summarized in Table 1.

Data treatment

Raw fractograms were translated into size distribution profiles using the Postnova FFF Analysis software version 2.0 (Postnova Analytik, Landsberg, Germany). Peak evaluation, baseline adjustment, and integration were performed using PeakFit™ (SPSS, IL, USA).

Results and discussion

The need for sample preparation before particle size characterization of titanium dioxide in cosmetics by using SdFFF

By knowing the exact geometry of the SdFFF channel, the field, flow rate, and the density difference between particle and carrier liquid, diameter of the separated particle can be calculated directly from the experimental retention time [22]. The average density of titanium dioxide particles was 4.05 $g mL^{-1}$ [23], and therefore, the density difference between the particles and the carrier liquid ($\Delta\rho$) was 3.05 $g mL^{-1}$. To apply SdFFF for particle size characterization of titanium dioxide in sunscreen samples, various experimental conditions were examined to demonstrate the reproducibility and reliability of SdFFF for particle size characterization of titanium dioxide in sunscreen products. Various initial field strengths (500, 600, and 800 rpm) were applied to fractionate titanium dioxide particles in a 30 SPF sunscreen as illustrated in Fig. 1. Fractograms of 1% (*w*/*v*) 30 SPF sunscreen (brand B) showed two separated peaks at different retention times. With higher field strength, the peaks shifted towards longer retention times (Fig. 1a). Nonetheless, the particle size distributions obtained from various experimental conditions did not agree well with each other, indicating the erroneous results in particle size determination by the SdFFF technique. This error might be due to the fact that the cosmetic sample contains not only the titanium dioxide particles, but also some other types of particles. Alternatively, it might be due to the fact that the titanium dioxide particles were coated by some organic components in the sunscreen sample, which could make the approximation of the particles density of 4.05 $g mL^{-1}$ to be incorrect.

Therefore, it was necessary to carry out sample preparation before introduction of sunscreen samples into SdFFF channel. To remove the organic components from the titanium dioxide particles, hexane extraction was performed [13]. Hexane removes the organic compounds contained in the sunscreen products, which could cause some interaction between organic component and SdFFF channel, and affected on particle size fractionation of sunscreen sample. With hexane removal of organic components from the sunscreen samples, the resulting samples were called "defatted sunscreen samples." Various initial field strengths (400, 500, and 600 rpm) were applied to fractionate titanium dioxide particles in the defatted sunscreen as illustrated in Fig. 2a with the resulting particle size distributions shown in Fig. 2b. The particle size distributions in Fig. 2b obtained from various experimental conditions were all similar showing the particle size range of 0.1–0.6 μm with the peak maximum at around 0.52 μm. This suggests that the particle size determination of titanium dioxide in sunscreen products is possible with SdFFF with the necessity of sample preparation before analysis, and hexane extraction is considered effective for such purpose. The initial field strength of 400 rpm was selected for further use as it was sufficient to separate the

Table 1 SdFFF and ICP-MS operating conditions

SdFFF operating conditions	
SdFFF channel dimensions (cm^3)	89.5×2.0×0.0254
SdFFF rotor radius (cm)	15.1
Carrier liquid	0.02% (*v*/*v*) FL-70 containing 0.02% (*w*/*v*) sodium azide
Channel flow rate ($mL min^{-1}$)	1.0
Equilibration time (min)	10
Power field programming	initial applied field, 400 rpm [obtained field, 397 rpm or 26.6×*g*] for 8 min; field decay parameter, −64; final field, 50 rpm [obtained field, 49 rpm]
ICP-MS operating conditions	
Rf generator frequency (MHz)	40
Rf power (W)	1,150
Nebulizer gas flow rate ($L min^{-1}$)	0.99
Coolant gas flow rate ($L min^{-1}$)	15
Auxiliary gas flow rate ($L min^{-1}$)	1.0
Isotopes monitored (*m*/*z*)	^{47}Ti and ^{49}Ti

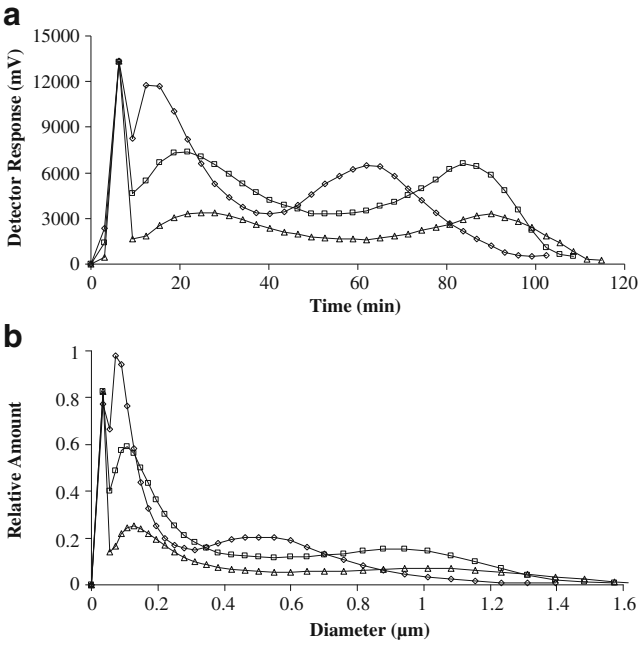

Fig. 1 Effect of field strength on fractionation of 30 SPF sunscreen (brand B). **a** Raw fractograms and **b** particle size distributions of 30 SPF sunscreen (brand B) obtained from various initial fields as 500 (*diamond*), 600 (*square*), and 800 rpm (*triangle*). The SdFFF operating condition was as follows: initial field hold time 8 min, field decay parameter −64, final field 50 rpm, and $\Delta\rho$=3.05 gmL^{-1}. The channel flow rate was constant at 1 mLmin^{-1}

particles from the void fraction with minimized analysis time.

Particle size distribution of titanium dioxide in sunscreen products of various brands and SPF values

With the selected SdFFF operating conditions, particle size distributions of titanium dioxide in the defatted sunscreen products of various brands and SPF values were investigated by using SdFFF-ICP-MS. With the UV detector, the particle size distributions of sunscreen samples are shown in Fig. 3. It can be seen that different brands of sunscreen products showed different particle size distribution patterns. For a particular brand of sunscreen products, the sample with higher SPF values showed larger particle size than that of the smaller SPF values. With the ICP-MS detector, the particle size distributions of titanium dioxide in sunscreen samples were obtained as illustrated in Fig. 4. For brand A, the signal of titanium was only slightly observed for sunscreen of 0 SPF value, whereas the distribution of titanium was found in the range of 0.1–0.5 μm for the sunscreen of 50 SPF value. For brand B, the distribution of titanium in sunscreen of various SPF values were different, but ranging between 0.1 and 0.4 μm. Titanium was found to present in a smaller particle size for the sunscreen of 15 SPF values as compared to that of 0 and 30 SPF values, suggesting that the manufacturer might have different strategies to formulate the products of different SPF values within the same brand. The manufacturer of brand B might not use the same titanium dioxide particle size for the products of different SPF values. For brand C, the distribution of titanium in sunscreen of 0 and 15 SPF values were found in the range of 0.2–0.6 μm. Higher titanium content was found in the product of higher SPF value.

Particle size distributions of titanium dioxide in all sunscreen samples investigated in this work were larger than 100 nm size range, except for the brand B of 15 SPF value. The particle size distributions of titanium dioxide in the defatted sunscreen samples (Fig. 4) were not well corresponded with the particle size distribution profiles (Fig. 3) except for the sunscreen brand A. For brand B, titanium (Fig. 4b) was found to associate with the small particle size range of the particles found in the defatted sunscreen samples (Fig. 3b). For brand C, titanium (Fig. 4c) was found to associate with the large particle size range of the particles found in the defatted sunscreen samples (Fig. 3c). These data suggest that the manufacturer of brand A might use titanium dioxide solely to adjust the SPF values of their products, whereas the manufacturers of brands B and C might adjust the SPF values of their

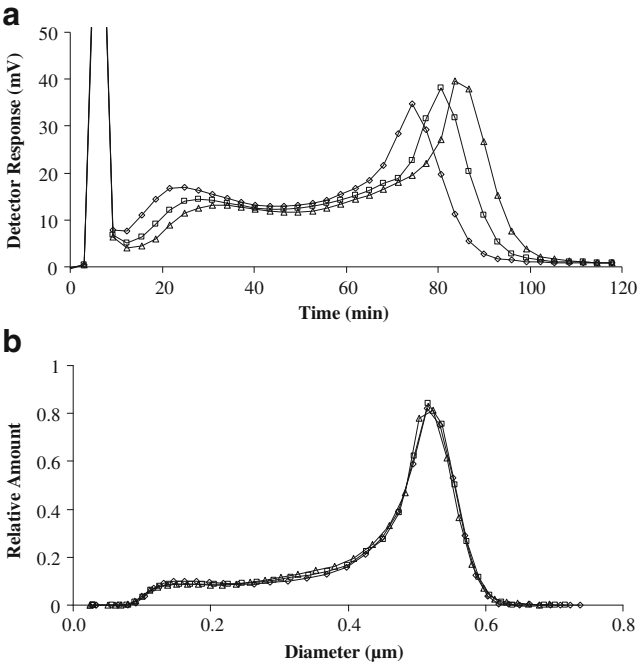

Fig. 2 Effect of field strength on fractionation of the defatted 30 SPF sunscreen (brand B). **a** Raw fractograms and **b** particle size distributions of 30 SPF sunscreen (brand B) obtained from various initial fields as 400 (*diamond*), 500 (*square*), and 600 rpm (*triangle*). The SdFFF operating condition was as follows: initial field hold time 8 min, field decay parameter −64, final field 50 rpm, and $\Delta\rho$=3.05 gmL^{-1}. The channel flow rate was constant at 1 mLmin^{-1}

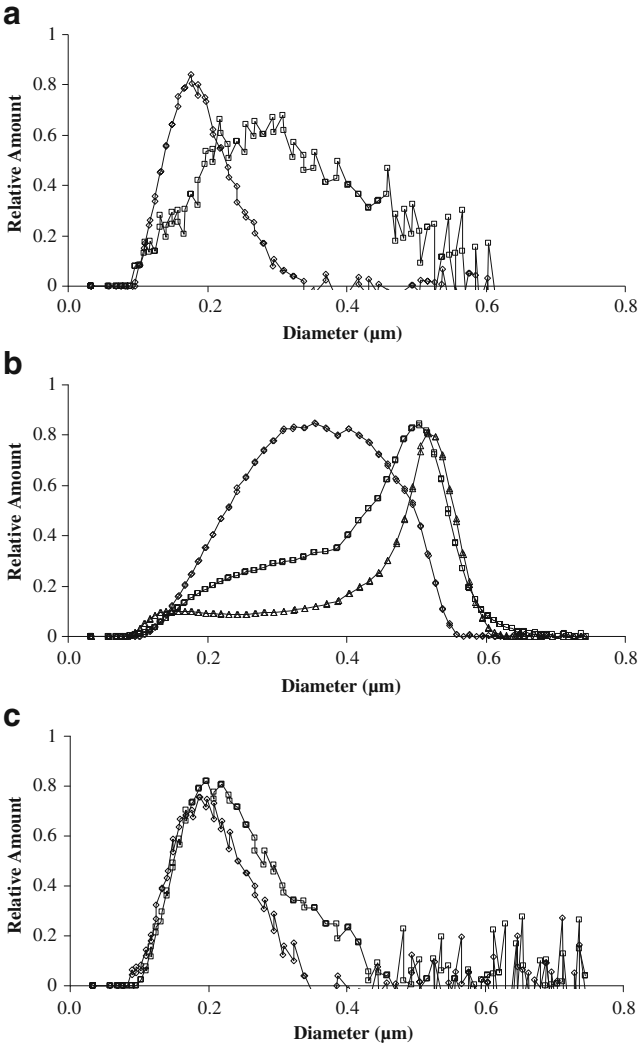

Fig. 3 Particle size distributions of defatted sunscreen samples. **a** Brand A, where *diamond* and *square* represent 0 and 50 SPF, respectively. **b** Brand B, where *diamond*, *square*, and *triangle* represent 0, 15, and 30 SPF, respectively. **c** Brand C, where *diamond* and *square* represent 0 and 15 SPF, respectively

products by adding both organic and inorganic components other than titanium dioxide as UV filters.

Titanium dioxide concentrations in sunscreen samples

Not only the particle size information, but it is also important to provide quantitative information on the titanium dioxide concentration in the sunscreen products, as its maximum allowable concentration in the sunscreen products has been declared by many countries such as European Union, Japan, and USA. In the European Union legislation, titanium dioxide is the only inorganic UV filter which is allowed at 25% maximum concentration [7]. The determination of titanium dioxide content (% *w*/*w*) in sunscreen products of various brands and SPF values was carried out using ICP-MS detection of titanium.

In this study, ICP-MS determination of titanium concentrations was performed with various approaches as follows: as an online detector for SdFFF, off-line detection of the collected fraction from SdFFF after acid digestion, and direct detection of the acid digested samples. The titanium dioxide concentrations in all sunscreen samples from various approaches are summarized in Table 2, which illustrates that the concentrations found from all approaches were similar. The closeness in the titanium dioxide concentrations obtained from the collected fraction from SdFFF after acid digestion with those directly determined after acid digestion of the samples indicates that titanium dioxide was not loss

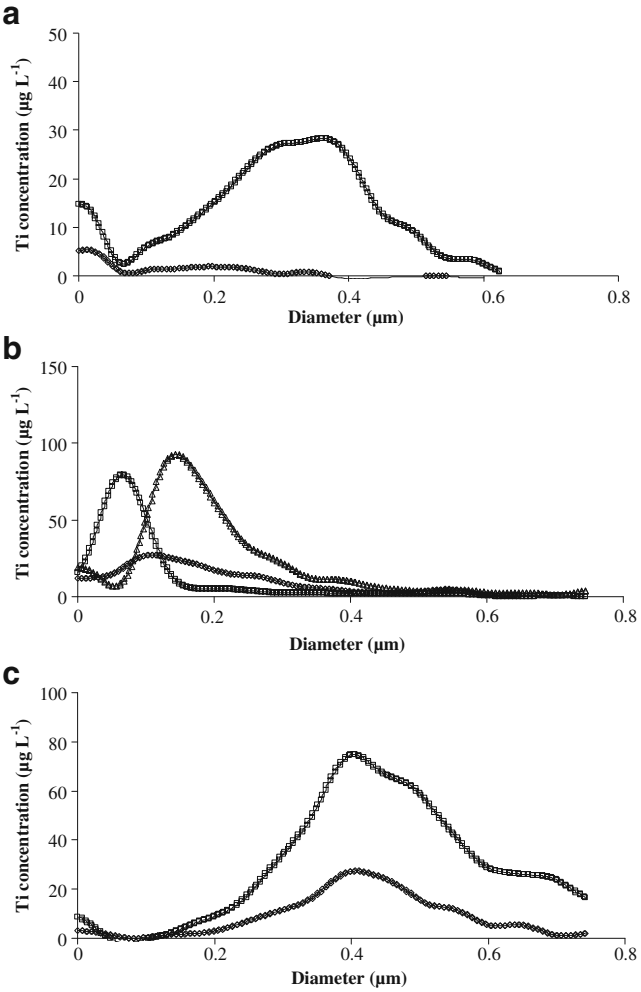

Fig. 4 Particle size distributions of titanium dioxide in defatted sunscreen samples. **a** Brand A, where *diamond* and *square* represent 0 and 50 SPF, respectively. **b** Brand B, where *diamond*, *square*, and *triangle* represent 0, 15, and 30 SPF, respectively. **c** Brand C, where *diamond* and *square* represent 0 and 15 SPF, respectively. Data were smoothed with Savitzsky–Golay function (PeakFit, SPSS, Chicago, IL, USA) with a smoothing level of 10%

Table 2 TiO_2 concentrations in sunscreen samples of various brands and SPF values

Samples	TiO_2 concentration (% *w*/*w*) [average±SD], *n*=3		
	Method A	Method B	Method C
0 SPF brand A	n.d.	n.d.	<0.04
50 SPF brand A	n.d.	n.d.	3.84±0.28
0 SPF brand B	n.d.	n.d.	0.09±0.02
15 SPF brand B	n.d.	n.d.	0.37±0.05
30 SPF brand B	0.84±0.10	0.74±0.10	0.82±0.20
0 SPF brand C	n.d.	n.d.	0.12±0.02
15 SPF brand C	1.16±0.16	0.94±0.06	0.93±0.05
LOQ	<0.06	<0.03	<0.04

The concentration of titanium is represented as TiO_2 percentage in the sample (% *w*/*w*). Method A is an online SdFFF-ICP-MS. The concentration of titanium dioxide in the samples was obtained by online SdFFF-ICP-MS measurement with external calibration using standard solutions prepared in the SdFFF carrier liquid. Total titanium dioxide concentration was determined by integration of the signal through the whole fractionation time using a PeakFit™ program (SPSS, IL, USA). Method B is an off-line SdFFF and ICP-MS determination of titanium dioxide in the fractionated samples. Method C is ICP-MS determination of titanium after acid digestion of samples

n.d. not determined

during the SdFFF fractionation of samples. The closeness in the titanium dioxide concentrations obtained from the online SdFFF-ICP-MS with those from the SdFFF fraction after acid digestion suggests that the ICP-MS could effectively atomize and ionize the titanium dioxide particle without the need for acid digestion. Therefore, the online coupling between SdFFF and ICP-MS could be effectively used to provide the quantitative information of titanium dioxide concentrations across particle size distribution profiles.

For all sunscreen samples in this study, the titanium dioxide contents were below the maximum allowable concentration (25%) as set by the European legislation. Different brands of sunscreen products showed different titanium dioxide contents. Nevertheless, higher titanium dioxide contents were observed for the sunscreen of the same brand but with increasing SPF values.

Conclusions

SdFFF-ICP-MS was demonstrated feasible to provide quantitative information of titanium dioxide concentrations across particle size distribution profiles. Nonetheless, sample preparation was necessary prior to SdFFF particle size characterization. Various brands and SPF values of sunscreen products showed different particle size distributions and different titanium dioxide contents. The information obtained from SdFFF-ICP-MS can be useful for quality control of the finished sunscreen products.

Acknowledgments The Center for Innovation in Chemistry: Postgraduate Education and Research Program in Chemistry (PERCH-CIC), Commission on Higher Education, Ministry of Education is gratefully acknowledged for the studentship support for A. Samontha, the partial research support for A. Siripinyanond, and the purchase of the SdFFF equipment. Thanks are also due to the Thailand Research Fund for the research support for A. Siripinyanond. This paper was presented in part at the Pure and Applied Chemistry Conference 2010 (PACCON 2010), Ubonratchathani, Thailand, January 21–23, 2010, Oral Presentation Number ANC-OR-17.

References

1. De Fabo EC, Noonan EP (1983) J Exp Med 158:84–98
2. Heck DE, Vetrano AM, Mariano TM, Laskin JD (2003) J Biol Chem 278:22432–22436
3. Agar NS, Halliday GM, Barnetson RS, Ananthaswamy HN, Wheeler M, Jones AM (2004) Proc Natl Acad Sci USA 101:4954–4959
4. Krutmann J (2000) J Dermatol Sci 23:S22–S26
5. Popov AP, Lademann J, Priezzhev AV, Myllylä R (2005) J Biomed Opt 10:1–9
6. Anderson MW, Hewitt JP, Spruce SR (1997) In: Lowe NJ, Shaath NA, Pathak MA (eds) Broad-spectrum physical sunscreens: titanium dioxide and zinc dioxide. Marcel Dekker Inc., New York, pp 353–398
7. Salvador A, Chisvert A (2005) Anal Chim Acta 537:1–14
8. Kim YS, Kim BM, Park SC, Jeong HJ, Chang JS (2006) J Cosmet Sci 57:377–381
9. Mason JT (1980) J Pharm Sci 69:101–102
10. Salvador A, Pascual-Martí MC, Adell JR, Requeni A, March JG (2000) J Pharm Biomed Anal 22:301–306
11. Kawauchi A, Ishida M, Saitoh I (1996) Spectrosc Lett 29:345–366
12. Melquiades FL, Ferreira DD, Appoloni CR, Lpoes F, Lonni AG, Oliveira FM, Duarte JC (2008) Anal Chim Acta 613:I35–I43
13. Contado C, Pagnoni A (2008) Anal Chem 80:7594–7608
14. Zattoni A, Reschiglian P, Montalti M, Zaccheroni N, Prodi L, Picca RA, Malitesta C (2007) Inorg Chim Acta 360:1063–1071
15. Contado C, Blo G, Fagioli F, Dondi F, Beckett R (1997) Colloid Surf A 120:47–59
16. Saeseaw S, Shiowatana J, Siripinyanond A (2006) Anal Bioanal Chem 386:1681–1688
17. Saeseaw S, Shiowatana J, Siripinyanond A (2005) Food Res Int 34:777–786
18. Cardot PJP, Rasouli S, Blanchart P (2001) J Chromatogr A 905:163–173
19. Rasouli S, Blanchart P, Clédat D, Cardot PJP (2001) J Chromatogr A 923:119–126
20. Koliadima A, Gavril D, Karaiskakis G (1999) J Liq Chromatogr Relat Technol 22:2779–2793
21. http://fscimage.fishersci.com/msds/06352.htm
22. Kirkland JJ, Rementer SW, Yau WW (1981) Anal Chem 53:1730–1736
23. (2006) In: Ó Neil MJ (ed) The Merck Index: an encyclopedia of chemicals, drugs, and biological, 14th ed. Merck Research Laboratories: Whitehouse Station, NJ

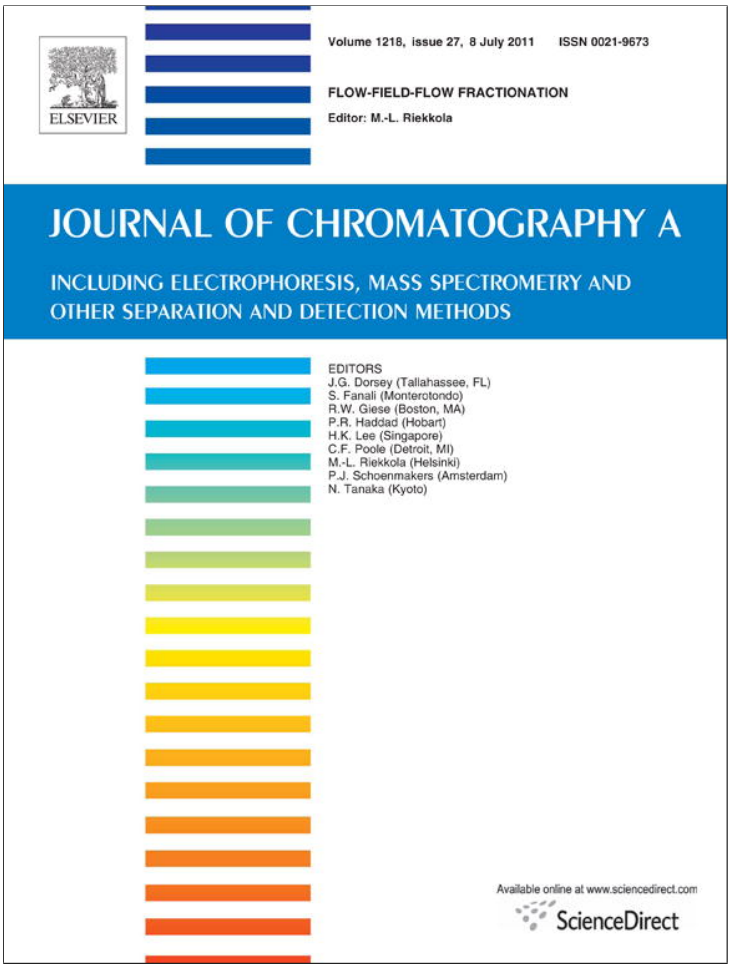

Journal of Chromatography A, 1218 (2011) 4213–4218

Contents lists available at ScienceDirect

Journal of Chromatography A

journal homepage: www.elsevier.com/locate/chroma

Flow field-flow fractionation with off-line electrothermal atomic absorption spectrometry for size characterization of silver nanoparticles

Kanchana Songsilawat, Juwadee Shiowatana, Atitaya Siripinyanond*

Department of Chemistry and Center for Innovation in Chemistry, Faculty of Science, Mahidol University, Rama VI Rd., Bangkok 10400, Thailand

ARTICLE INFO

Article history:
Available online 21 December 2010

Keywords:
Silver nanoparticles
Flow field-flow fractionation
Electrothermal atomic absorption spectrometry
Humic acid

ABSTRACT

Flow field-flow fractionation (Fl-FFF) with off-line electrothermal atomic absorption spectrometry (ETAAS) detection was developed and employed for particle size characterization of Ag NPs stabilized by citrate, pectin, and alginate. Citrate stabilized-Ag NPs were prepared from sodium borohydride reduction of silver nitrate. Sodium citrate was used as the capping agent to stabilize Ag NPs and prevent the aggregation process. Pectin stabilized- and alginate stabilized-Ag NPs were prepared from ascorbic acid reduction of silver nitrate. Pectin and alginate were used as the capping agent for pectin stabilized- and alginate stabilized-Ag NPs, respectively. Three types of Ag NPs were characterized by using FlFFF, zeta potentiometer, and TEM technique. The mean particle sizes of Ag NPs as characterized by FlFFF were 9 nm, 19 nm, and 45 nm for citrate stabilized-, pectin stabilized-, and alginate stabilized-Ag NPs, respectively, in deionized water. Further, FlFFF with ETAAS detection was employed to observe the aggregation of Ag NPs of various types in environmental water in the absence and presence of humic acid. Citrate stabilized-Ag NPs underwent aggregation more rapid than the pectin stabilized- and alginate stabilized-Ag NPs as the latter two types were sterically stabilized. Further, humic acid could prolong the stability of Ag NPs in the environment.

1. Introduction

Silver nanoparticles (Ag NPs) are one of common engineered nanoparticles (ENPs) with at least one dimension within the size from approximately 1 nm to 100 nm [1]. Owing to their antibacterial properties, Ag NPs have been used in various consumer products including textiles, personal care products, food storage containers, and laundry additives. The release of Ag NPs into water and their mobilities in water should therefore be investigated. Silver ions (Ag^+) can be released from consumer products by oxidation of metallic silver (Ag^0) in contact with water [2,3]. Blaser et al. studied the model of total silver in the form of Ag^+ ions or AgNPs released from plastic and textile into water and indicated that up to 15% of the total Ag discharged into the environment [4]. Moreover, recent studies by Benn and Westerhoff confirmed that Ag NPs were easily released from nanosilver-coated socks during the washing process [5].

Recently, the issue of mobility and toxicity of Ag NPs has gained significant attention. In general, the smaller size can transport faster and has much higher toxicity than the larger size. Moreover, smaller size Ag NPs (<5 nm) are more toxic than any other forms of silver [6]. The aggregation is also one of the primary controls on both transport and toxicity of Ag NPs in the aquatic environment. Not only temperature, pH, ionic strength of environmental water, and concentration of Ag NPs show significant effect on the aggregation process, but also the surface property of Ag NPs is important [7]. The surface property of Ag NPs depends on how Ag NPs are synthesized. Ag NPs can be synthesized using various methods resulting in different shapes, sizes, and surface properties for numerous applications [8]. Normally, Ag NPs are synthesized via reduction of silver nitrate in water using reductants and stabilizing agent or capping agent for control of particle size to ensure a stable suspension [9,10]. The reductant and stabilizing agents commonly used are sodium borohydride and sodium citrate, respectively. Greener processes for the production of greener nanomaterials were reported by use of nontoxic chemicals [11].

As the particle size of Ag NPs plays important roles to their mobility and hence toxicity, particle size characterization of Ag NPs is necessary. Size characterization techniques for Ag NPs include dynamic light scattering (DLS) [12], transmission electron microscopy (TEM) [7,13], atomic force microscopy (AMF) [14], size exclusion chromatography (SEC) [15], hydrodynamic chromatography (HDC) [15], and flow field-flow fractionation (FlFFF) [13]. The use of FlFFF coupled off-line with AFM to observe the structure of the smaller size fraction of aquatic colloids was reported to fractionate citrate-stabilized Ag NPs at environmentally relevant conditions [14]. In this study, the use of ETAAS as an off-line detector for the Ag NPs fractionated by FlFFF was evaluated. FlFFF with

* Corresponding author. Tel.: +66 2 201 5195; fax: +66 2 354 7151.
E-mail address: scasp@mahidol.ac.th (A. Siripinyanond).

0021-9673/$ – see front matter © 2010 Elsevier B.V. All rights reserved.
doi:10.1016/j.chroma.2010.12.040

ETAAS detection was employed for size characterization of Ag NPs in environmental water. The aggregation phenomenon of Ag NPs from different synthesis methods including common method (citrate stabilized) and green synthesis (polysaccharide stabilized) in various types of water was investigated. The effect of humic acid on the aggregation of Ag NPs was also examined.

2. Experimental

2.1. Chemicals and samples

Silver nitrate was purchased from Carlo Erba (Rodano, MI, Italy). Sodium borohydride, sodium hydroxide, and sodium azide were purchased from Merck (Darmstadt, Germany). Humic acid and sodium citrate tribasic dihydrate were purchased from Sigma–Aldrich (Steinheim, Germany). Pectin and alginate were from Fluka (Buchs, Switzerland). Gold nanoparticle standard (Au NPs) of 10 nm diameter (Sigma–Aldrich) was used to calibrate the FlFFF channel. The humic acid stock solution (2000 mg L^{-1}) was made by dissolving 0.050 g of humic acid in 25 mL of deionized water.

Water samples were collected from three different sites including sea water from the Jausumran beach (Phetchaburi, Thailand), ground water from the Lopburi farm (Lopburi, Thailand), and tap water (Bangkok, Thailand). The samples were stored in a refrigerator and filtered through 0.45 μm membrane filters before use.

2.2. Silver nanoparticles synthesis

Citrate stabilized-Ag NPs were prepared as described previously by Yang et al. [16]. Briefly, 100 mL of 0.3 M silver nitrate and 8 mL of 12.6 M sodium citrate were mixed together in a conical flask, and then stirred at 50 rpm. Stirring was continued and 2 mL of 37 mM $NaBH_4$ was added into solution. The yellow solution was then observed.

For polysaccharide stabilized-Ag NPs, Ag NPs were prepared by the reduction of silver ion using ascorbic acid. Polysaccharide, i.e., pectin and alginate, were used to stabilize nanoparticles. Briefly, 100 mL of 0.1% (w/v) polysaccharide solution (pectin or alginate) were mixed together with freshly prepared ascorbic acid of 1 mM (50 mL) and vigorously stirred. Fifty milliliters of 2 mM silver nitrate solution was added into the solution and 0.3 M NaOH (0.1 mL) was added quickly. Stirring was continued and the final yellow solution was observed.

2.3. Instrumentation

The FlFFF system is a PN-1201-FO model (Postnova Analytics, Landsberg, Germany). The FlFFF channel dimensions are 27.7 cm length, 2.0 cm wide, and 254 μm thick. A 1-kDa regenerated cellulose membrane (Postnova) was used. The carrier liquid was 0.02% FL-70 and 0.02% NaN_3 was diluted in deionized water and adjusted to pH 9.2–10. Sample volume of 20 μL was introduced into FlFFF via the Rheodyne injector valve. A high pressure liquid chromatography (HPLC) pump (Model PN 2101, Postnova Analytics, Germany) was used to deliver the channel flow at 1 mL min^{-1}. The cross flow rate fixed at 1 mL min^{-1} was delivered by another HPLC pump of the same model. After fractionation, the effluent was directed through a UV detector (Model S3210 UV–visible detector; Postnova Analytics) and the detector was set at 400 nm for detection of the Ag NPs. The automatic fraction collector (Waters, Milford, MA, USA) was used to collect fraction from UV detector outlet. The FlFFF operating conditions are shown in Table 1.

A Perkin Elmer Model AAnalyst 100 (Norwalk, CT, USA) with deuterium background corrector was used for detection of silver after the UV absorption detector. The Perkin Elmer Model AS-72 autosampler was used to introduce solution into a graphite tube. The furnace operating condition for silver and silver nanoparticles measurement is summarized in Table 2.

Table 1
FlFFF operating condition.

FlFFF: Model PN-1021-FO	
Channel dimension/cm × cm × cm	27.7 long × 2.0 wide × 0.02 thick
Carrier liquid	0.02% FL-70 and 0.02 NaN_3 (pH 9.5)
Channel flow rate/mL min^{-1}	1.0
Cross flow rate/mL min^{-1}	1.0
Equilibration time/min	2.2
Membrane	1 kDa MWCO poly(regenerated cellulose acetate)

Table 2
Electrothermal atomic absorption spectrometer operating condition for silver detection.

ETAAS: Perkin Elmer Analyst 100-HGA-800				
Step		Temperature (°C)	Ramp time (s)	Hold time (s)
1	Drying	130	20	30
2	Ashing	800	20	30
3	Atomization	1800	0	8
4	Clean up	2600	1	5

The UV–visible absorption spectra of Ag NPs were observed by using UV–visible spectrophotometer (Model V-530, Jasco, Easton, MD, USA). Zeta potential measurements were carried out using the Zetasizer Nano ZS (Malvern Instruments Zetasizer1000 Hs, Malvern, UK). A transmission electron microscope (TEM), JEOL JEM-1230 (Peabody, MA, USA), was used to acquire images of the Ag NPs. The TEM was operated at 25 °C and 80 kV.

3. Results and discussion

3.1. Particle size characterization of the synthesized silver nanoparticles

Particle size characterization of three types of Ag NPs was performed by using FlFFF as illustrated in Fig. 1. Particle sizes at peaks were 9 nm, 19 nm, and 45 nm for citrate stabilized-Ag NPs, pectin stabilized-Ag NPs, and alginate stabilized-Ag NPs, respectively. The particle size values obtained from FlFFF were in good agreement with those from TEM (Fig. 2) and zetasizer as summarized in Table 3, by which the particle size of alginate stabilized-Ag NPs was larger than pectin stabilized- and citrate stabilized-Ag NPs, respectively.

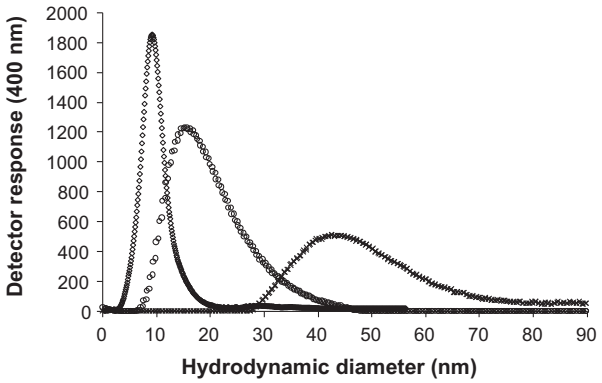

Fig. 1. Hydrodynamic diameter distributions of Ag NPs: (◊) citrate stabilized Ag-NPs; (○) pectin stabilized-Ag NPs; (×) alginate stabilized-Ag NPs. The FlFFF conditions were as follows: channel flow 1 mL min^{-1}, cross flow 1 mL min^{-1}, RC membrane (1 kDa), 0.02% FL-70 and 0.02% NaN_3 as carrier liquid. UV–visible was used as FlFFF detector.

Table 3
Particle size of silver nanoparticles (Ag NPs) as determined by various techniques.

Ag NPs	Particle diameter (nm)			
	TEM	Zetasizer	FlFFF with UV–visible[a]	FlFFF with ETAAS[a]
Citrate-stabilized	11.3 ± 3.5	13.6 ± 3.1	9.50 ± 0.0	10.5 ± 0.5
Pectin-stabilized	10.5 ± 5.1	18.3 ± 9.4	19.1 ± 0.1	18.2 ± 0.7
Alginate-stabilized	37.5 ± 2.3	48.8 ± 11	45.5 ± 0.1	40.1 ± 0.4

[a] The mean particle size (d_{mean}) and associated standard deviation ($n = 3$).

With UV–visible absorption spectrometry, the surface plasmon resonance peaks were observed at 390 nm, 400 nm, and 412 nm for citrate stabilized-, pectin stabilized-, and alginate stabilized-Ag NPs, respectively, as shown in Fig. 3, suggesting the same trend as those observed by the FlFFF, TEM, and zetasizer, as the smaller particles exhibit plasmon resonance band as shorter wavelength and the larger particles exhibit the plasmon band at longer wavelength [17]. Nonetheless, the particle sizes of Ag NPs obtained from different techniques were slightly different owing to the fact that different techniques provide different particle size information. TEM measures a number based size distribution of the core particle excluding the stabilizing agent, while FlFFF and zetasizer measure a mass based size distribution or hydrodynamic volume [13].

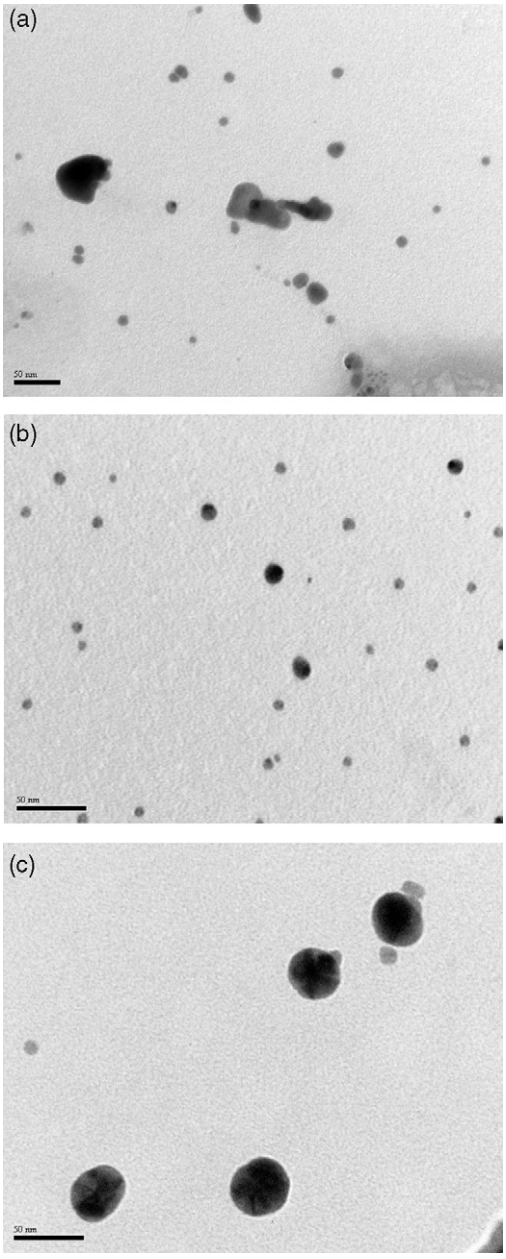

Fig. 2. TEM images of (a) citrate stabilized-Ag NPs, (b) pectin stabilized-Ag NPs, and (c) alginate stabilized-Ag NPs.

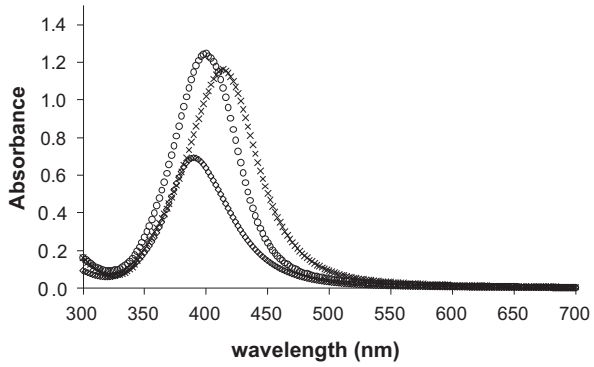

Fig. 3. UV–visible absorption spectra of silver nanoparticles prepared by different stabilizer agents: (◊) citrate stabilized-Ag NPs; (◯) pectin stabilized-Ag NPs; (×) alginate stabilized-Ag NPs.

3.2. FlFFF with off-line ETAAS detection of silver

Electrothermal atomic absorption spectrometer (ETAAS) was investigated as an off-line detector for FlFFF, as it was previously illustrated possible for SdFFF [18,19]. With the ashing temperature of 800 °C and atomization temperature of 1800 °C for ETAAS determination of silver, it was possible to completely atomize the fractionated particulate sample thus avoiding complex and lengthy sample digestion steps [20]. Nonetheless, to confirm the similarity between the atomization behaviors of the Ag NPs and silver ions, calibration experiments were performed for Ag NPs of various types and silver ions. Calibration curves obtained from all silver types indicate that the slopes were not significantly different, suggesting that the analytical sensitivities were the same for silver of all types. It was 0.0227, 0.0214, 0.0235, and 0.0210 for silver ion, citrate stabilized-, pectin stabilized-, and alginate stabilized-Ag NPs, respectively. The standard t tests with a significance value of 0.05 were performed for data comparison and indicated that the calibration slopes were not significantly different. Table 4 summarizes the characteristic masses, the limits of detection (LOD), and the limits of quantification (LOQ) obtained for silver determination for various

Table 4
The characteristic mass (m_o), slope, the limit of detection (LOD) and the limit of quantification (LOQ) for silver determination by ETAAS for various types of Ag NPs and silver ion.

Sample	Slope	m_o (pg)	LOD ($\mu g\,L^{-1}$)	LOQ ($\mu g\,L^{-1}$)
Ag ion	0.0227	0.8	2.6	8.7
Citrate stabilized-Ag NPs	0.0214	0.9	2.8	9.3
Pectin stabilized-Ag NPs	0.0235	1.0	2.5	8.4
Alginate stabilized-Ag NPs	0.0210	0.9	2.8	9.4

Table 5
The particle size of Ag NPs dispersed in various environmental waters.

Ag NPs	Particle size (nm) of Ag NPs in various types of water as determined by FlFFF-ETAAS		
	Deionized water	Tap water	Ground water
Citrate stabilized	10.5	16.7	n.d.
Pectin stabilized	18.2	19.7	21.2
Alginate stabilized	40.9	40.9	36.7

n.d.: not detectable.

types of silver. As the analytical sensitivities obtained for all types of silver examined in this work were not significantly different, it was possible to use the standard calibration prepared from silver ions for determination of silver in the fractionated silver nanoparticles.

3.3. Ag NPs stability in environmental waters

The stability of Ag NPs in various environmental waters including tap, sea, and ground water was investigated. UV–visible spectrophotometry and FlFFF with ETAAS detection were employed for such investigation. As reported earlier, the shift of the plasmon resonance band of Ag NPs towards the red end or the blue end depends upon the particle size, shape, state of aggregation, and the surrounding dielectric medium [17,21,22]. The blue shift is observed when the particles are smaller, and vice versa the red shift is observed when the particles grow larger. Therefore, UV–visible absorption spectrum can be used to examine the stability and the aggregation behavior of citrate stabilized-Ag NPs, as illustrated in Fig. 4. The maximum absorption of Ag NPs occurred at approximately 400 nm. Upon incubation of Ag NPs in various types of water for 180 min, two bands were observed suggesting that the nanoparticles formed aggregation or deviated from spherical symmetry [17]. Among the three types of Ag NPs synthesized in this study, the stability of alginate stabilized-Ag NPs was higher than that of pectin stabilized- and citrate stabilized-Ag NPs, respectively.

Flow FFF with ETAAS detection was also employed to observe the changes in particle size distribution of various types of Ag NPs upon incubation in various types of water for 180 min as summarized in Table 5. No peak was observed for Ag NPs dispersed in seawater, suggesting that seawater caused change in Ag NPs into free Ag ion or other non-detectable forms. Changes in particle size of Ag NPs were very significant when dispersed in ground water, as compared to those in tap water. In ground water, no peak was observed for citrate stabilized-Ag NPs, whereas it was detectable for other types of Ag NPs, suggesting that the stability of citrate stabilized-Ag NPs was poorer than that of other types of Ag NPs. Fig. 5 illustrates the hydrodynamic diameter distribution of citrate stabilized-Ag NPs dispersed in various types of water. Further experiments are necessary to investigate parameters affecting changes in particle size of Ag NPs. Tap water was selected to be investigated.

3.4. Parameters affecting particle size of Ag NPs in tap water

In environmental waters, the stability of Ag NPs depends on their surface properties, pH, ionic strength, and the presence of natural organic macromolecules and their concentrations [1,7,13,23]. The stability of the colloidal systems in natural water can be governed by two fundamental mechanisms, which are steric repulsion and charge stabilization or electrostatic interaction [24,25]. The steric repulsion refers to the adsorption of polymers or macromolecules onto the particle surface preventing the particle surfaces coming into close contact with each other. Charge stabilization or electrostatic interaction refers to the distribution of charge species in the system.

For this reason, stabilizing agent was added in the Ag NPs synthesis process to prevent nanoparticles from aggregation and control the particle size of the Ag NPs. Various stabilizing agents, including alginate, citrate, and pectin, were used in the synthesis of Ag NPs. The stability of Ag NPs prepared from different stabilizing agents in environmental waters including tap, sea, and ground water was examined.

3.4.1. Types of stabilizing agent

Ag NPs were dispersed in tap water and UV–visible spectrophotometer was employed to investigate the stability of Ag NPs prepared from various stabilizing agents as shown in Fig. 6. Among the three types of Ag NPs synthesized in this study, the stability of Ag NPs stabilized by alginate was found higher than those stabilized by pectin and citrate, respectively. This information is in good agreement with the zeta potential value (mV) of each Ag NPs as -51.3 ± 1.6, -35.6 ± 2.3 and -34.7 ± 2.4 for alginate, pectin, and citrate stabilized Ag NPs, respectively. The nanoparticles with zeta potential more negative than -30 mV or more positive than

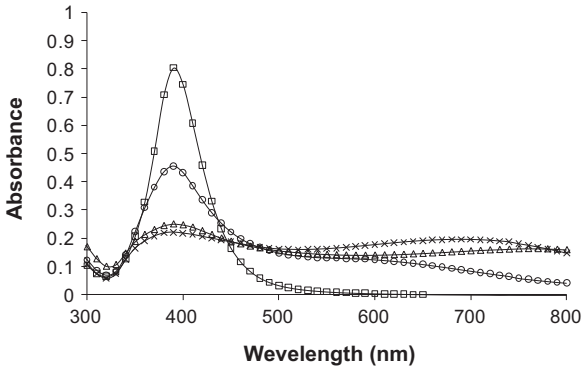

Fig. 4. UV–visible absorption spectra obtained for citrate stabilized-Ag NPs in different types of environmental water: (□) deionized water; (○) tap water; (△) ground water; (×) sea water, at contact time of 180 min.

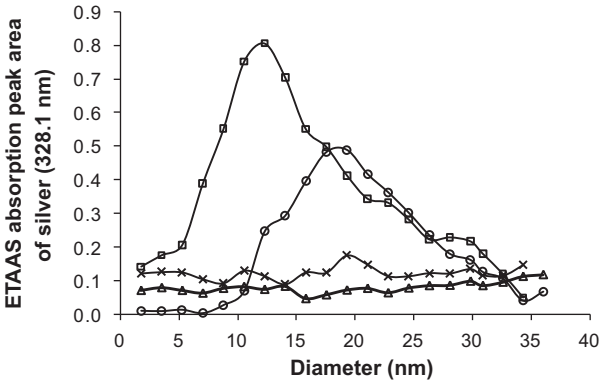

Fig. 5. Hydrodynamic diameter distributions of citrate stabilized-Ag NPs in different types of environmental water: (□) deionized water; (○) tap water; (△) ground water; (×) sea water, at contact time of 180 min. ETAAS was used as FlFFF detector.

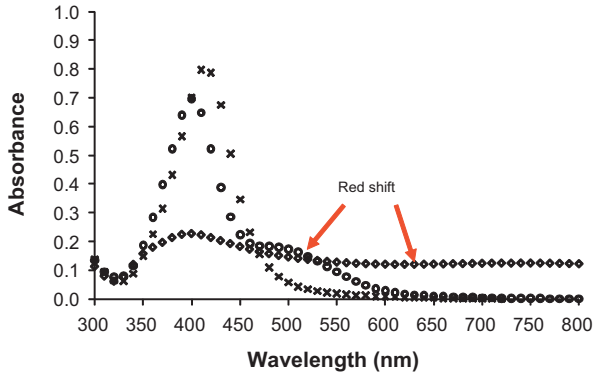

Fig. 6. UV–visible absorption spectra obtained for Ag NPs prepared from different stabilizing agents: (◊) citrate stabilized-Ag NPs; (○) pectin stabilized-Ag NPs; (×) alginate stabilized-Ag NPs in tap water, at contact time of 180 min.

+30 mV are electrically stabilized while nanoparticles with low zeta potentials tend to form aggregates [25].

These findings can be described by steric repulsion. The structure of stabilizing agent is the key factor to control Ag NPs stability; larger steric structure offers higher stability than the smaller steric structure [17]. Therefore, alginate stabilized Ag NPs should have higher stability than pectin and citrate stabilized Ag NPs, respectively, according to the molecular weight of citrate, pectin, and alginate as 258, 30,000–100,000, and 100,000–200,000 g mol^{-1}, respectively.

3.4.2. Effect of contact time

The particle size information obtained from FlFFF with ETAAS detection and zeta potential value from zeta potentiometer were used to provide evidence on Ag NPs aggregation. The aggregation of 20 mg L^{-1} citrate-stabilized Ag NPs in tap water was temporally investigated as demonstrated by shifts in size distributions with increasing contact time. With increasing contact time, the size distributions slightly broadened. The peak maximum appeared at larger diameter size, showing clear evidence of Ag NPs aggregation. The particle size at peak maximum (d_p) and the mean particle size (d_{mean}) increased with increasing contact time (Fig. 7a), suggesting that the aggregation process gradually occurred. The aggregation of Ag NPs was confirmed by zeta potentiometer, and the results are shown in Fig. 7b. The zeta potential values were less negative with increasing contact time, suggesting that the nanoparticles became less stable.

3.4.3. Effect of Ag NPs concentration

The concentration of silver nanoparticles also affects on stability of nanoparticles in water. Therefore, the effect of Ag NPs concentration was examined, as shown in Fig. 8. The mean particle size (d_{mean}) increased when the concentration of Ag NPs decreased. This might be explained by using the DLVO theory, by which the ions present in water cause charge shielding effect, reducing the diffuse layer size and thereby allowing NPs to come into contact sufficiently closely to produce aggregation [26,27]. The very low ion concentrations in tap water were not effective to shield charge of high amount of nanoparticles, but they were sufficient to shield charge of small amount of nanoparticles.

3.4.4. Effect of humic acid

The dissolved organic matter and natural organic macromolecules (NOM) in natural water may react with Ag NPs, which influenced on the stability of Ag NPs. As humic substances are the most important class of NOM in aquatic environment, citrate stabilized-Ag NPs were investigated for their stability in tap water, both in the absence and presence of humic acid using FlFFF with

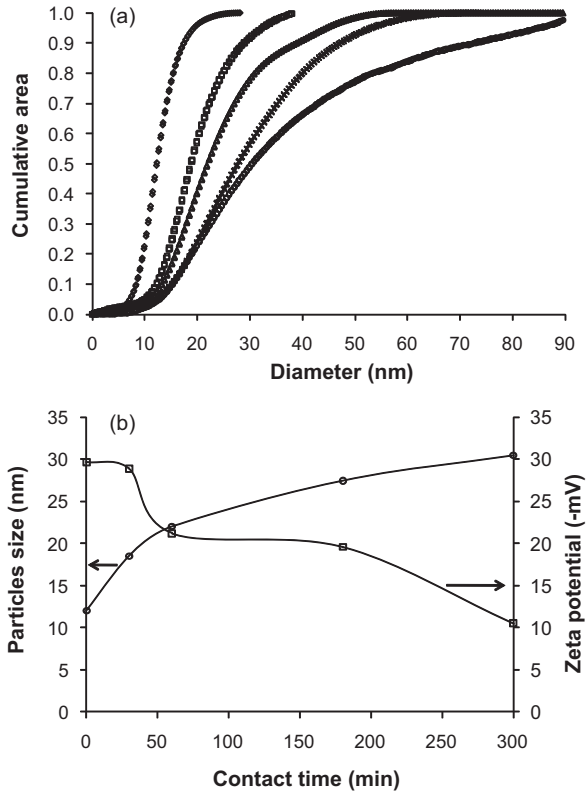

Fig. 7. (a) The cumulative area plot of 20 mg L^{-1} citrate stabilized-Ag NPs in tap water at various contact times: (◊) 0 min; (□) 30 min; (△) 60 min; (×) 180 min; (○) 300 min. (b) Diagram showing the particle size and zeta potential value at various contact times.

ETAAS detection and zeta potential measurement, as illustrated in Figs. 9 and 10, respectively. In the absence of humic acid, the particle sizes of citrate stabilized-Ag NPs increased with longer contact time, as shown in Fig. 9a and the zeta potential values also became less negative with increasing contact time (Fig. 10). In the presence of humic acid of 200 mg L^{-1}, the particle sizes remained unchanged in tap water even at 180 min contact time (Fig. 9b), suggesting that Ag NPs were stabilized with humic acid. This was further confirmed by the observation that the zeta potential values of Ag NPs in the presence of humic acid remained stable with increased contact time, as shown in Fig. 10. These findings are related with the previous reports by Hahn and Stumm [28] who discussed about the effect of NOM to stabilize inorganic colloids in natural waters

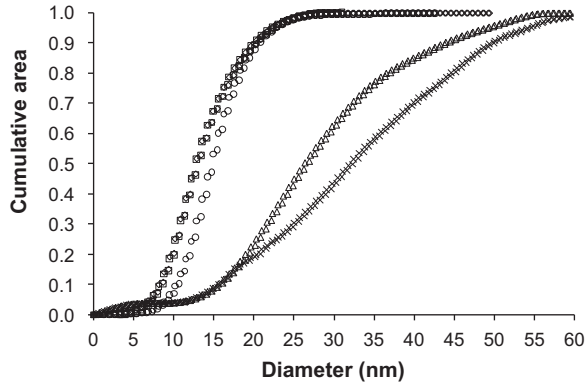

Fig. 8. The cumulative area plot of particle size of citrate stabilized-Ag NPs in tap water at varying concentrations of Ag NPs: (◊) 53 ppm; (□) 40 ppm; (○) 30 ppm; (△) 20 ppm; (×) 10 ppm

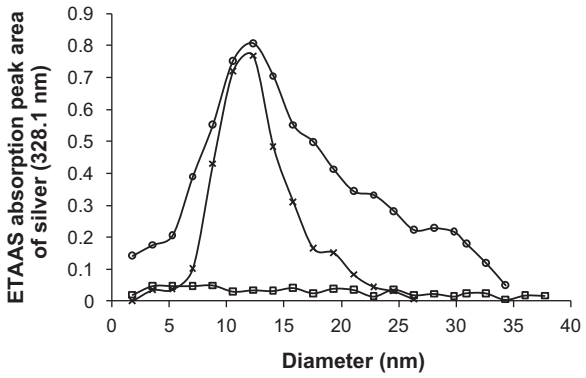

Fig. 9. Particle size distribution of citrate stabilized-Ag NPs: (◯) without humic acid in deionized water; (□) without humic acid in tap water; (×) with 200 mg L^{-1} humic acid in tap water, at contact time of 180 min. ETAAS was used as FlFFF detector.

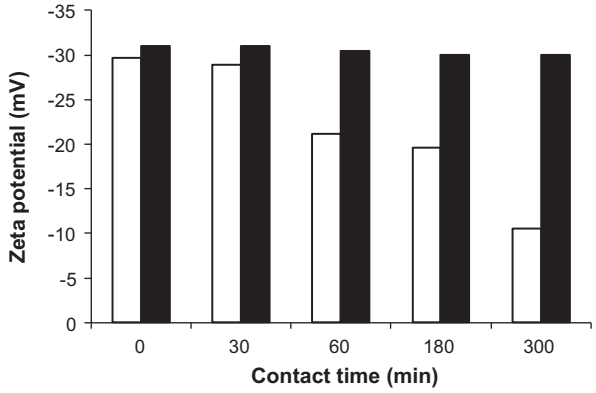

Fig. 10. Zeta potential values of citrate stabilized-Ag NPs in tap water in the absence (□) and presence (■) of 200 mg L^{-1} humic acid.

and Diegoli et al. [17] who reported that humic acid could stabilize the gold colloids in natural waters. Humic acid might cause aggregates to re-disperse or stabilize Ag NPs by steric repulsion [23,29,30].

4. Conclusions

Electrothermal atomic absorption spectrometry (ETAAS) was found efficient as an element specific detector for detection of silver in Ag NPs samples fractionated by FlFFF. In environmental water, citrate stabilized-Ag NPs undergo rapid aggregation than pectin and alginate stabilized-Ag NPs, suggesting that the surface property is the key factor that control the stability of Ag NPs in aquatic system. Humic acid affects on the stability of Ag NPs in the environment. In summary, the stability of Ag NPs in environmental water depends on the environment conditions such as types of stabilizing agent, contact time, Ag NPs concentration, and the presence of humic acid.

Acknowledgements

We gratefully acknowledge the research grants from the Thailand Research Fund (TRF) and Center for Innovation in Chemistry: Postgraduate Education and Research Program in Chemistry (PERCH-CIC), Commission on Higher Education, Ministry of Education, Thailand.

References

[1] S.N. Luoma, PEN Report, Woodrow Wilson International Center for Scholars and The Pew Charitable Trusts, Washington, DC, USA, 2008.
[2] J. Liu, R.H. Hurt, Environ. Sci. Technol. 44 (2010) 2169.
[3] L. Geranio, M. Heuberger, B. Nowack, Environ. Sci. Technol. 43 (2009) 8113.
[4] S.A. Blaser, M. Scheringer, M. MacLeod, K. Hungerbühler, Sci. Total Environ. 390 (2008) 396.
[5] T.M. Benn, P. Westerhoff, Environ. Sci. Technol. 42 (2008) 4133.
[6] O. Choi, Z. Hu, Environ. Sci. Technol. 42 (2008) 4583.
[7] J. Fabrega, S.R. Fawcett, J.C. Renshaw, J.R. Lead, Environ. Sci. Technol. 43 (2009) 7285.
[8] T.M. Tolaymat, A.M. Badawy EI, A. Genaidy, K.G. Scheckel, Sci. Total Environ. 48 (2010) 999.
[9] D.D. Evanoff Jr., G. Chumanov, Chem. Phys. 6 (2005) 1221.
[10] A. Panácek, L. Kvítek, R. Prucek, M. Kolár, R. Vecerova, N. Pizúrová, V.K. Sharma, T. Nevecna, R. Zboril, J. Phys. Chem. B 110 (2006) 16248.
[11] P. Raveendran, J. Fu, S.L. Wallen, J. Am. Chem. Soc. 125 (2003) 13940.
[12] R.F. Domingos, M.A. Baalousha, Y.J. Nam, M.M. Reid, N. Tufenkji, J.R. Lead, G.G. Leppard, K.J. Wilkinson, Environ. Sci. Technol. 43 (2009) 7277.
[13] S.A. Cumberland, J.R. Lead, J. Chromatogr. A 1216 (2009) 9099.
[14] M. Baalousha, J.R. Lead, Sci. Total Environ. 386 (2007) 93.
[15] K. Tiede, A.B.A. Boxall, S.P. Tear, J. Lewis, H. David, M. Hassellöv, Food Addit. Contam. A 25 (2008) 795.
[16] J. Yang, J.Y. Lee, L.X. Chen, H.P. Too, J. Phys. Chem. B 109 (2005) 5468.
[17] S. Diegoli, A.L. Manciulea, S. Begum, I.P. Jones, J.R. Lead, J.A. Preece, Sci. Total Environ. 402 (2008) 51.
[18] G. Blo, A. Ceccarini, C. Conato, C. Contado, F. Fagioli, R. Fuoco, A. Pagnoni, F. Dondi, Anal. Bioanal. Chem. 384 (2006) 922.
[19] C. Contado, G. Blo, F. Fagioli, F. Dondi, R. Beckett, Colloid Surf. A 120 (1997) 47.
[20] P. Liang, L. Peng, Microchim. Acta 168 (2010) 45.
[21] I.E. Sendroiu, S.F.L. Mertens, D.J. Schiffrin, Phys. Chem. Chem. Phys. 8 (2006) 1430.
[22] P. Mulvaney, Langmuir 12 (1996) 788.
[23] E. Navarro, A. Baun, R. Behra, N.B. Hartmann, J. Filser, A.J. Miao, A. Quigg, P.H. Santschi, L. Sigg, Ecotoxicology 17 (2008) 372.
[24] W. Kreyling, M. Semmler-Behnke, W. Möller, J. Nanopart. Res. 8 (2006) 543.
[25] Zeta Potential, An Introduction in 30 Minutes, Zetasizer Nano Series technical note (MRK654-01), Malvern Instruments, Worcestershire, UK, 2006.
[26] H. Christenson, J. Chem. Soc. 80 (1984) 1933.
[27] S. Elzey, V. Grassian, J. Nanopart. Res. 12 (2009) 1945.
[28] W. Stumm, Chemistry of the Solid–Water Interface: Processes at the Mineral-water and Particle-water Interface in Natural Systems, John Wiley & Sons, New York, USA, 1992.
[29] M. Farré, K. Gajda-Schrantz, L. Kantiani, D. Barceló, Anal. Bioanal. Chem. 393 (2009) 81.
[30] J. Buffle, K.J. Wilkinson, S. Stoll, M. Filella, J. Zhang, Environ. Sci. Technol. 32 (1998) 2887.